Dept. of Defense Center for Geoscience/Atmospheric Research
Under Agreement DAAL01-98-2-0078

PROTOTYPE REAL-TIME BOUNDARY LAYER PREDICTION IN SUPPORT OF THE CASES-99 NOCTURNAL BOUNDARY LAYER EXPERIMENT

by Douglas C. Schuster

William R. Cotton, P.I.

Colorado State University

DEPARTMENT OF ATMOSPHERIC SCIENCE

PAPER NO. 716

PROTOTYPE REAL-TIME BOUNDARY LAYER PREDICTION IN SUPPORT OF THE CASES-99 NOCTURNAL BOUNDARY LAYER EXPERIMENT

by

Douglas C. Schuster
Department of Atmospheric Science
Colorado State University
Fort Collins, Colorado 80523

Research Support by

Department of Defense Center for Geosciences/Atmospheric Research
under Agreement #DAAL01-98-2-0078

February 5, 2002

Atmospheric Science Paper No. 716

ABSTRACT

PROTOTYPE REAL-TIME BOUNDARY LAYER PREDICTION IN SUPPORT OF THE CASES-99 NOCTURNAL BOUNDARY LAYER EXPERIMENT

In September 1999, a modified version of the Regional Atmospheric Modeling System (RAMS), version 4.29, was implemented to provide 48 hour forecasts initialized at 12z in support of the CASES-99 nocturnal boundary layer experiment centered at Leon, KA. The research objective, through use of a forecast model, was to predict the structure of the nocturnal boundary layer, including temperature, relative humidity, and position/direction of the low level jet to provide guidance for field operations, and study the model's effectiveness in predicting such variables. In this effort the RAMS model was run throughout October 1999 over the study area. Additional runs were performed off-line after the CASES-99 project to examine how the model performed under varied configurations. Configuration 1, run at the time of the field project, implemented the Mahrer/Pielke radiation scheme at 35% homogeneous volumetric soil moisture (MP-35). Configuration 2 implemented the Harrington radiation scheme at 35% soil moisture (HAR-35), and configuration 3 implemented Harrington radiation at 25% soil moisture (HAR-25). Through investigation of two representative study days, one in which the model resolved the formation of a low level jet (LLJ) that developed high shear zones near its boundaries, RAMS demonstrated its general functionality as a high resolution forecast tool in all configurations when compared to observations. Specific results from the individual forecast studies displayed a tendency for all model configurations to produce inversion layers 800m to 1000m above ground level (AGL) that did not exist in the observations, or several hundred meters below observed inversion levels at initial nighttime forecast hours. As the model forecast progressed through the night, the fictitious, or lower than observed inversion layer tended to wash out causing the temperature and RH structure to match up well with observations taken around 12Z. In IOP#9, it appears that the erroneously predicted inversion may coincide with fictitious directional wind shear displayed in model winds near 800m AGL. Near the surface, southerly flow strengthened through the night in association with LLJ development at 80m to 100m AGL. Observations and model predicted winds displayed a similar pattern of directional shear with height strengthening through the nighttime hours. Additionally, near the surface, a warm model temperature bias existed as the near-surface temperature inversion developed through the night. MP-35 and HAR-25 produced the warmest temperature readings, while HAR-35 produced the coolest temperatures and highest RH values in the near surface inversion layer. In all cases, temperatures were 1 to 3 degrees warmer than observed, with RH readings up to 20% RH less than observations within 150m of the surface. In addition to the individual forecast analysis, a comprehensive forecast analysis of several CASES-99 Intensive Operational Periods (IOP's) compares model and observed values at 4 sounding sites and a central fixed 55m tower site. Wind fields displayed little change between configurations, while temperature and relative humidity fields varied with respect to configuration. Wind fields for all configurations were generally within 4 m/s in magnitude of observed values. HAR-

35 produced results closest in magnitude to observed values of temperature and RH through the nighttime hours of forecast periods. Additionally, HAR-35 produced the coolest temperatures and highest RH values of all three configurations, especially within 200m of the surface.

Douglas C. Schuster
Department of Atmospheric Science
Colorado State University
Fort Collins, Colorado 80523
Fall 2001

ACKNOWLEDGMENTS

Many thanks to advisor, Dr. William Cotton, co-advisor, Dr. Tom Vonder Haar, and committee member, Dr. Paul Mielke Jr. for giving their time and providing valuable insight. I would also like to thank Ray McAnelly, Dr. Bob Walko, and Dr. Rolf Hertenstein for helping me get the project started and providing support throughout. Additionally, I would like to acknowledge my entire research group, atmospheric science friends, and project coordinator Brenda Thompson for the support they have provided through my years at CSU.

This work was supported by the Department of Defense Center for Geosciences/Atmospheric Research Agreement #DAAL01-98-2-0078.

TABLE OF CONTENTS

1. Introduction

1.1 Operational Numerical Forecast Models

Operational numerical weather models have become some of the most utilized tools in modern weather prediction. Primarily, governmental and military agencies across the globe are charged with development and implementation of a variety of forecast models. In the United States, The National Centers for Environmental Prediction/Environmental Modeling Center (NCEP/EMC) oversees the operations of short and medium range forecast models including the ETA, NGM, AVN, and MRF. Centers in Canada, Europe and Japan provide similar support for their own numerical forecast models. The various models vary in scale and resolution from coarse global domains to higher resolution continental scales. Currently, the Environmental Modeling Center is operating an experimental 12km resolution configuration of the ETA model over the continental U.S. This is a marked improvement in resolution from other ETA configurations, which operate at 48km, 32km, and 29km resolutions respectively. Increases in computing power have greatly facilitated the development and implementation of higher resolution model configurations covering broader spatial regions such as the ETA. Additionally, decreasing costs for higher power computing components have allowed for Universities and research institutions to produce their own specialized forecasts.

1.2 Specialized Forecast Models

Numerous research institutions have implemented research numerical mesoscale models in operational real-time forecast environments. These models provide localized model output products, which can be developed specific to a forecast location. Successful simulations of a variety of mesoscale weather phenomena, including thunderstorm morphology, see-breeze circulations, and flow over complex terrain have demonstrated the utility a mesoscale model may provide as a localized forecast tool. Highly detailed topography, prognostic soil and vegetation models, in combination with more complete physical parameterizations and finer vertical and horizontal resolution give mesoscale models the complexity required to provide detailed localized model forecasts. Specialized forecasts can be made for guidance in industrial, military, and environmental applications. Model guidance of fog at an airport can provide airlines information to re-direct flights from the affected area. Wind and humidity guidance can be used as a tool in the prediction of wildfire intensity and propagation. Predicted evolution of boundary layer structure can be used to diagnose pollution dispersion in a populated area, or noxious gas dispersion on the battlefield.

Numerous research institutions have implemented mesoscale models to operate in various real-time configurations focused on specific local forecast needs. The Pennsylvania State University / National Center for Atmospheric Research (PSU/NCAR) MM5 is currently operated in real-time at the Mesoscale and Micro scale (MMM) division of NCAR along with several universities (Warner and Seaman, 1990). The Army's Battle scale Forecast Model (BFM) provides high-resolution forecasts specific to the needs of the battlefield (Henmi and Dumais, 1998). At Colorado State University (CSU), the Regional Atmospheric Modeling System (RAMS) has been configured to produce

mesoscale forecasts specific to the Colorado region initialized at 0z since 1991 on a cluster of seven IBM workstations using version 4a (Cotton et al., 1994). In September 1999 a modified version of the latest model release (version 4.29) was implemented on a heterogeneous cluster of eight single processor and eight dual processor 400Mhz Pentium Linux PC's. The initial 4.29 real-time configuration was developed to provide higher vertical and horizontal resolution boundary layer forecasts, than the previous workstation version, in support of the CASES-99 nocturnal boundary layer experiment (Poulos et al. 2001). Nested fine grids were centered over Leon, KA to provide forecast support for the field project over October 1999. After successful configuration and operation of the model in support of the CASES-99 project, the nested grids were re-located to several regions in the U.S. in support of field projects and general forecast interests. Once the new forecast system proved to operate effectively, all real-time model operations were moved to the version 4.29 PC cluster, which produced forecasts in a much more timely manner than the original workstation cluster. Daily 12z (user specified boundary layer location) and 00z (fixed Colorado location) initialized model runs could both be produced due to the increased power provided by the cluster.

1.3 Scientific Objectives

Scientific objectives to be accomplished through this study included three primary goals. The initial objective of the project was to provide real-time forecast support for the CASES-99 field project. This objective involved setting up an operational real-time forecast system that produced realistic information for forecasters to utilize in support of field operations. Model output was used to complement operational observation planning and provide information for near real-time interpretation of observed events. The second objective of this study was to examine a mesoscale model's (RAMS) utility

as a specialized forecast tool in support of a field project. In this case, the model's unique function was to resolve boundary layer and near-boundary layer structure and morphology through the period of the CASES-99 nocturnal boundary layer experiment, which occurred over October 1999. Observational data recorded through soundings and fixed tower instrumentation provided the means to analyze model effectiveness. The final objective involved determining potential model biases and a preferential configuration for the forecasting situation. To accomplish the final objective, three model configurations were investigated to determine which appeared best for predicting the desired boundary layer and near-boundary layer variables. Mahrer/Pielke radiation at 35% homogeneous soil moisture was implemented at the time of the forecasts following the standard configuration in the 4a model. Off-line runs implemented the Harrington Two-Stream radiation scheme at 35% and 25% homogeneous soil moisture over identical forecast times. The 25% soil moisture value was chosen to be more representative of local observed values, which were released upon completion of the experiment. For both the second and third objectives, four separate sounding sites provided the necessary observations to compare model output to observed thermodynamic and wind variables through the lowest 1 km of the atmosphere. The central 55m tower provided wind and thermodynamic variables at fixed levels located at 45m above ground level (AGL), and thermodynamic variables for comparison at 5m AGL. Two individual examinations of model performance during separate intensive operational periods (IOP's) compare evolution of model structure to observed atmospheric structure for all three-model configurations through the lowest 1500m AGL at the Leon sounding site. Additionally, model output is compared against thermodynamic and wind observations recorded at the central observing tower and large scale synoptic conditions recorded during the IOP's. A composite analysis investigates model performance through the duration of the field project. Model performance and

potential model biases are examined through simple statistical comparison at fixed levels through the lowest 1km AGL of the atmosphere. Thermodynamic and wind variables are examined with sounding data from a combination of all four launch sites. Model vs. tower data at fixed levels is also examined over the same time period.

Chapter 2 gives an overview of the CASES-99 field project. Scientific objectives and experimental setup are discussed, along with the role of RAMS as a real-time forecast system in support of the field project. Background information on specific instruments utilized for model performance analysis will also be provided.

Chapter 3 provides background on the setup of the real-time forecast system. General model features, and specific model configuration for the CASES-99 field project will be described. Initialization and time-dependent lateral boundary conditions utilizing the ETA gridded pressure data set will also be explained. Finally, examples of grid mobility and a description of computer resources will be presented.

Chapter 4 investigates model performance over two individual IOP's including IOP #7 (Oct 18, 1999), and IOP #9 (Oct 21, 1999) which presented defined atmospheric features that were representative of the general conditions observed through all IOP's. Three model configurations will be analyzed to determine which setup provided the most reliable forecast data for each individual period. Configurations utilizing Mahrer/Pielke radiation at 35% homogeneous volumetric soil moisture, Harrington radiation at 35% soil moisture, and Harrington radiation at 25% soil moisture will be compared against RH, temperature, U-wind, V-wind, and wind direction sounding data taken from the Leon sounding site over the first 1500m AGL, through the time evolution of each IOP. Synoptic scale features will also be examined to determine what role large scale forcing may have played in affecting fine grid output. Finally, model and central tower data will be compared at 5m and 45m AGL. RH and Temperature will be examined at 5m AGL, with RH, Temperature, U-wind, and V-wind compared at 45m AGL. Upon examination

of the data, discrepancies between model configurations, and discrepancies between model and observations for each configuration will be discussed.

Chapter 5 investigates composite model performance for each configuration through much of the CASES-99 operational period. Mean difference, mean absolute difference, and root mean square error were calculated for fixed forecast times at 100m, 200m, 500m, and 915m AGL incorporating data from all 4 sounding sites. Model bias and discrepancy from observed values for each configuration are discussed through examination of the rough statistics. Baseline plots of model and tower data at 5m and 45m AGL provide a general sketch of each model configuration's performance for forecast times less than 24 hours, and forecast times greater than 24 hours in terms of RH and temperature at 5m AGL, and RH, temperature, U-wind, and V-wind at 45m AGL. Data points for statistical comparison and baseline plots were chosen according to observational data availability.

Chapter 6 presents a summary of model performance for each configuration, interpretation of results, and suggestions for further research. The summary and interpretations of results will combine the findings of individual IOP analyses with the findings from the comprehensive statistical analysis. Any model biases or large discrepancies for specific configurations and variables will be highlighted.

2. CASES-99 Experimental Overview

This section provides an overview of the setup and objectives of the CASES-99 field experiment. Scientific objectives and ideal observing conditions are first defined. Types and placement of measurement systems are then discussed, along with the role of RAMS as a real-time forecast system in support of the field project.

2.1 CASES-99 Background and Scientific Objectives

The Cooperative Atmospheric Surface Exchange Study October 1999 (CASES-99) field observational program represents a study to investigate linkages between the atmosphere and the earth's surface. This study was designed to examine events in the nighttime boundary layer, and to investigate the physical processes associated with evening and morning transition periods. Broad goals of the CASES-99 field program included identifying the sources and quantifying the physical characteristics of the mixing phenomena that occur within stable boundary layers, utilizing an optimal arrangement of a variety of observational tools. Phenomena including internal gravity waves, Kelvin-Helmholtz (KH) billows, inertial oscillations, shallow drainage flows, and turbulent bursts that occur intermittently under clear sky and light wind conditions were the focus of the study (Poulos et al., 2001). Specific goals of the one-month field program listed in Poulos et al., 2001 included:

1) provide a time history of internal gravity waves, KH shear instabilities, and turbulence events in the nighttime stable boundary layer, and to evaluate the relative contributions to intermittent heat, moisture, and momentum fluxes that can be associated with these phenomena. Sources of turbulence bursts include, but are not restricted to, surface and elevated shear layers and KH instability, internal gravity waves within the stable boundary layer, drainage currents, and surface vortex shredding.

2) measure heat and momentum fluxes and their divergences accompanying the events contributing to turbulence, transports, and mixing throughout the nocturnal boundary layer, and especially within the surface layer (~10 to 20m), to assess the departures from similarity theory under weakly stable and very stable conditions.

3) define the relative importance of surface heterogeneity, particularly under very stable light wind conditions, on the initiation of shallow drainage currents, and the horizontal and vertical transports that accompany such boundary undulations.

4) improve our current understanding of the diffusion, dispersion, meandering and concentration fluctuations of plumes that emanate from ground-based and possibly, elevated sources, during both clear and cloud-topped nocturnal boundary layer conditions.

5) acquire data during the transition from a convective to a stable boundary layer regime and vice-versa to compare with existing models of this transition, and to assess the role of this transition period in the initiation of internal oscillations and the enhancement of low-level jets ~ 100m-300m above the surface.

2.2 Study Period and Instrumentation

The month long field experiment took place from October 1-31, 1999 on the Walnut River Watershed field site near Leon, Kansas (Fig. 2.1). That period was chosen for its

climatologically high frequency of clear, calm nights and therefore increased likelihood of stable boundary layer development. The region was chosen due to its relative lack of obstacles, relatively flat terrain, and reasonable access to power and phone lines. Over the month of October, 10 Intense Observing Periods (IOP's) occurred, where conditions were considered ripe to observe the desired nocturnal boundary layer phenomena. Ripe conditions were defined by periods with clear sky, light near-surface wind, nocturnal boundary layer conditions which are conductive to stable ($Ri > 0.25$) and very stable conditions ($Ri > 1.0$) (Poulos et. al., 2001).

A large number of instruments were deployed within the study area to capture observations of the desired phenomena during the IOP's. These instruments included a heavily instrumented 55m tower, six 10m towers, multiple radars, lidars, scintillometers, tethersondes, rawinsondes, and research aircraft. Instrument data utilized for model performance analysis included 55m tower data collected at the central Leon site, and data collected at four rawindsonde sites including Leon, Beaumont, Smileyberg, and El Dorado (Fig. 2.2). All sites provided measurements of wind and thermodynamic variables, which could be compared to model output.

National Center for Atmospheric Research / Atmospheric Technology Divisions (NCAR/ATD) provided and operated the GPS/Loren Atmospheric Sounding System (GLASS) at the four fixed sounding sites. The system is composed of a VAISALA RS80-15GH rawinsonde containing a 403 MHz band transmitter, a GPS receiver, pressure, temperature, and relative humidity sensors. Thermodynamic data are transmitted from the sonde roughly every 1.5 seconds. GPS radionavigation signals are received by the sonde and re-transmitted to the surface station. The surface station in composed of a navigation data processor, a meteorological data processor, and a personal computer with specialized software.

Pressure, temperature, relative humidity, and wind information are the primary variables recorded through the GLASS system. The pressure sensor is an encapsulated steel aneroid sensor with a range from 3 to 1060mb, an accuracy of 0.5mb, and a 0.1 mb resolution. The temperature sensor is a capacitive bead in glass encapsulation possessing a range of -90 C to 60 C, an accuracy of 0.2 C, and 0.1 C resolution. Relative humidity measurement is done through a thin-film capacitive type sensor with a range of 0 to 100% RH, an accuracy of 2.0% RH, and 0.1% RH resolution. Wind and position measurements are done with a GPS receiver. Winds derived from GPS have a constant accuracy of 0.5m/s once the minimum number of satellites (typically four) are received. Resolution and averaging time for derived winds are 0.1m/s and 0.5 seconds respectively.

NCAR/ATD additionally conducted the measurements taken using the Integrated Surface Flux Facility (ISFF) located on the central site 55m tower. Figure 2.3 diagrams the layout of sensors on the 55m tower. Generally there is a wind and temperature measurement every 5m, with turbulent wind, temperature, and humidity measured at least every 10m. Observations taken at 45m and 5m AGL were utilized for comparison against model data calculated at similar heights. Variables included U-wind, V-wind, temperature and RH at 45m, and temperature and RH at 5m AGL.

A hygrothermometer developed at NCAR with VAISALA components recorded temperature (C) and RH (%) measurements. The hygrothermometer is composed of integrated sensors which utilize a platinum resistance thermometer and solid state RH sensor inside an aspirated radiation shield enclosure. Accuracies range from 0.1 C for temperature, and 2% RH for the relative humidity.

Wind measurements were recorded by a prop-vane anemometer produced by R.M. Young, and modified at NCAR to obtain a high-resolution vane azimuth using an optical encoder. Instrument range covers wind speeds from 0 to 60 m/s, and has an accuracy

of 0.3 m/s. Accuracy in wind direction is 3.0 degrees. All information described above can be obtained from the NCAR/ATD website located at http: //www.atd.ucar/edu/facilities.html.

2.3 Real-time Forecast Support

Real-time forecast support involved providing model guidance for forecasters overseeing CASES-99 field operations. Model guidance was used, as a forecast tool in determining what types of observational operations would proceed, if any, on a given night. In order to provide this support, RAMS version 4.29 was implemented on a cluster of 16 Linux PC's, and automated over September 1999. Automation involved scripts to ingest and degrib initialization data, execute the parallel model run, and convert the model output into graphical products, which could be viewed through a web-site interface. Some of the automation scripts were simply taken from the previous IBM workstation cluster and modified to run under the Linux operating environment. The final system included an IBM workstation to ingest and degrib data, the PC cluster to perform the parallel forecast model run and produce graphical output, and a PC web server to access the graphical model output.

Several types of graphical products were produced daily to provide CASES-99 forecasters with relevant information to assist in their forecasts. Products included mapped views of forecast variables for all model grids, longitudinal and latitudinal cross sections of forecast variables for the fine grids (see chapter 3), and a Skew-T/LogP thermodynamic diagram plotted at the central field project site. Forecasters were provided with specific products that helped in determining the development and evolution of the low level jet (LLJ), temperature inversions, and moisture fields. Mapped products, including U-wind, V-wind, total wind speed, potential temperature,

temperature, and RH, were available on the high resolution boundary layer grid (Grid 3) at 25m, 125m, 225m, 475m, and 1000m AGL. Longitudinal and latitudinal cross-sections centered within the grid-3 domain provided forecasters similar variables, and were the primary tools used in determining development and positioning of the LLJ over the field project domain. Correspondence with field forecasters allowed for model products to be modified if the need arose.

Timeliness in producing model products was required to provide forecasters enough information by the time a decision had to be made on what operations, if any, would commence on a given evening. Typically, forecasters needed the products by 2:00PM mountain daylight time (MDT), the scheduled time of their daily operations meeting. Model runs were started when ETA initialization and nudging data (Chapter 3) became available, around 10:30AM MDT, and completed through all 48 hours by 5PM MDT. Graphical products were generated as model data became available through the course of a model run. On days where no system problems occurred, 24 hours of hourly forecast products were typically available by 2PM MDT. On certain occasions, problems occurred within the forecast system, causing graphical output to be delayed, or not generated at all. One typical problem involved downloading incomplete ETA gridded pressure files for model initialization and boundary nudging (Chapter 3). When this occurred, the model would run up to the hour that it encountered the incomplete nudging data and stop, or not run at all if the incomplete data file occurred at the initialization time. Another problem involved communication errors between machines within the PC cluster. When a communication error randomly occurred, this would bring the model run to a halt. Finally, software problems involving the graphical post-processing, and network problems between the web-server and PC-cluster prevented forecasters from accessing model output. Frequency of these problems decreased as the field project progressed, and familiarity with the forecast system grew. Causes of many of the

problems ranged from insufficient network hardware to too many processes running on one machine. Most of the problems have been addressed in the time following the field project.

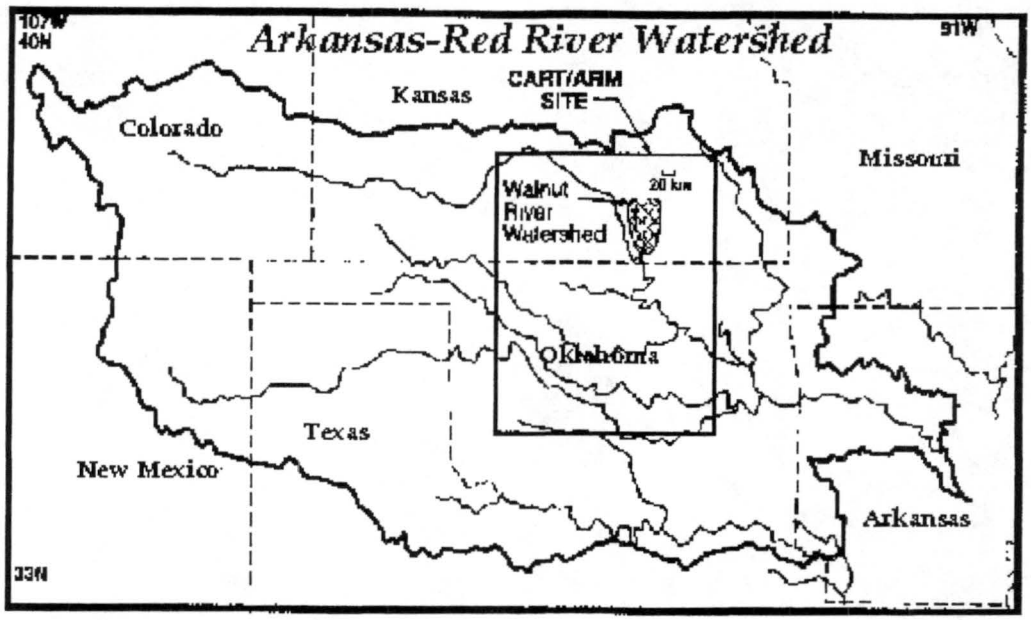

Figure 2.1 – Walnut River Watershed Site.

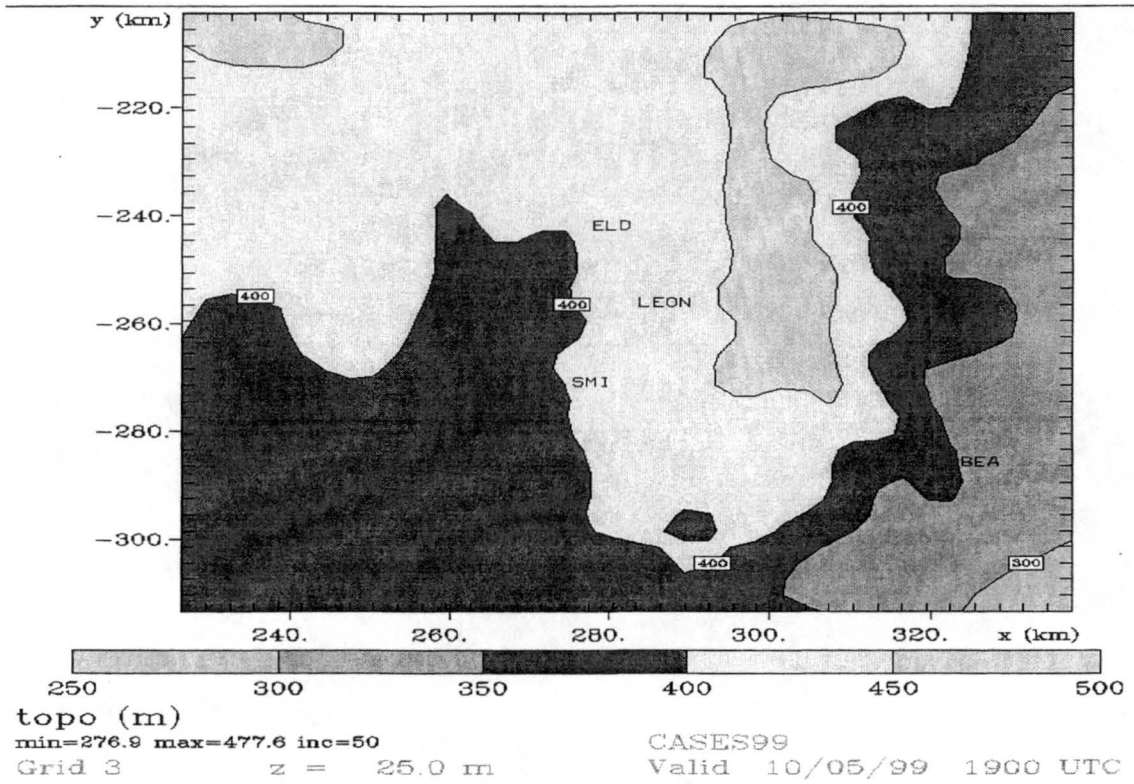

Figure 2.2 – CASES-99 Rawinsonde Sites Within Model Grid 3.

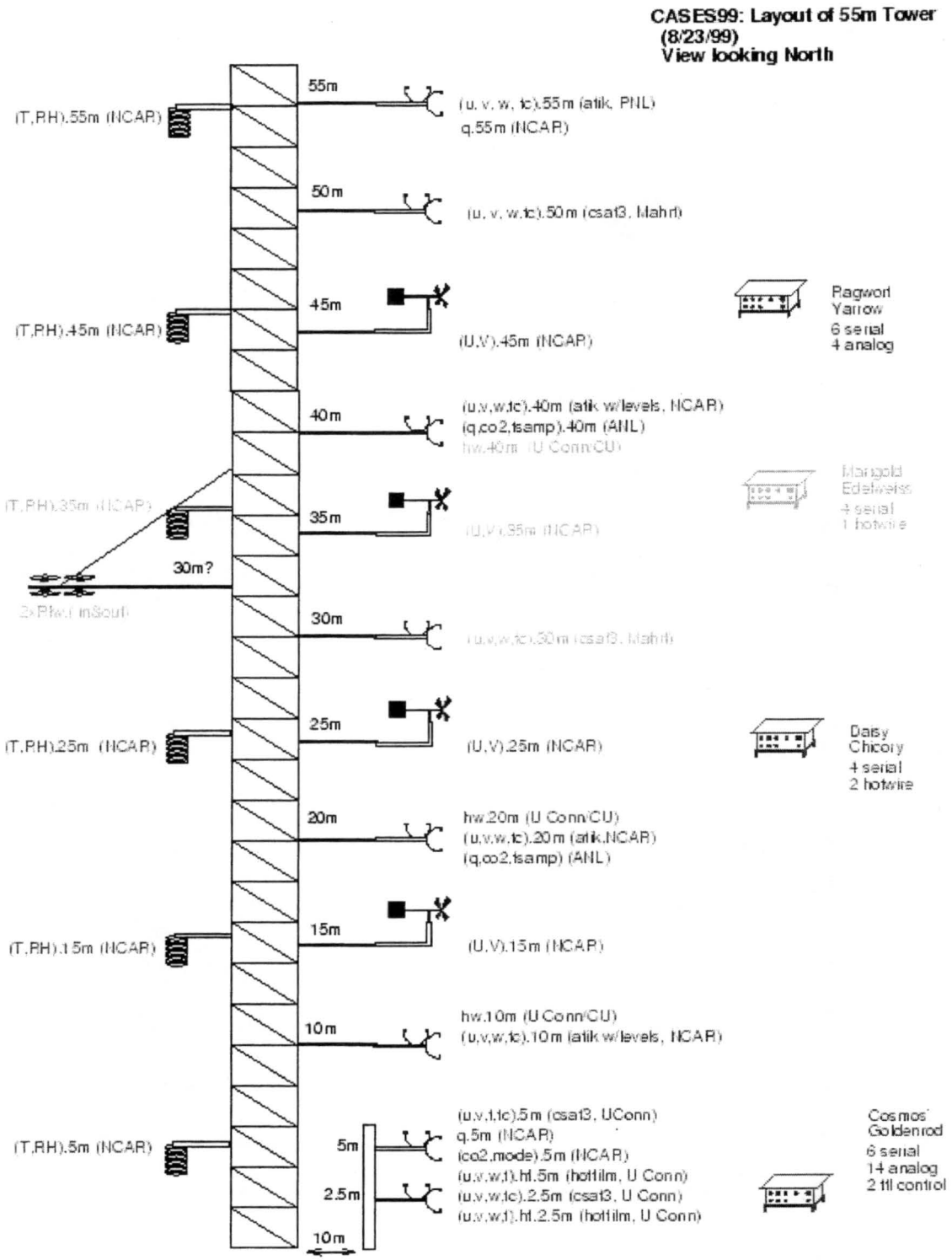

Figure 2.3 – 55m Tower Observing System.

3. Real-time Forecast System

This section contains a general description of the features implemented in the real-time RAMS 4.29 setup. Specific characteristics of the high-resolution boundary layer configuration are discussed, along with computer performance and resources needed to support the real-time implementation. Examples of grid-3 relocation, to provide forecast support over varied geographical regions, are displayed. ETA initialization and boundary nudging data are also discussed.

3.1 General Model Description

The Regional Atmospheric Modeling System (RAMS), developed at Colorado State University (CSU) has been run as a prototype real-time mesoscale forecast model since 1991. The code is a merger of a non-hydrostatic cloud model (Tripoli and Cotton, 1982) and a hydrostatic mesoscale model (Mahrer and Pielke, 1977). A general model description can be found in Cotton et al. (1982), Tripoli and Cotton (1982), Tremback et al. (1985), Tripoli (1986), Tremback (1990), and Pielke et al. (1992). The non-hydrostatic version of RAMS v4.29 was employed for this project with the numerical procedures described in Tripoli and Cotton (1982) and Tripoli (1986). This version of the non-hydrostatic model uses a leapfrog time differencing scheme formulated with "time-split" time differencing schemes (Tripoli and Cotton, 1982; Tremback et al., 1985) to integrate fast wave modes, including acoustic and gravity waves, on short time steps,

and all other terms on long time steps. A second order leapfrog scheme is used for advection. Predicted RAMS variables include *u*, *v*, and *w* wind components, ice/liquid water equivalent potential temperature, dry air density, total water mixing ratio, and the mixing ratios of the various water variables (rain, snow, pristine ice, hail, aggregates and graupel). From these, pressure, potential temperature, vapor mixing ratio, and cloud mixing ratio are diagnosed.

The standard C grid (Mesinger and Arakawa, 1976) is the grid stagger used in RAMS, staggered in both the vertical and horizontal directions. All thermodynamic and moisture variables are defined at the same grid point with the velocity components *u, v,* and *w* staggered 1/2 Δx, 1/2 Δy, and 1/2 Δz, respectively. The horizontal grid uses a rotated polar-stereographic projection with user specified spacing, where the pole of the projection is rotated to an area near the center of the domain, in order to minimize the distortion of the projection in the main area of interest. The grid vertical structure uses the σ_z terrain-following coordinate system (Gal-Chen and Somerville, 1975; Clark, 1977; Tripoli and Cotton, 1982) with user specified spacing. In this coordinate system, the top of the model domain is exactly flat and the bottom follows the terrain. Horizontal and vertical grids are composed of a parent grid, which covers a large domain at low resolution, and higher resolution nested grids, which occupy a region within the computational domain of the coarser parent grid, and coincide with the parent grid mesh in that region. Mesh refinement on a nested grid may be prescribed for the horizontal or vertical directions, or both. The refinement is always required to be an integer ratio; such that a whole number of nested grid cells are contained within a parent grid cell.

Specific features to particular model configurations are mentioned in subsequent sections however, additional common features between study configurations follow. The turbulence scheme combines the Mellor/Yamada turbulent kinetic energy (TKE) scheme

(Mellor and Yamada, 1974) to predict vertical eddy mixing coefficients and a local deformation scheme for horizontal mixing (Tripoli and Cotton, 1982). The surface parameterization uses the Land-Ecosystem-Atmosphere Feedback model (LEAF2) (Walko et al. 2000) sub-model which prognoses soil, vegetation, snow cover, and canopy air temperature and moisture fields based on vertical diffusion and exchange with the atmosphere of both quantities. For this study, surface vegetation type was set constant through the entire domain to crop/mixed farming with 8 soil levels. The "wall on top" condition, where *w* is set to zero at the model top, is used as a top boundary condition.

Two radiation schemes were employed in this study, one described by Mahrer and Pielke (1977), and one described by Harrington (1997). The Mahrer/Pielke scheme is the simpler of the two, accounting for the influence of water vapor absorption and scattering by oxygen, ozone, and carbon dioxide on shortwave and longwave radiative transfer. It does not consider radiative influences due to condensate or microphysical species. For this reason, the model does not account for reflected/absorbed shortwave radiation due to clouds nor does it include additional downward longwave radiation. The Harrington parameterization accounts for many of the effects ignored by the Mahrer/Pielke model. The Harrington parameterization accounts for each form of condensate as well as water vapor, and even utilizes information on ice crystal habit. It is the most sophisticated and computationally expensive radiation option in RAMS. With the previous workstation cluster, the Harrington option would have been too computationally expensive to use in a real-time forecast environment.

Four basic levels of moisture complexity are available in RAMS v4.29. The first level is completely dry, eliminating any process, which influences or is influenced by any phase of moisture. The second level includes advection, diffusion and surface flux of water vapor. The third level activates condensation of water vapor to cloud water

whenever supersaturation is attained. No other forms of liquid or ice water are considered. The final option, utilized under the single moment scheme in the boundary layer configuration of this study, has the highest complexity microphysics including the precipitation process. It activates the bulk microphysics parameterization, which includes cloud water, rain, pristine ice, snow, aggregates, graupel, and hail species (Walko et al. 1995).

3.2 Real-time BL Model Configuration

The real-time forecast model configuration is designed to provide higher spatial resolution through the lowest kilometer of the atmosphere then the previous forecast model configuration. A three-grid structure, with vertical nesting on grid 3, accomplishes this. The parent grid with 100 x 72 grid points and horizontal spacing of 48 km covers the continental U.S. The second grid, with 46 x 46 grid points and horizontal spacing of 12 km, can be located anywhere within the parent grid. Grid 3, the boundary layer (BL) grid with 38 x 38 grid points and 3 km horizontal grid spacing, can be located anywhere within grid 2. Grids 1 and 2 have 36 vertical levels with spacing starting at 150m near the ground, stretching to 1000m near the model top, which is fixed at 19,191m. Grid 3 has 46 vertical levels and is vertically nested within grid 2 at 50m spacing over the first 12 grid levels, up to 600m above ground level, where the spacing increases to 75 m over the next 4 grid levels. Above this level, grid 3 vertical spacing coincides with that of grids 1 and 2. Over the period of October 1999, grids 2 and 3 were centered over Leon, KA in support of the CASES-99 field project (Fig 3.1). Model runs were initialized daily with 1200 UTC data and, as often as data allowed, would forecast out to 48 hours. A 48-hr simulation on the PC cluster typically took from 5 to 6 hours of wall-clock time.

3.3 Initialization - ETA

Model initialization data were provided by the NCEP ETA model observational analysis. The ETA data assimilation system (EDAS) is patterned after the NCEP global spectral statistical interpolation analysis (Parrish and Derber, 1992). It utilizes the regional 3-dimensional variational analysis (3DVAR) to interpret several observational data sources. Data sources include surface land observations, surface marine observations, rawinsondes, conventional and Aircraft Communication Addressing and Reporting System (ACARS) aircraft data, cloud-tracked winds from GOES, Japanese, and European satellites via visible, IR and WV imagery, Special Sensor Microwave/Imager (SSM/I) wind speeds, dropwindsondes, microwave radiances from polar-orbiting and geostationary (GOES) satellites, GOES precipitable water data, profiler wind data, and Velocity Azimuth Display (VAD) wind profiles from next generation radar (NEXRAD) stations. 3DVAR analyzes wind, specific humidity, geopotential height, and temperature. The analysis of temperature, instead of inferring temperature from the analyzed thickness, allows for easy assimilation of "isolated" temperature observations, such as high density (ACARS) temperature data (Rogers et al. 1998). Observational data are interpolated to the ETA grid. A gridded pressure ETA analysis dataset with approximately 81 km x 81 km horizontal resolution on a Lambert-Conformal grid, covering North America and surrounding oceans, is used for RAMS initialization. The ETA dataset provides horizontal wind components, heights, temperatures and relative humidity at 19 pressure levels from 1000 mb to 100 mb at 50 mb intervals (Day, 1998). The portion of the ETA dataset, which covers the continental U.S. and border regions, is accessed and interpolated onto the RAMS polar-stereographic grids, creating a polar-stereographic/pressure coordinate dataset. Then

the data are linearly interpolated vertically to both the isentropic vertical coordinate and the terrain following, σ_z coordinate.

3.4 Time-Dependent Lateral Boundary Conditions – ETA

Time-dependent lateral boundary conditions are necessary for variably initialized simulations. RAMS lateral boundary nudging is an implementation of the Davies (1978) scheme where a number of grid points in a boundary region are nudged toward the data analysis. This allows for the introduction of time-varying information into the model domain. In RAMS lateral boundary nudging scheme, boundary values of *u, v, theta, r* and π are forced to externally specified values although the model's internally defined tendencies are used in the model integration (Cram, 1990). To accomplish this, an extra tendency term is added to each model prognostic equation, which forces the predicted variable towards the available observations or forecasts.

In the boundary layer forecast configuration, ETA model forecasts provided lateral boundary conditions. A comprehensive description of the ETA model can be found in Mesinger et al. 1999. The ETA model forecasts were run at 32km resolution covering much of North America and adjacent oceans, with 45 vertical levels (Rogers et al. 1998). ETA forecast datasets have the same structure as the initialization data discussed previously. The forecast datasets were available at the following forecast hours: 0, 6, 12, 18, 24, 30, 36, 42 and 48 hours. As discussed previously, the 0 forecast hour dataset is used for model initialization. Lateral boundary conditions were first updated at 6 hours and then at all subsequent ETA forecast times listed. The boundary conditions were linearly interpolated between the listed time intervals. This implies the variables on a zone of points along the domain's lateral boundaries were assumed to undergo a linear transition from initialization to 6 hours, 6 to 12 hours and so on. Five horizontal

nudging points were chosen for the boundary layer configuration, following the setup used for the previous forecast model.

Obtaining a complete set of 6-hourly nudging files presented the greatest challenge in generating a complete 48-hour forecast cycle over the CASES-99 study period. On several occasions incomplete data were transmitted from the NOAA ftp site to the RAMS ftp server. Either the data were incomplete, unavailable, or there was a problem in the transmission process. If one of the six hourly nudging files was incomplete or missing, it caused the model to blow up at the time of the bad file, or prevented the model from starting at all if the bad file occurred at 0 or 6 hours. On some occasions, a manual re-start, reconfigured to skip a bad or missing nudging file, allowed for a forecast to be completed, but usually in an untimely manner for forecasters on the field site. Time issues also occurred on several occasions in the data transmission process preventing a timely model forecast due to late initialization. Both problems seem to have been alleviated with the implementation of a new ftp server for the RAMS real-time forecast system. The previous server was a workstation of late 1980's vintage, which had several processes running along with ftp service, causing the ftp service to be slow and, at times, incomplete. The new PC server is dedicated to the ftp process, and seems to have been much more efficient and reliable.

3.5 Grid Mobility

One of the goals of the boundary layer forecast model design was to provide enough flexibility to allow for the fine resolution grids to be relocated to a desired site anywhere within the continental U.S. given a days notice. To accomplish this, model output products were required to remain fixed for any site location. Additionally, model configuration had to be modified according to site location. This was especially evident

when the forecast grids were relocated over Tucson, AZ in May 2000. Model predicted temperatures were 10 degrees C cooler than observed in initial model runs. The soil moisture parameter needed to be lowered to reflect the dry surface conditions of the desert region. Once the soil moisture parameter was reduced, temperature forecasts were observed to be much closer to surface observations in the Tucson area.

Over the years of 1999 and 2000, RAMS grid mobility was demonstrated through the relocation of the fine grids to several different U.S. sites. Sites were chosen for forecaster interest, availability of direct feedback on model performance, and field project support. Operational forecast locations included White Sands, NM, Littlefield, TX, Tucson, AZ, WLEF Tower, WI, southern MN, Leon, KA, north central and northeast Colorado (Fig 3.2). In addition to the CASES-99 project support discussed throughout this paper, model forecast support was provided for the August 2000 COBRA field project in northern Wisconsin. The RAMS forecast model was interfaced with Dr. Marek Uliasz's Lagrangian Particle Dispersion Model (LPDM) to provide source location information on the air mass that was sampled at the WLEF tower site. The Littlefield, TX location was chosen to provide guidance for a soaring contest. Other locations were chosen due to forecaster interest. Future goals of grid relocation include a web user interface where a designated user could chose a forecast location from a map of possible grid center-points. "Canned" configurations would be set for each pre-defined forecast point, allowing for grid location to be specified with ease.

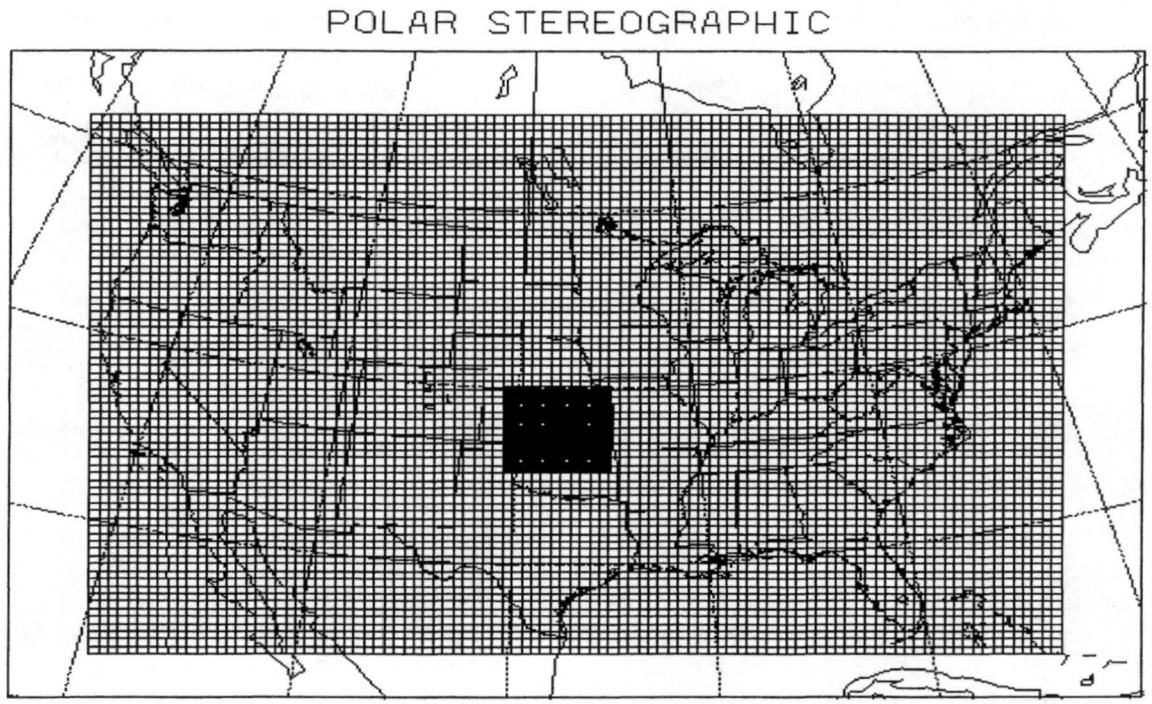

Figure 3.1a – CASES-99 Grid 1 and 2 Location.

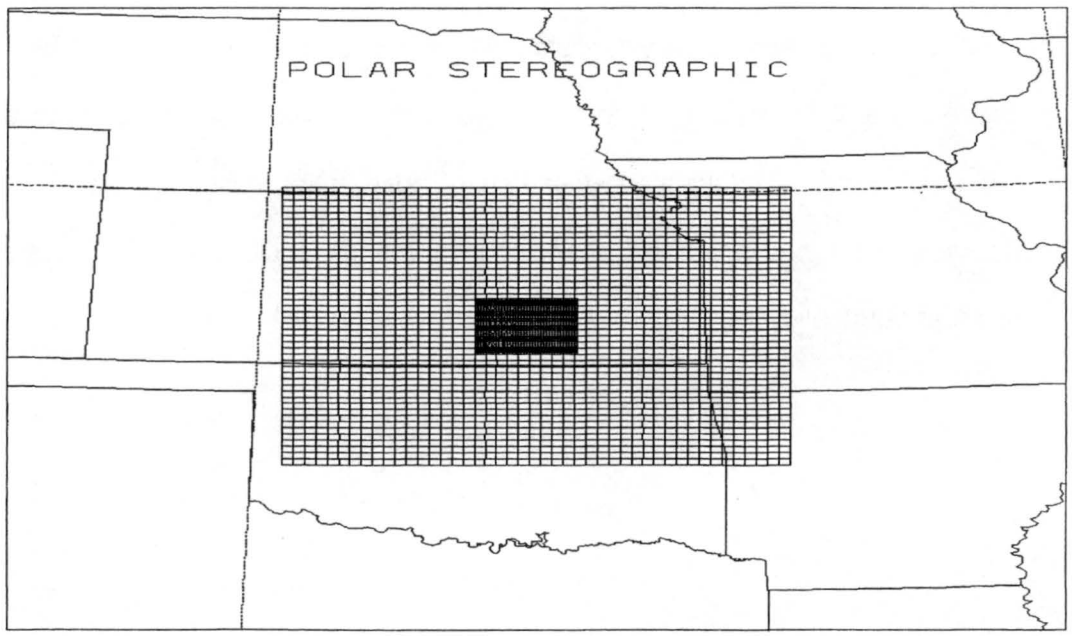

Figure 3.1b – CASES-99 Grid 2 and 3 Location.

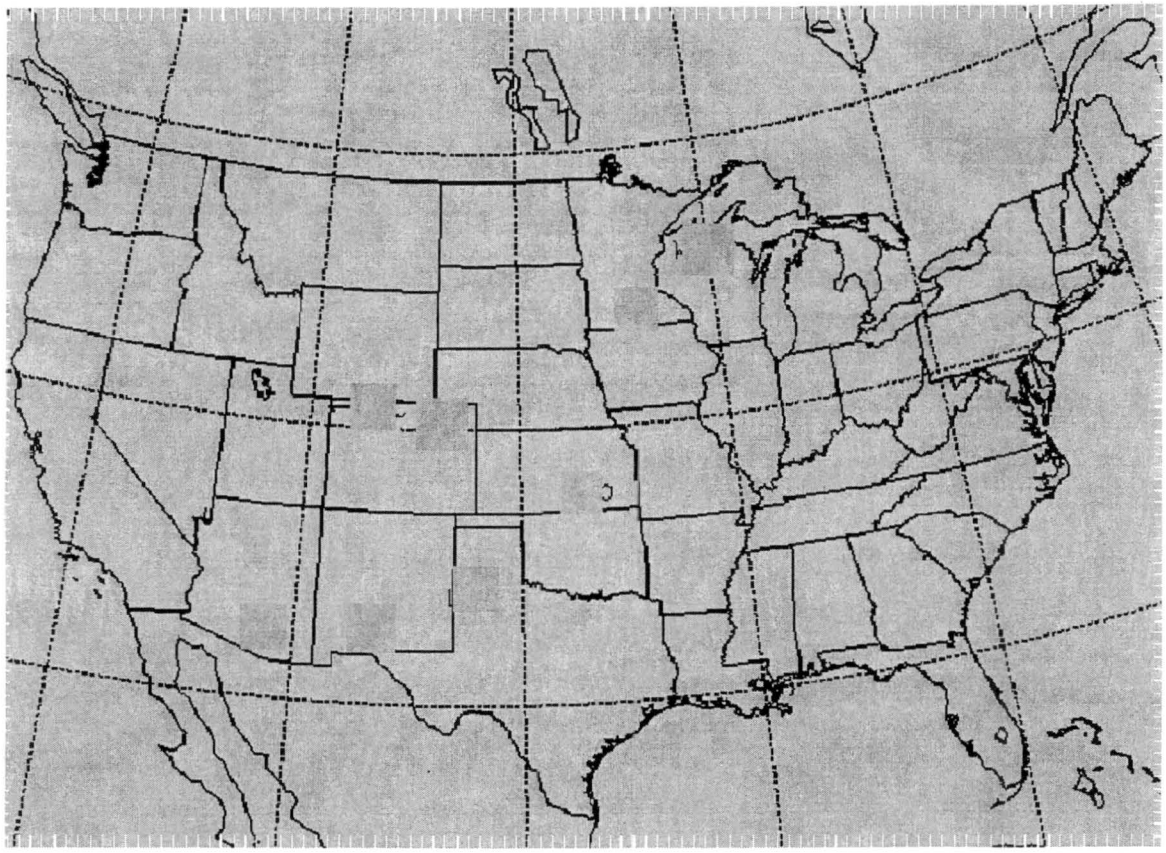

Figure 3.2 – 1999/2000 Forecast Grid Locations.

4. CASES-99 Real-time Boundary Layer Forecasting Investigations

This section investigates model performance over two individual IOP's including IOP #7 (Oct. 18, 1999), and IOP #9 (Oct. 21, 1999) which presented defined atmospheric features that were representative of the general conditions observed on all IOP's. Three model configurations are analyzed to determine which setup provided the most reliable forecast data for each individual period. Configurations utilizing Mahrer/Pielke radiation at 35% soil moisture, Harrington radiation at 35% soil moisture, and Harrington radiation at 25% soil moisture are compared against RH, temperature, U-wind, V-wind, and wind direction sounding data taken from the Leon sounding site over the first 1500m AGL, through the time evolution of each IOP. Examination of synoptic scale features helps determine what role large scale forcing may have played in affecting fine grid output. Finally, model and central tower data are compared at 5m and 45m AGL. RH and Temperature are examined at 5m AGL, with RH, Temperature, U-wind, and V-wind compared at 45m AGL. Upon examination of the data, discrepancies between model configurations, and discrepancies between model and observations for each configuration are discussed.

4.1 Description of Model Configurations

Model configuration follows the general format described in chapter 3 with the exception of the manipulation of the soil moisture parameter, the choice of radiation scheme, and the size of grid 1. Forecasts through IOP #7 implemented a parent grid that excluded sections of the continental U.S. (CONUS). Excluded sections included the extreme western portion of northern California, the SE tip of Florida, and much of the east coastal region. Model runs starting with IOP #8 were modified to include the entire CONUS within the parent grid to allow for future movement of the fine grids to any location within the CONUS. The manipulation of parent grid size should have little if any impact on the Kansas study due to the large distance from the parent grid boundaries. Manipulation of radiation and soil moisture parameters were the focus of this study. The configuration used in the on-line real-time forecast setup implemented the Mahrer/Pielke scheme with 35% (MP-35) volumetric soil moisture as a continuation of the configuration used in the version 4a forecast model. Once the Harrington scheme became operational within version 4.29, that scheme was implemented in the on-line 4.29 model after completion of the CASES-99 project. Off-line runs were completed utilizing the Harrington scheme at 35% soil moisture (Har-35) with the identical model setup as that used on-line for all other parameters for the period of CASES-99 field project. Additionally, the soil moisture parameter was lowered to 25% (Har-25) volumetric soil moisture in one of the off-line runs in accordance with soil moisture observations taken at the Smileyberg location within CASES-99 field site. Thus, three model configurations were used in the forecast analysis: 1) Mahrer/Pielke radiation scheme at 35% soil moisture (MP-35); 2) Harrington radiation scheme at 35% soil moisture (Har-35); 3) Harrington radiation scheme at 25% soil moisture (Har-25).

4.2 Discussion of Forecasts for the Study Period.

Daily forecasts were completed through an automated process of data ingest, model execution, and post processing data presentation. Initial forecasts for the period were completed by manually starting the processes described above. Manual starts had to be done due to problems with the automation code discussed in chapter 3. Also, a minimal number of graphical forecast products were available due to the late implementation of parallel 4.29 on the PC cluster. Model runs became operational on September 27, 1999 with a combination of manual and automated runs, as the automation code was tested and became operational. Problems within the graphics package had to be resolved before a complete set of forecast products would be available to investigators. Over the first week of October 1999, most of the graphical problems were resolved allowing for a more complete set of model output, including cross-sectional plots bisecting the center of the grid-3 domain in longitudinal, and latitudinal directions. Sounding plots were also implemented at the center of grid 3. Input from the PI's of the CASES-99 project allowed for modification of model output products, as the project was ongoing. Additional cross-section and mapped products for wind components were added to assist project forecasters in analysis of desired meteorological features, such as direction and position of the low level jet.

Model instability presented a further obstacle to producing timely forecasts. On some forecast days, numerical instability caused the model to crash in the middle of a forecast run. Typically the cause of numerical instability came from the violation of the Courant-Friedrichs-Levy (CFL) stability criterion depending on atmospheric conditions. In order to alleviate the problem, more conservative time steps were chosen for model operation. Initially, the coarse grid time step was set to 90 seconds to allow for forecasts to be produced in the most efficient manner. Experimentation through the initial week of

forecasts displayed a coarse grid time step of 60 seconds as a consistently stable value. Forecasts could still be generated out to approximately 24 hours by the 2:00 PM mountain daylight time (MDT) deadline forecasters required the information, and the model proved to be much more reliable in completing forecast cycles without numerical instability problems. With a 60 second coarse grid time step, a 12z forecast cycle executed at 10:30AM MDT was typically complete by 5:00PM to 5:30PM MDT providing forecasters with information regarding the following day.

4.3 Examination of Model Performance Over IOP # 7

Background and Field Description of Event

IOP #7 occurred over the period from October 18, 00z to October 18 15z. The model data used for this forecast period was initialized at 12z on October 17. Field observational logs described some of the events observed through the IOP. A northerly flow was observed at the beginning of the IOP above the surface with speeds of about 5-7 m/s. The winds rotated throughout the evening, and were southeasterly by the morning hours. Winds at the surface remained essentially calm for the whole period. Lidar instrumentation observed a low level jet developing about 0230Z in the 200m to 300m layer. Turbulence below the jet was also observed by about 0330Z, when the jet reached a peak speed of about 10m/s. Kelvin-Helmholtz (KH) waves were also reported before 0400Z. The jet descended below 100m AGL at about the same time, with speeds decreasing slightly to about 9m/s. The jet direction rotated from northerly flow to east southeasterly flow during the night and stayed at east southeasterly in the morning hours until the end of the IOP.

Synoptic Scale Analysis

Synoptic conditions for the period were favorable for the development of stable boundary layer formation. Surface winds were light under a ridge of high pressure. A trough of low pressure was situated to the west of the study area from eastern Colorado, north through the Dakotas into southern Canada. Figure 4.1 displays the surface setup at 00z on October 18 in terms of surface observations and model forecast winds and model forecast sea level pressure at 75m AGL for each model configuration. A wind shift occurred near the region of the study area from the north/northeasterly flow in SE Kansas to south/southeasterly flow in NC Kansas as displayed on figure 4.1.a. Examination of all model configurations show that none of the configurations, with output displayed in 4.1.b – 4.1.d, tended to pick up the southeasterly flow displayed in the observations from NC Kansas to NE Minnesota. The positioning of the trough appears to be fairly consistent with the observations. Additionally, a closed region of high pressure appeared on all model analysis from SE Kansas to W Texas that did not appear in the analysis of the surface observations. As time progressed to 06Z, the trough dug and progressed to the east with winds observed to shift to a more south/southwesterly direction over NC Kansas (Fig. 4.2.a). A southeasterly flow continued to be observed from eastern Nebraska to NW Minnesota. All model configurations were fairly consistent with the observational analysis in the progression of the trough to the east (Fig. 4.2.b – 4.2.d). This progression placed a wind-shift boundary over the field study site by 06z, which may have affected model performance on the local scale depending on the timing of the wind shift. Additionally, the observed synoptic scale winds continued to be analyzed as south/southeasterly from NC Kansas to NW Minnesota, while model analysis showed a southerly flow from NC Kansas to NW Minnesota, which may have been a function of the difference in height between observational analysis and model analysis. Problems with synoptic scale wind direction

may also have impacted model performance in resolving the correct wind direction on the local scale. The closed high pressure from S. New Mexico to E Kansas displayed in model analysis appears to be fairly consistent with a similar feature seen in the observational analysis at 06Z with the center located over New Mexico. At both times of synoptic scale analysis, little difference can be detected between model configurations. Additionally, most large-scale features appear to be consistent between model and observational analysis at both times.

Leon Sounding Analysis

Model data vs. high resolution observed sounding data is analyzed from the central sounding site over six individual time periods on October 18: 00Z; 03Z; 05Z; 09Z; 13Z; and 19Z according to the availability of quality sounding data. This approach is taken to compare the evolution of the model predicted boundary layer structure to observed evolution of boundary layer structure. Atmospheric variables including RH (%), temperature (C), U-wind (m/s), V-wind (m/s), and wind direction (degrees) are the focus of the analysis.

Examination of the results shows little difference between model configuration in the evolution and structure of predicted wind fields, with some consistent differences displayed in the temperature and relative humidity fields. Figure 4.3 displays the evolution of model and observed relative humidity from the surface to 1500m AGL. Over the IOP #7 forecast period, the Har-25 simulation had the lowest relative humidity values, with Har-35 generally 10% RH greater than Har-25 through 700 to 1000m AGL. Above that height, all runs tended to converge to similar values, indicating the height where the increased soil moisture contribution to atmospheric humidity may have lost its influence in this case. Below the 700 to 1000m AGL level, the MP-35 and Har-35 were consistently 5% to 10% RH higher than Har-25 values. A comparison between model

predicted RH and observed atmospheric RH shows no great preference between model runs. At 05Z, the greatest preference is seen with Har-35 and MP-35 more closely mimicking the observed values through the lowest 800m AGL. All configurations tended to dry out well below the observed drying height, with the difference increasing with time. The drop in RH was consistent with the observed drop at 00Z, but after that time, the height of the model drop in RH decreased to about 600m below the observed RH drop by 13Z. By 19Z, after daytime heating had commenced, the difference jumps to about 1000m. The observed differences in RH drop were most likely due to the fact that the model inversion tended to develop at a lower height than what was observed, as can be seen in figure 4.4.

When figure 4.3 and 4.4 are compared, it can readily be seen that the drop in observed RH coincides with the start of the inversion level. For example in 4.4.c, the observed inversion starts at approximately 1225m AGL, coinciding with the height of the observed drop in RH values displayed in 4.3.c. Similar comparisons of model data show corresponding trends. In figure 4.4.a, model and observed inversion height correspond fairly well as do the drop in RH values at a height of 1225m AGL. At 09Z (Fig. 4.4.d), the model inversion develops at about 900m AGL while the observed inversion starts at about 1225m AGL. Once again, the inversion heights correspond well with the heights of drop in RH seen in figure 4.3.d. From these results, it appears that all model configurations tend to evolve an inversion level at too low of a height through the course of the night.

Examination between model runs of temperature forecasts shows MP-35 produced the highest temperature values of all configurations. MP-35 values are generally 1 to 2 degrees C greater than values produced in the Har-35 run, especially below inversion height. Temperature values produced in the Har-25 run generally fall between Har-35 and MP-35 values. Once again, no configuration is preferential through the complete

forecast period when compared with observed temperature values. At 00Z and 03Z (Fig. 4.4.a and 4.4.b), Har-25 and MP-35 more closely replicate the observed temperature structure below the inversion level. In the remaining forecast times, up to 13Z, Har-35 does the best job of predicting the temperature values over the first 200 to 300m AGL with no preference between runs above that height. By 19Z, no configuration does a very good job at predicting the observed temperature structure. As discussed above, the inversion heights are consistently too low for all runs.

Examination of U, V-wind, and wind direction profiles (Fig. 4.5, 4.6, and 4.7) shows no large differences in the structural evolution of the wind between model configurations. Additionally, no preference can be found between model configurations when comparing model predicted winds to observed winds. Figure 4.5 displays the model and observed evolution of the U-wind field through the forecast period. The structural pattern of model and observed wind correspond best starting at 05Z through the rest of the forecast period. A lack of sounding data at times other than 05Z prevents comparison over the first 100m AGL. At 05Z, the structure of a 5m/s easterly maximum wind speed, observed at 100m AGL, was captured by the model although the magnitude was off by 3 m/s. The same model feature was displayed at 80 to 100m AGL from 03Z to 13Z. This model feature appears to correspond with the easterly component (Fig. 4.7b - e) of a low level jet that was reported by surface field observers with speeds up to 10m/s at an altitude of 80 to 100m AGL. At 09Z, the model captured the observed easterly to westerly directional wind shear with height from 300m AGL to 1100m AGL (Fig. 4.7.d). By 19Z, model and observed winds were both westerly and of similar magnitude.

Examination of V-wind evolution (Fig. 4.6) shows model structure and magnitude fairly close to observed values from 03Z to 13Z. A transition from northerly to southerly winds can be seen from 05Z to 09Z in the lowest 200m AGL. This corresponds with the available observations displayed in figure 4.7.c and 4.7.d, along with field log reports of a

low-level jet transitioning from northerly flow to east/southeasterly flow through the night. It appears that the model was able to resolve the low-level jet position, and transition from northerly to southeasterly flow in this case. The primary deficiency in the model guidance was in the wind magnitude.

Central Site Tower Analysis

The purpose of the tower data analysis is to compare model and observations at a fixed site with fixed heights near the surface. The location of the tower site, near the Leon sounding release point allows for addition of low level data that was not captured through the sounding process. Also, a complete time series evolution through the forecast period is examined due to the frequency of observations taken at the tower site. Model and observed atmospheric variables including RH (%), temperature (C), U-wind (m/s), and V-mind (m/s) are compared at 45m AGL. At 5m AGL, model and observed RH (%) and temperature (C) are compared.

The 45m AGL analysis displays very little difference between model configurations in U-wind (Fig. 4.7.c) and V-wind values (Fig. 4.8.d) through the time evolution of the IOP #7 forecast period. MP-35 displays a warm bias in the temperature plot (Fig. 4.8.b), approximate 2 degrees C greater than Har-35 throughout the forecast period with Har-25 temperatures falling in between the other configurations. RH results in figure 4.8.a show that the Har-25 configuration consistently produced RH values 10% RH less than the values produced with the Har-35 configuration. RH values produced with the MP-35 configuration generally split the difference between the values produced by the other two configurations.

Comparison of model and observational data once again shows no distinct preference between configurations with respect to predicting closer to observed values of U and V-wind. Over the hours from 00Z to 15Z the Har-35 configuration appears to fit

closer to observations than the other two configurations with respect to temperature and RH. All model configurations approximately followed observed patterns displayed through time evolution of RH and temperature from 00Z to 15Z. A problem occurred during the transition from a stable nocturnal environment to one with daytime heating. Temperatures lagged below observed values after 15Z by up to 5 C, while RH values were slightly greater than observed. Model U-wind component was the same direction as observed easterlies from 10Z to 13Z, but as in the sounding comparisons, the magnitude was up to 6 m/s below observed values. The pattern of model U-wind evolution generally followed observations other than magnitude problems, and a 2-hour lag behind the observed transition to a westerly U-wind component. The transition and possibly magnitude problem may have been due to wind direction discrepancies between model and observed winds discussed in the synoptic scale features of the model output. The model V-wind component followed observed patterns and magnitudes better than the U-wind component at 45m AGL. In the case of V-wind, the transition from northerly to southerly flow lagged about one-hour behind the observed transition. From 00Z to 14Z, the V-wind magnitude stayed within 2m/s of the observed magnitude. After 14Z the magnitude became about 5m/s too strong.

Comparison between configurations at 5m AGL display similar biases to those displayed at 45m AGL. Har-35 produced RH values 10% RH greater than Har-25 values with MP-35 values falling in between (Fig 4.9.a). In temperature, MP-35 produced the warmest values, approximately 2 C warmer than Har-35 at times, with Har-25 temperatures values falling in between (Fig 4.9.b). An exception to the biases in both temperature and RH is seen around the initiation of daytime heating at 13Z. At that time, the values of all configurations virtually coincide before diverging back to their biases as daytime heating progresses.

Comparison between model and observed values at 5m AGL show a 2 to 5 degree C warm bias in model temperature above observed values from 00Z to 14Z, with a corresponding low RH bias 10% to 20% RH over the same period. As in the 45m data, model temperatures lagged behind observations in the transition from night to day from 13Z to 20Z. The observed warming of the atmosphere begins at 13Z, while the modeled warming does not commence until 16Z. A moist bias in RH values corresponds with the lag in temperature transition. Observed RH values begin dropping at 13Z, while model RH doesn't start dropping until about 16Z.

4.4 Examination of Model Performance Over IOP # 9

Background and Field Description of Event

IOP #9 occurred over the period from October 21, 00z to October 21 15z. The model data used for this forecast period was initialized at 12z on October 20. Field observational logs described some of the events observed through the IOP. Weather in the region was defined by high-pressure conditions over the CASES-99 main site but a hard-to-define geostrophic pressure gradient. IOP #9 was characterized by notable directional shear with height throughout the night. Winds at the surface were from the S to SSW, turning nearly straight west by 500m AGL. The winds in the low level jet were from the S and SW at up to 15 m/s, but generally were 10-12 m/s after about 04Z. The increase in jet speed with time corresponded to nearly continuous, but weak turbulence developing at the surface. Until 07Z the low level jet developed strong shear both above and below the jet resulting in turbulence above the jet. Sometime after midnight the jet nearly disappeared over the site, apparently being mixed out. The jet was re-established by 10Z and turbulence began again both above and below the jet, with some pockets of moderate turbulence at altitudes up to 900m. AGL.

Synoptic Scale Analysis

With high pressure in the region, synoptic conditions for the period were favorable for the development of stable boundary layer formation. Surface winds were light and from the south. Figure 4.10 displays the surface setup at 02Z on October 21 in terms of surface observations, model forecast winds and model forecast sea level pressure at 75m AGL for each model configuration. A surface trough of low pressure extended from central Manitoba southward through western Minnesota, eastern Nebraska, and diagonally from NC to SW Kansas (Fig. 4.10.a). The trough was a weak feature through Kansas mainly defined by a wind shift from south/southwesterly flow in eastern Kansas to westerly flow in western Kansas. Examination of model configurations shows that all of the configurations, with output displayed in 4.10.b – 4.10.d, produced a wind shift from south/southwesterly flow in eastern Kansas to westerly flow in western Kansas. The sea level pressure contours appear to be consistent between all model configurations with the trough located from central Manitoba through the eastern Dakotas. The model trough positioning is fairly consistent with the observations. The main difference between model and observational analysis would be that the model predicted trough flattens out by northern Nebraska while the observed trough extends to southern Nebraska. Additionally, observed SE winds across Missouri and Iowa are depicted as southerly in the model analysis. The wind direction problem once again may be due to the height of the model analysis, 75m AGL. The model high-pressure center located over south-central Texas appears consistent with observations in the 1025mb range. By 09Z, the observed trough and wind shift had progressed slowly to the east, positioned from eastern Manitoba through central Minnesota, extending to SE Nebraska, and diagonally from NE to SC Kansas (Fig. 4.11.a). All model configurations were once again similar in their synoptic progression (Fig. 4.11.b – d). Model trough positioning

appears to be slightly west of the observed trough running from eastern Manitoba through western Minnesota to SE Nebraska. The model analysis shows the trough base progressing south from central South Dakota to the SE Nebraska/Kansas border from 02Z to 09Z. High pressure in both model and observations is still centered over south central Texas. The model positioning of the wind shift through east central Kansas appears to agree with the wind shift displayed in the surface observations.

Leon Sounding Analysis

Model data vs. high resolution observed sounding data is analyzed from the central sounding site over four individual time periods including October 20, 23Z and October 21: 03Z; 07Z; and 12Z. As in the IOP #7 sounding analysis, atmospheric variables including RH (%), temperature (C), U-wind (m/s), V-wind (m/s), and wind direction (degrees) are the focus of the analysis.

Similar to IOP #7, examination of the results shows little difference between model configurations in the evolution and structure of predicted wind fields, with some consistent model predicted RH and temperature biases displayed in the layer below the model predicted inversion. Har-35 tended to produce the most cool, moist atmosphere of the model configurations below predicted inversion level. Figure 4.12 displays the time evolution of model and observed RH fields through the lowest 1500m AGL. Har-35 tended to produce the highest RH values from the surface to the inversion height at 800m AGL from 10/20 23Z to 10/21 07Z. Over the same period Har-25 produced RH values 10% RH less than Har-35, with MP-35 values splitting the difference. Above the inversion level, the predicted fields of all configurations become similar, as the surface influence decreases. By 10/21 12Z, the model inversion had subsided, so the trends described below inversion level at previous times extend to the top of the analysis. A comparison between model and observed values shows no preference between model

configurations in predicting closer to observed values. All configurations tended to be too moist below the inversion level, and too dry above the inversion level, which never existed in the observations. Figures 4.12.b and 4.12.c also display a tendency for the model to be too low in RH near the surface, associated with a warm bias seen near the surface in figure 4.13. By 10/21 12Z, all model configurations line up well with the observations as the model inversion had subsided.

Temperature fields, displayed in figure 4.13, reinforce some of the biases and features displayed in the RH fields. Har-35 produced the coolest temperatures below the inversion, while MP-35 produced temperatures 1 to 2 degrees C warmer through the same level. Har-25 produced similar temperature profiles as those produced by MP-35. As with the RH examination, no configuration excels above the other at producing results in close agreement with observed values. A temperature inversion 800m AGL was produced by all model configurations from 10/20 23Z to 10/21 07Z (Fig. 4.13.a – 4.13.c) that was not displayed in the observations. At 10/20 23Z (Fig. 4.13.a), before a distinct near-surface inversion was apparent, all model configurations produced temperatures 2 to 3 degrees cooler than observed. Once the near-surface inversion had developed, all model configurations produced temperatures warmer than observed near the surface, and cooler than observed above the surface inversion (Fig 4.13.b and 4.13.c). By 12z (Fig. 4.13.d), model output most closely resembled the observational profile with a strong 10 to 11 C near-surface inversion.

Consistent with the trend observed in IOP #7, examination of U, V-wind, and wind direction profiles (Fig. 4.14, 4.15, and 4.16) shows no large differences in the structural evolution of the wind profile between model configurations. Also, once again no preference can be found between model configurations in predicting the observed wind profile. Analysis of the U-wind profile time evolution shows that the model had the U-component in the correct direction (Fig. 4.16), with magnitude problems. Observed and

modeled winds were consistently westerly, with the modeled westerly component of a low level jet apparent by 10/21 12Z (Fig. 4.14.d and 4.16.d). A lack of measurements over the first 100m AGL prevents a detailed comparison between model and observations through that level. In terms of magnitude, the model was not consistently too strong or weak, with the greatest difference displayed at 4 m/s below observations at 10/20 23Z (Fig. 4.14.a), and 10/21 07Z (Fig. 4.14.c).

Examination of V-wind component and direction evolution (Fig. 4.15 and 4.16) shows that the model captured the observed pattern of directional shear with height. At 10/20 23Z (Fig.4.16.a) directional shear is displayed in the model field that doesn't exist in the observations at about 800m AGL. This abrupt directional shear from southwesterly to north/northwesterly winds may have contributed to the fictitious temperature inversion displayed at similar levels (Fig 4.13.a). From 10/21 03Z through the rest of the forecast period, model and observed wind profiles became more consistent, and the directional shear becomes less abrupt at 800m AGL (Fig. 4.15.b – 4.15.d and 4.16.b - 4.16.d). Correspondingly, the fictitious inversion washes out over the same period (Fig. 4.13.b - 4.13.d.). Consistent with field log reports, the model predicted low-level jet initially appeared around 03Z and strengthened through the night and morning hours to 12Z. Strong shear developed above and below the jet by 07Z, and persisted through 12Z. Field reports described strong shear above and below the jet consistent with model predictions. As was displayed in the plots of U-wind component, differences between predicted and observed magnitude existed.

Central Site Tower Analysis

Examination of the central tower data provides a complete time series evolution of atmospheric variables at fixed heights of 45m and 5m through the entire IOP, filling in low-level data that could not be resolved in the soundings. Model and observed

atmospheric variables including RH (%) and temperature (C) are compared at 45m and 5m. U and V-wind (m/s) components are added to the comparison at 45m due to additional instrumentation at that height.

Comparison between model configurations of RH and temperature at 45m AGL shows that Har-35 produced the most cool, moist atmosphere of the three configurations (Fig. 4.17.a and b) through the nocturnal hours from 00Z to 13Z. Har-25 produced the driest RH values with temperatures nearly the same as those produced by the MP-35 configuration. When the transition to daytime heating occurred, all three configurations converged to similar temperatures before warming with the same temperature biases that were seen during nocturnal hours. No distinct biases between configurations are displayed in the time evolution of the U and V-wind components (Fig. 4.17.c and d), except for a short aberration in the MP-35 U-wind component from the other two configurations from 15Z to 18Z.

Comparison between model and observational data shows no configuration bias in predicting wind fields. Har-35 appears to fit closest in magnitude to RH and temperature observations through the nocturnal hours from 00Z to 13Z. All model configurations followed the observed pattern through the nocturnal hours, with the previously discussed 2 to 3 hour lag in conversion from nighttime to daytime conditions occurring after 13Z. Analysis of U-wind comparison shows that the model produced a westerly component through the forecast period consistent with observations. The wind magnitude stayed within 2 to 3 m/s of observations through the nocturnal hours from 00Z to 12Z before diverging from observations at 15Z by 7 m/s. As in IOP #7, the modeled V-wind component was somewhat more consistent with observations than the modeled U-wind component. From 00Z to 16Z, the modeled wind direction followed the observed southerly pattern well with a positive difference in magnitude of about 2 m/s. After 16Z,

the modeled wind field turned to a northerly component, while observed winds remained light and southerly.

Analysis of temperature and RH values at 5m AGL (Fig. 4.18.a and b) displays model biases consistent with those displayed at 45m AGL. Har-35 produced the most cool, moist results through the entire forecast period, while Har-25 produced the lowest values of RH. MP-35 produced temperatures slightly warmer than Har-25, and RH values in between Har-25 and Har-35 through the forecast period.

Comparison between model and observed values at 5m AGL shows Har-35 to fit closest with observed temperature values through the nocturnal period from 00Z to 13Z. A warm temperature bias of 2 to 5 degrees C occurred for all configurations over the same period. Analysis of RH shows Har-35 to fit closest with observed values from 00Z to 10Z, with MP-35 closest from 10Z to 13Z. As at 45m, a 2 to 3 hour lag in conversion from nighttime to daytime conditions can be seen in both the RH and temperature fields.

4.5 Summary of IOP #7 and #9 Forecast Analysis

From the discussions of forecasts for two intensive operational periods in this chapter, it was shown how RAMS performed under various model configurations as a near surface high resolution forecasting tool on specific dates of a field project. Synoptic scale guidance displayed consistency between all model configurations in predicting the observed synoptic scale structure at various times. The main problem was with prediction of wind direction ahead of troughs approaching the Midwest. Observed winds tended to be southeasterly, while model winds were southerly. Model-predicted regions of high and low pressure spatially agreed with observations well. Comparison between model and observed sounding data showed a tendency of all model configurations to produce temperature inversions at heights lower than observed, or fictitious inversions

that never existed within the observations, which may have been associated with fictitious directional wind shear at similar heights, as displayed in IOP# 9. Below predicted inversion levels, model and observed values agreed fairly well in structural appearance. Within the sub-inversion air mass Har-35 consistently produced an atmospheric layer that had the lowest temperature and highest RH of all configurations. Har-25 consistently produced the lowest values of RH with temperatures near or slightly cooler than temperatures produced by MP-35. All configurations were similar to one another in predicting the profile of temperature and RH with height, with no preferential configuration in predicting closer to observed profiles. Additionally, no preference was displayed between model configurations in predicting the structure of the wind profile. All configurations did a decent job in predicting the observed direction of wind components, but had some problems with magnitude. The model configurations resolved the formation and development of low level jets near the surface, and indicated the presence of high-resolution wind features, such as the vertical shear observed in IOP #9, which indicated to forecasters that turbulence might develop. Analysis of tower data showed a preference to Har-35 in predicting the observed temperature and RH profiles through the nocturnal hours from 00Z to 13Z. As was displayed in the sounding data comparison, Har-35 consistently produced the coolest and correspondingly moistest near-surface atmosphere. Also consistent with the vertical profile comparison, no preferential model configuration was displayed in predicting closer to observed wind fields, while modeled U and V-wind components resolved the correct wind direction, with discrepancies in magnitude.

Upon consultation with Dr. Robert Walko, it was found that the transitional lag from nocturnal to daytime heating conditions, displayed in model temperature and RH values, was due to conservative settings in the version 4.29 LEAF-2 surface model. He provided two primary causes for the lag as deduced in his own operational runs

including, soil thermal conductivity values that were too low causing the surface to cool too much at night and then warm up more time before it could start warming the air, and too much heat capacity of canopy air and vegetation, both of which were made artificially large for computational stability and efficiency. These issues were addressed with code changes that became available in version 4.3, which will soon be implemented as the real-time forecast model. Even with the LEAF-2 problem, all model configurations demonstrated a useful effectiveness as forecasting tool for these specific days, with Har-35 producing slightly better results near the surface.

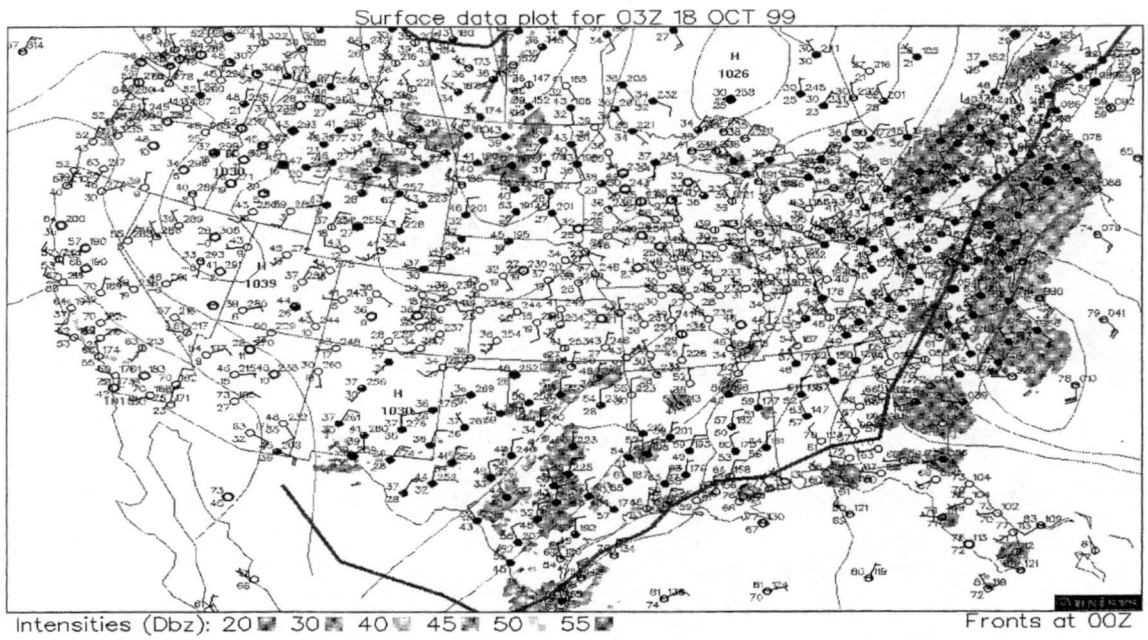

4.1.a.

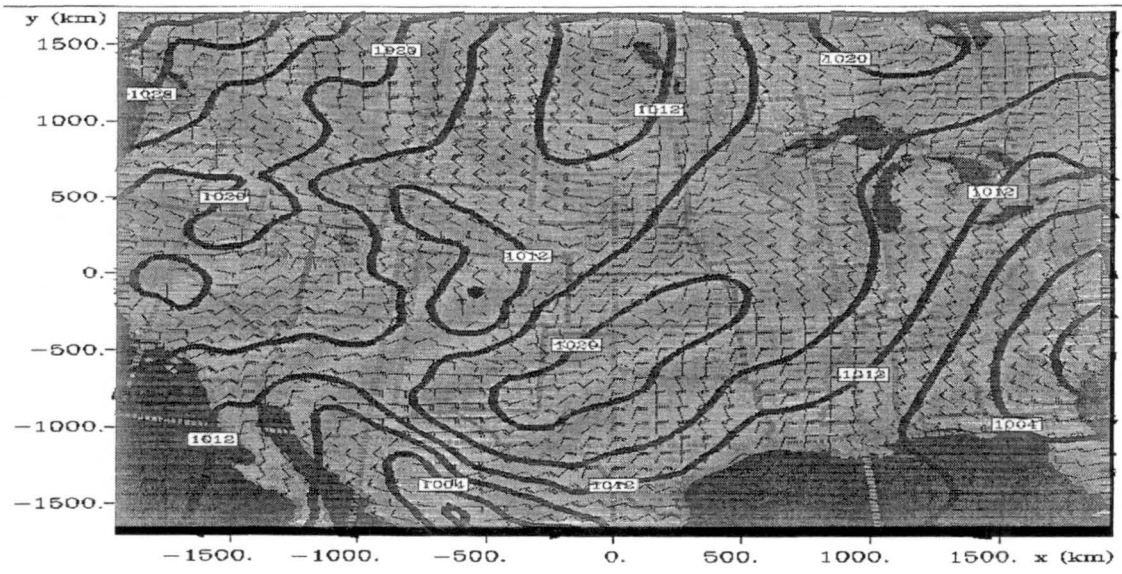

sea level pressure (mb)
min=996.5 max=1034 inc=4
Grid 1 z = 75.0 m IOP7
Valid 10/18/99 0300 UTC

4.1.b.

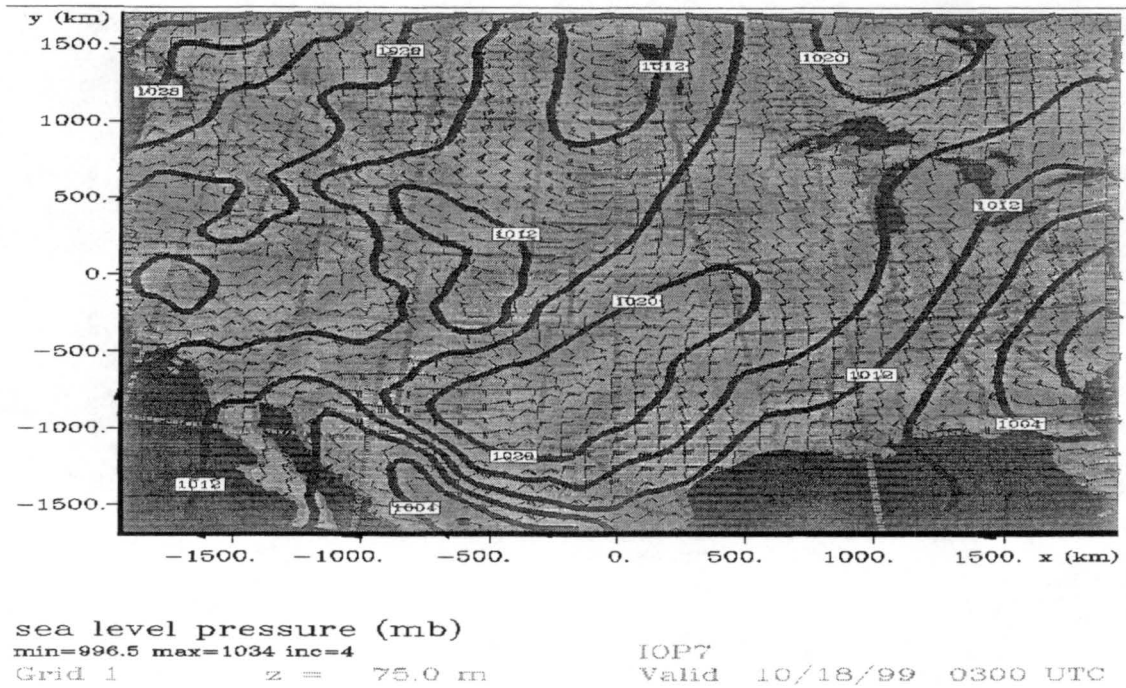

4.1.c.

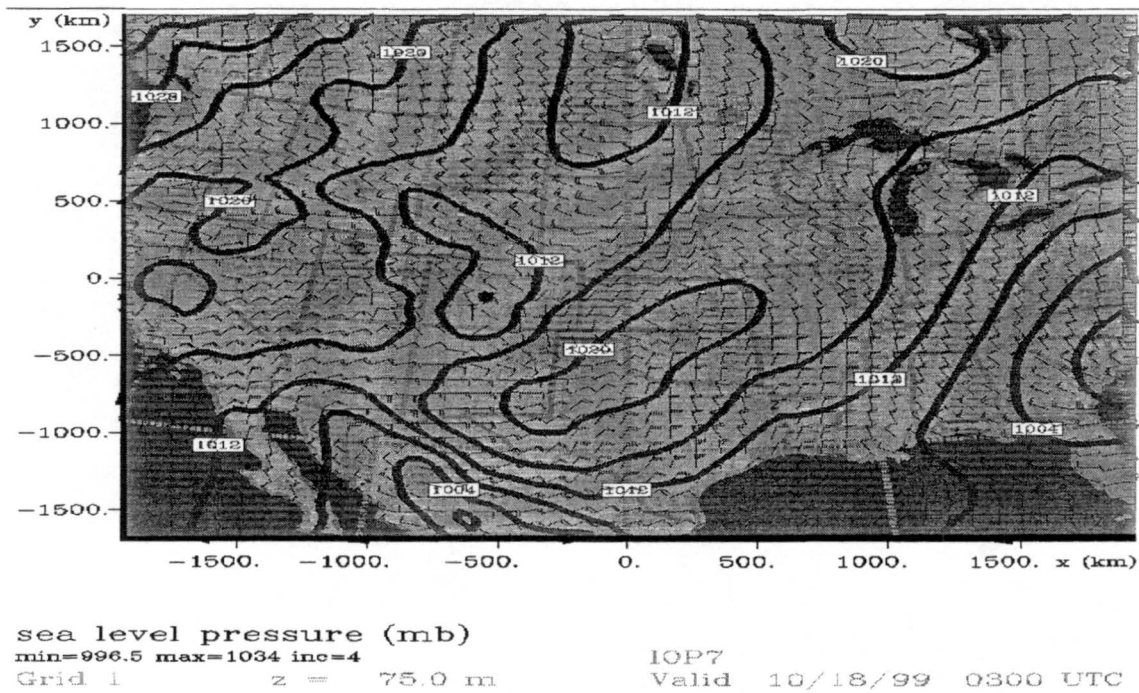

4.1.d.

Figure 4.1 – IOP #7 (10/18/1999) sea level pressure at 03Z: a) observed; b) Harrington-35% model; c) Harrington-25% model; and d) Mahrer/Pielke-35% model.

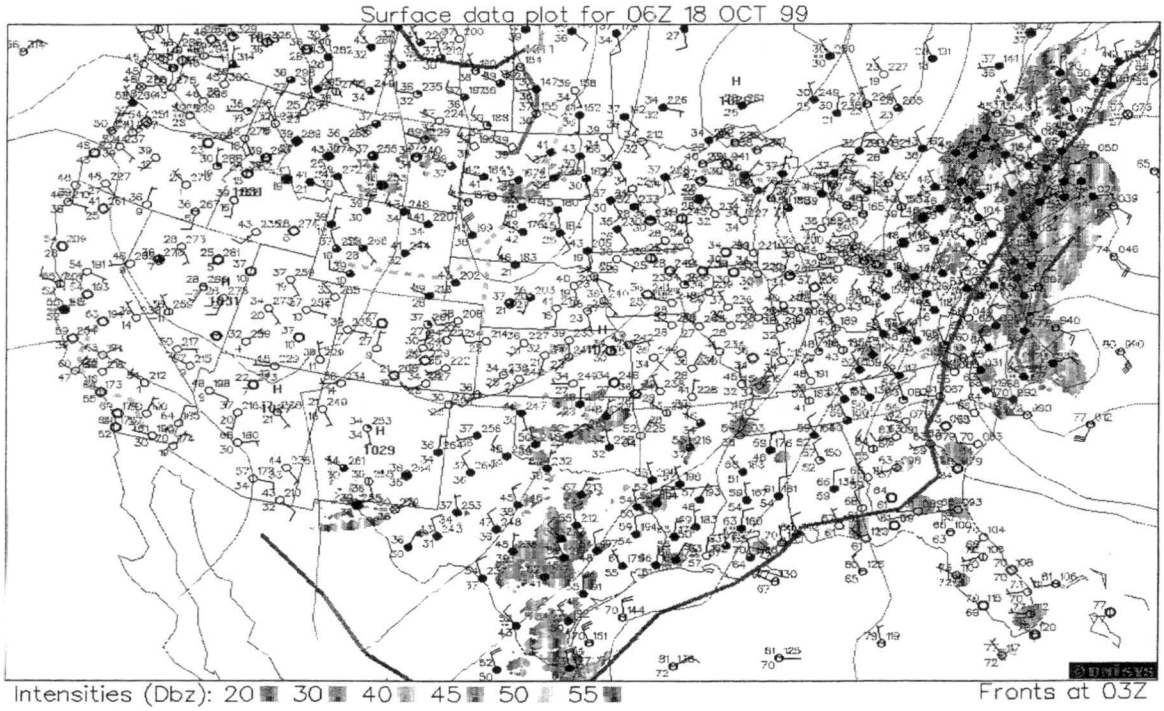
Surface data plot for 06Z 18 OCT 99
Intensities (Dbz): 20 30 40 45 50 55
Fronts at 03Z

4.2.a.

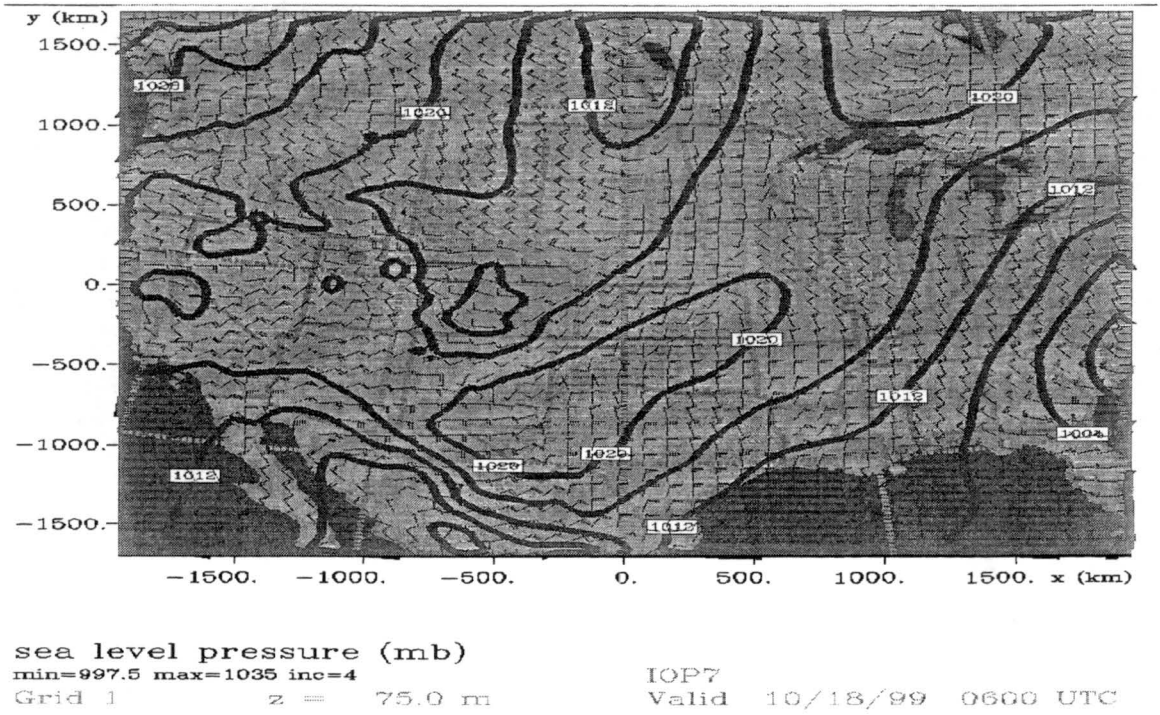
y (km)
1500.
1000.
500.
0.
-500.
-1000.
-1500.
1032
1020
1016
1020
1012
1020
1012
1024
1028
1028
1012
1012
-1500.
-1000.
-500.
0.
500.
1000.
1500. x (km)
sea level pressure (mb)
min=997.5 max=1035 inc=4
Grid 1 z = 75.0 m
IOP7
Valid 10/18/99 0600 UTC

4.2.b.

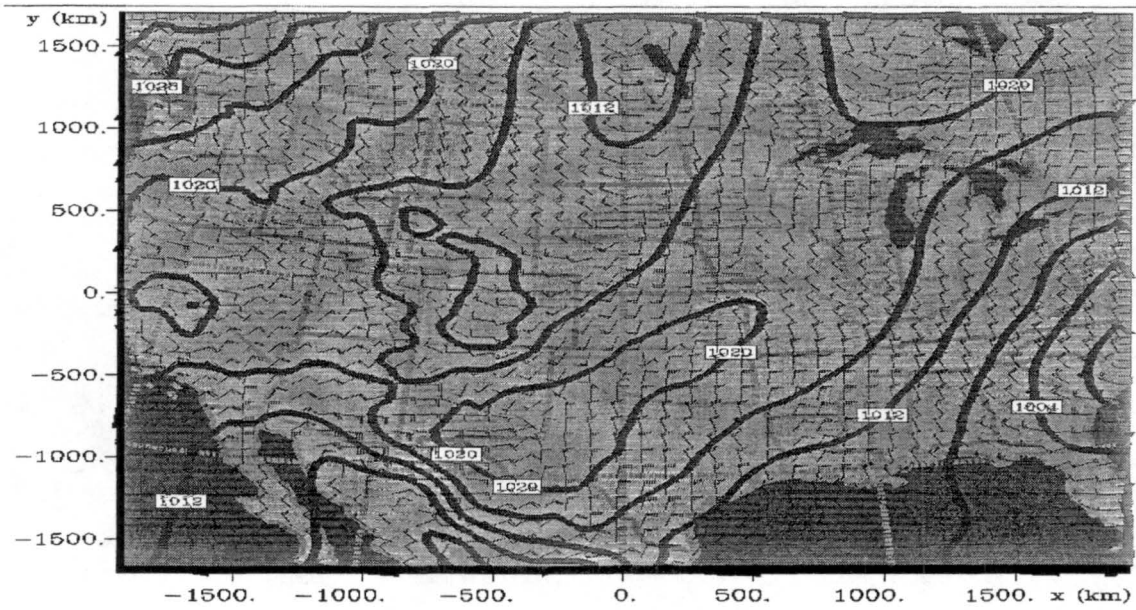

sea level pressure (mb)
min=997.5 max=1035 inc=4
Grid 1 z = 75.0 m
IOP7
Valid 10/18/99 0600 UTC

4.2.c.

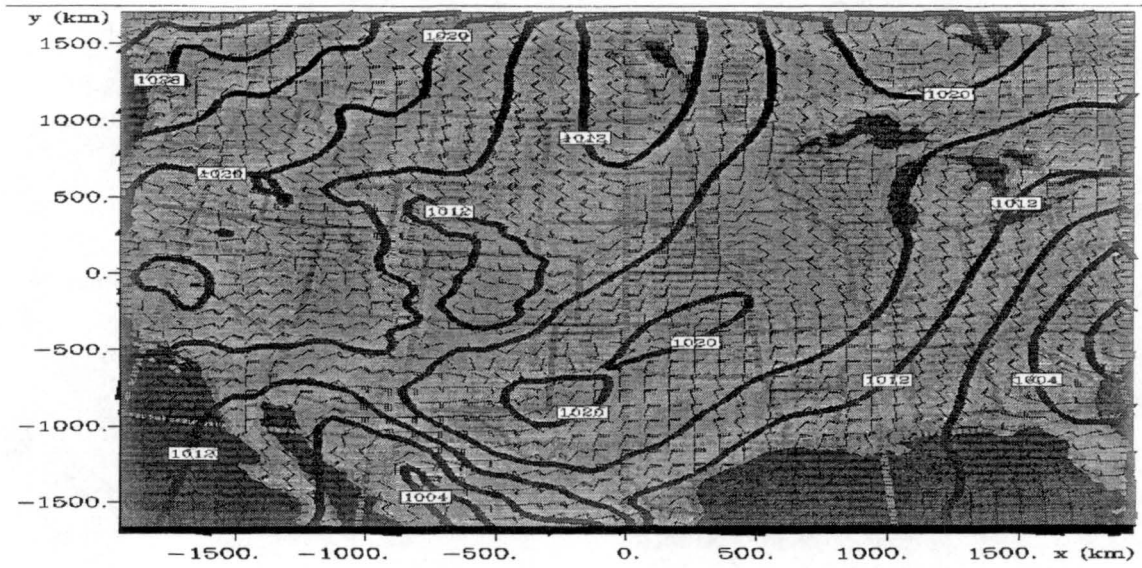

sea level pressure (mb)
min=997.5 max=1035 inc=4
Grid 1 z = 75.0 m
IOP7
Valid 10/18/99 0600 UTC

4.2.d.

Figure 4.2 – IOP #7 (10/18/1999) sea level pressure at 06Z: a) observed; b) Harrington-35% model; c) Harrington-25% model; and d) Mahrer/Pielke-35% model.

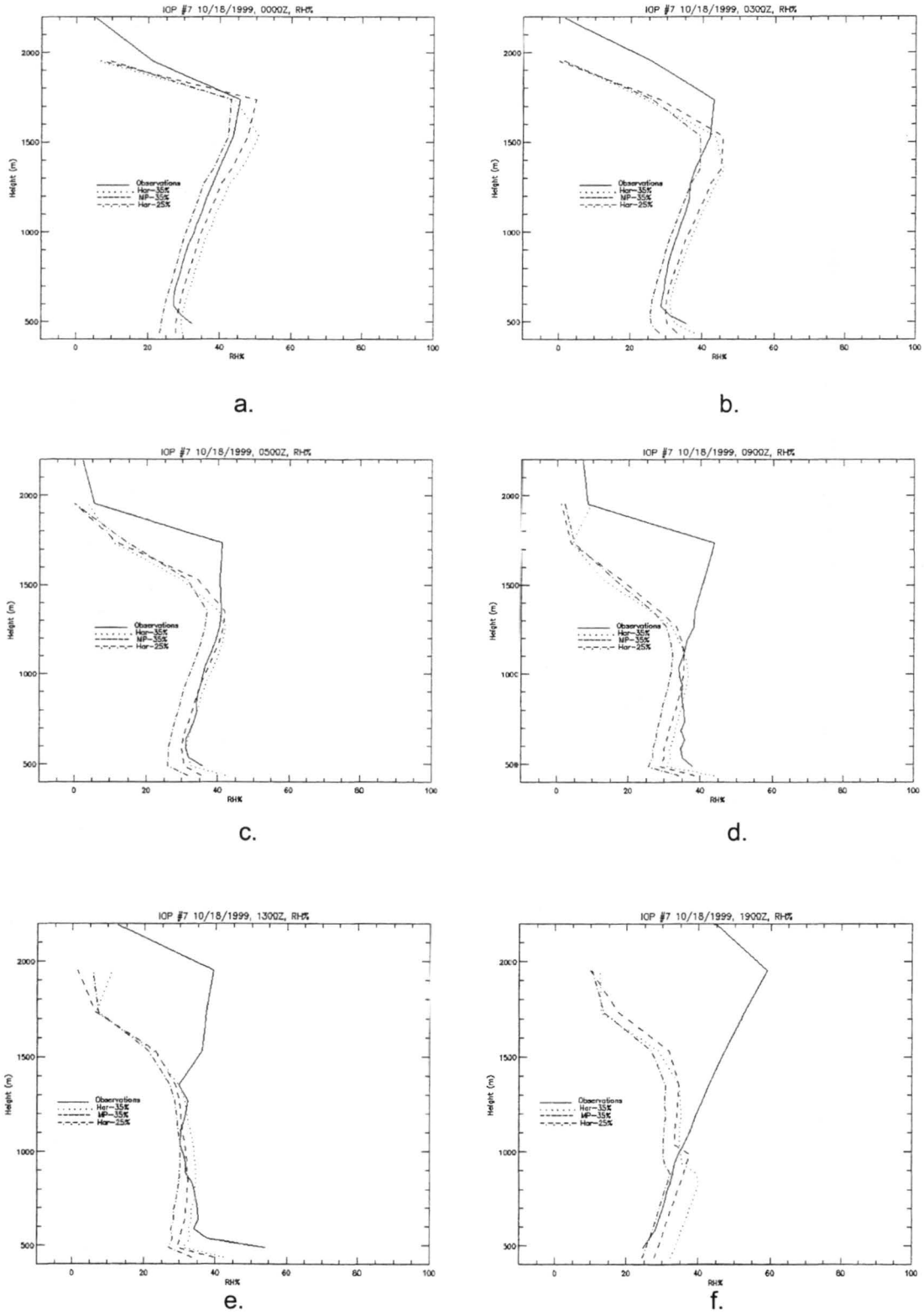

Figure 4.3 - IOP #7 (10/18/1999) relative humidity (%) profile at Leon, KA: a) 00Z; b) 03Z; c) 05Z; d) 09Z; e) 13Z; and f) 19Z. Legend: (.... Har-35, -.-.-.- Har-25, - - - - MP-35)

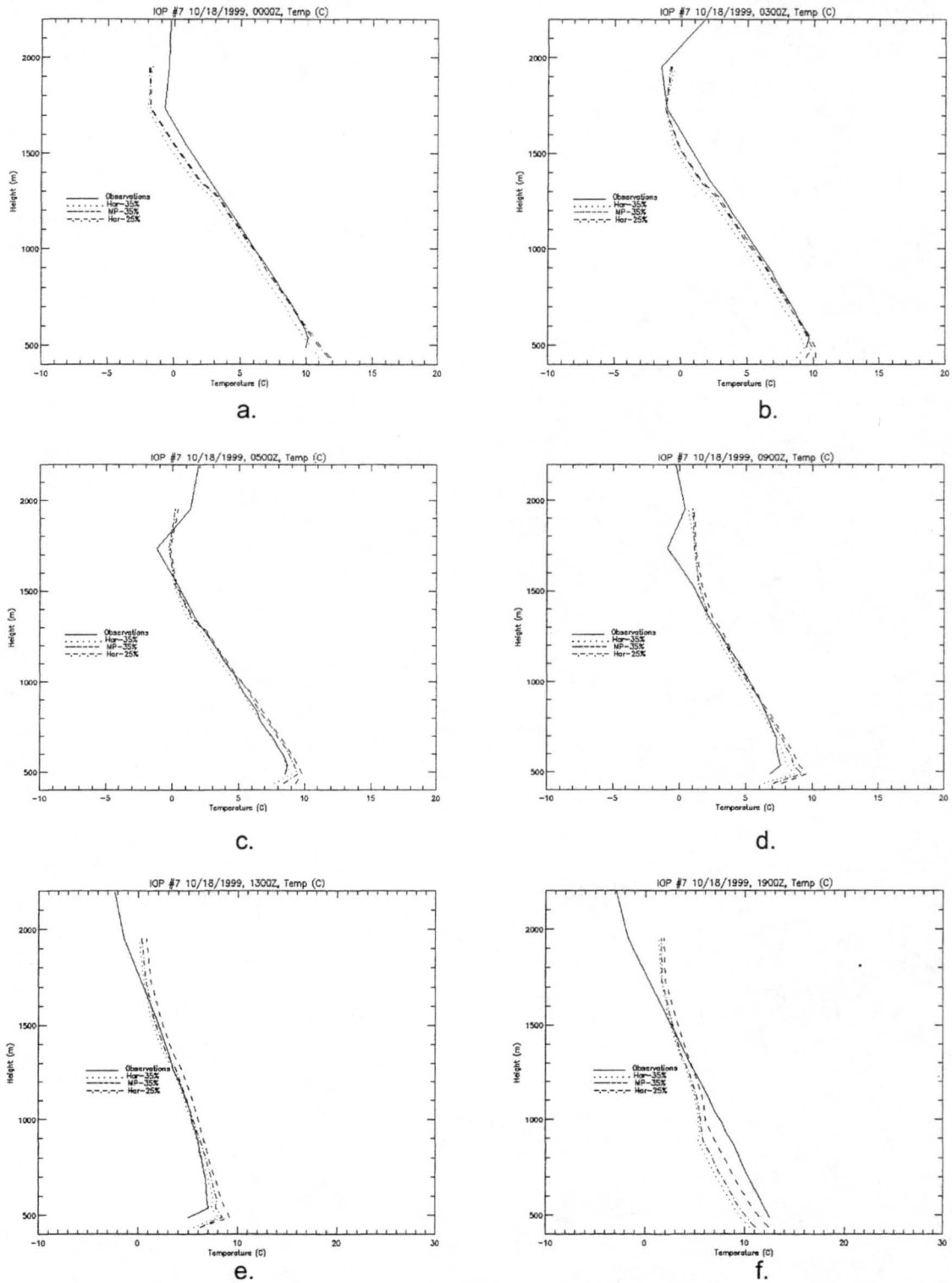

Figure 4.4 – IOP #7(10/18/1999) temperature (C) profile at Leon, KA: a) 00Z; b) 03Z; c) 05Z; d) 09Z; e) 13Z; and f) 19Z. Legend: (.... Har-35, -.-.-.- Har-25, - - - - MP-35)

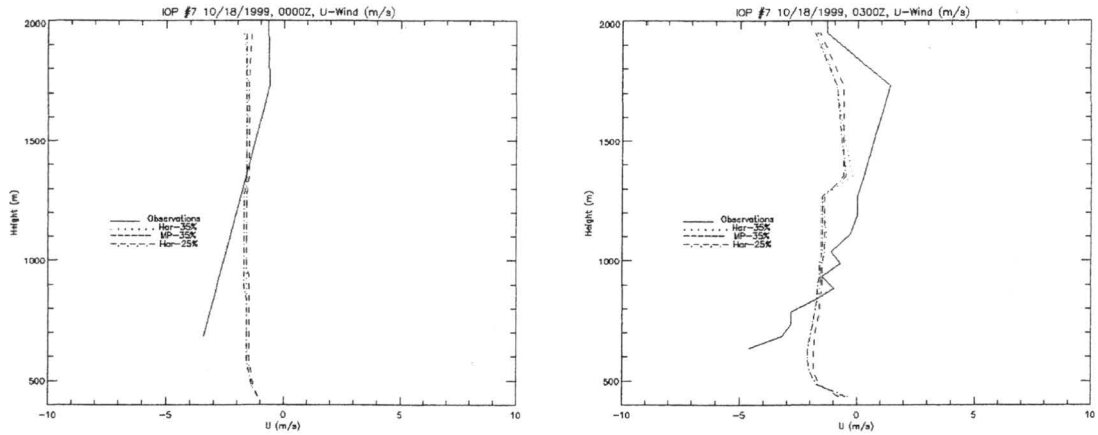

a.

b.

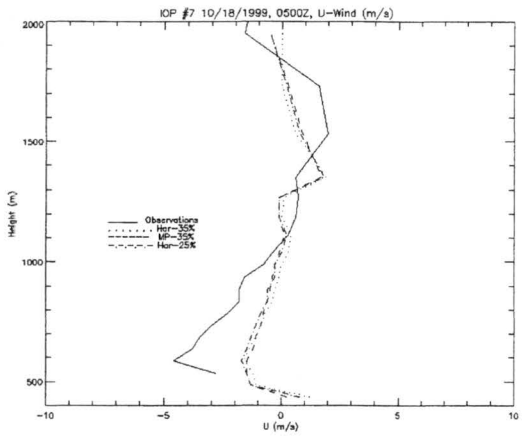

c.

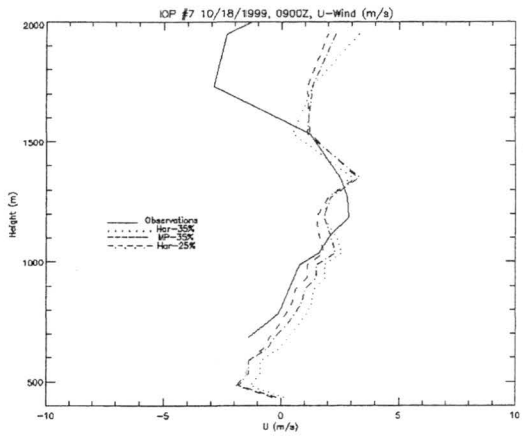

d.

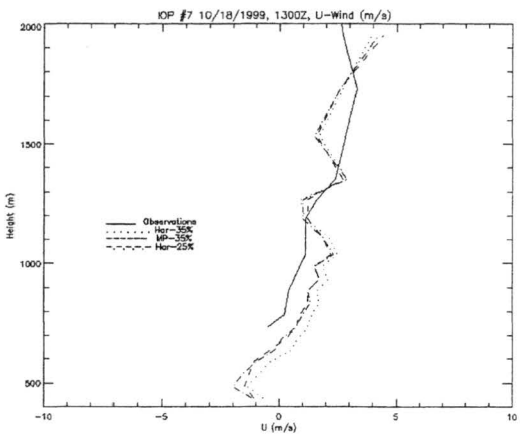

e.

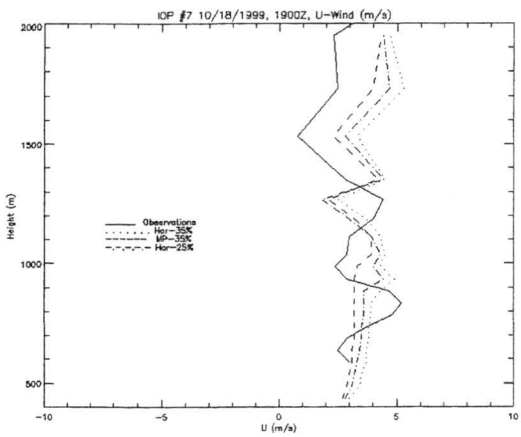

f.

Figure 4.5 – IOP #7 (10/18/1999) U-wind speed (m/s) profile at Leon, KA: a) 00Z; b) 03Z; c) 05Z; d) 09Z; e) 13Z; and f) 19Z. Legend: (.... Har-35, -.-.-.- Har-25, - - - - MP-35)

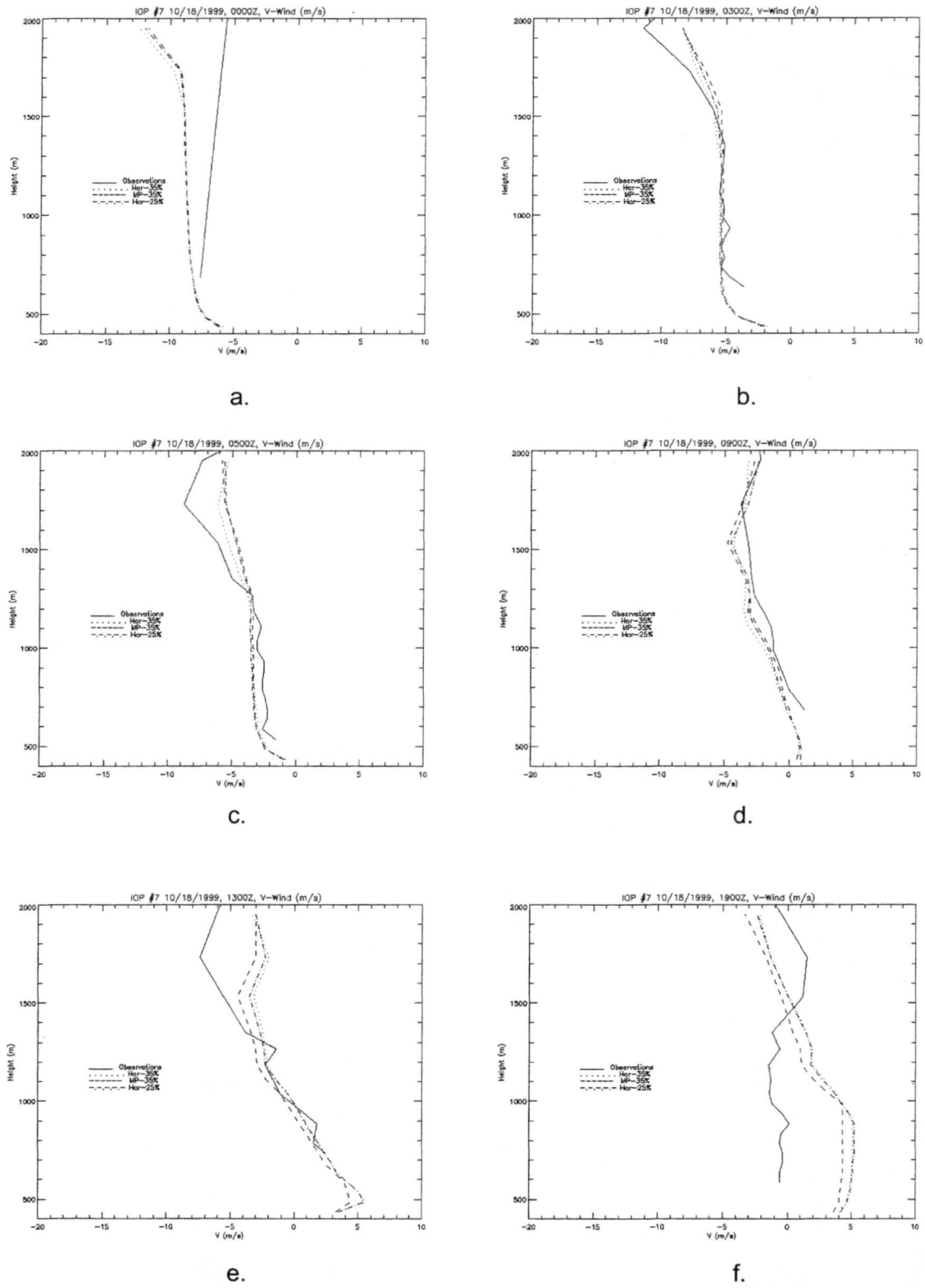

Figure 4.6 – IOP #7 (10/18/1999) V-wind speed (m/s) profile at Leon, KA: a) 00Z; b) 03Z; c) 05Z; d) 09Z; e) 13Z; and f) 19Z. Legend: (.... Har-35, -.-.-.- Har-25, - - - - MP-35)

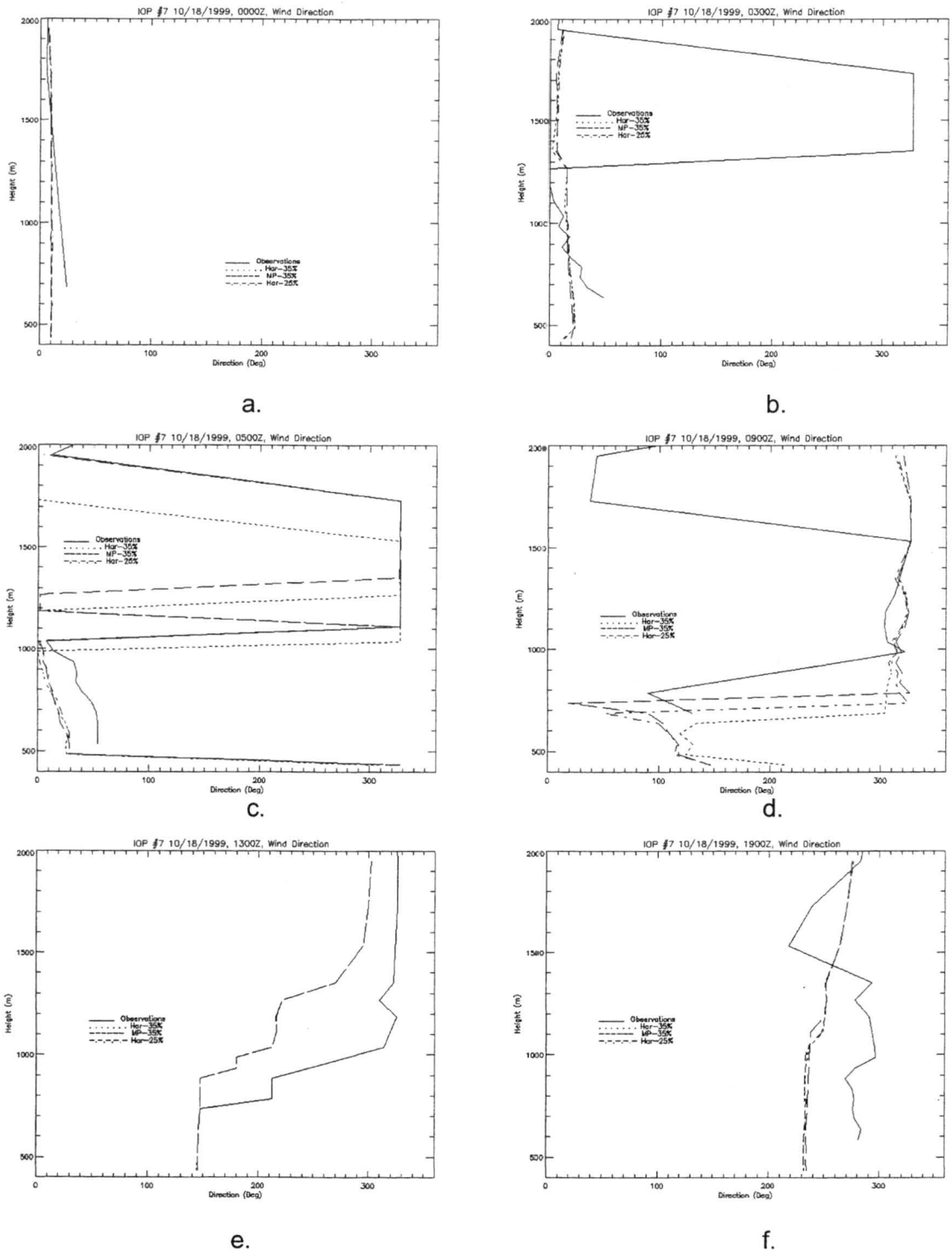

Figure 4.7 – IOP #7 (10/18/1999) wind direction (degrees) profile at Leon, KA: a) 00Z; b) 03Z; c) 05Z; d) 09Z; e) 13Z; and f) 19Z. Legend: (.... Har-35, -.-.-.- Har-25, - - - - MP-35)

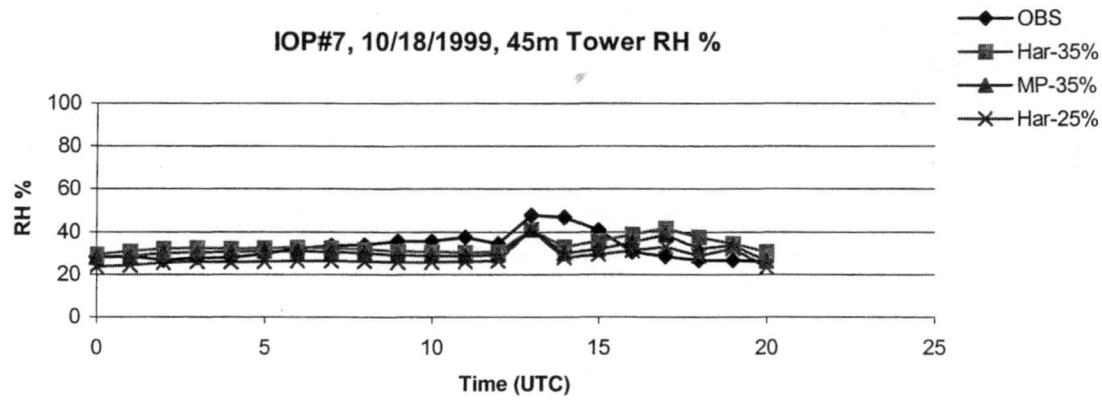
IOP#7, 10/18/1999, 45m Tower RH %
OBS
Har-35%
MP-35%
Har-25%
RH %
100
80
60
40
20
0
0
5
10
15
20
25
Time (UTC)

4.8.a.

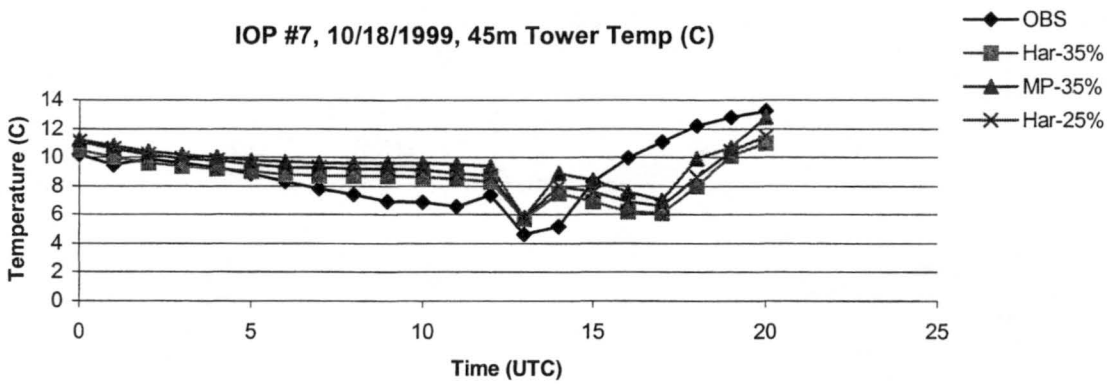
IOP #7, 10/18/1999, 45m Tower Temp (C)
OBS
Har-35%
MP-35%
Har-25%
Temperature (C)
14
12
10
8
6
4
2
0
0
5
10
15
20
25
Time (UTC)

4.8.b.

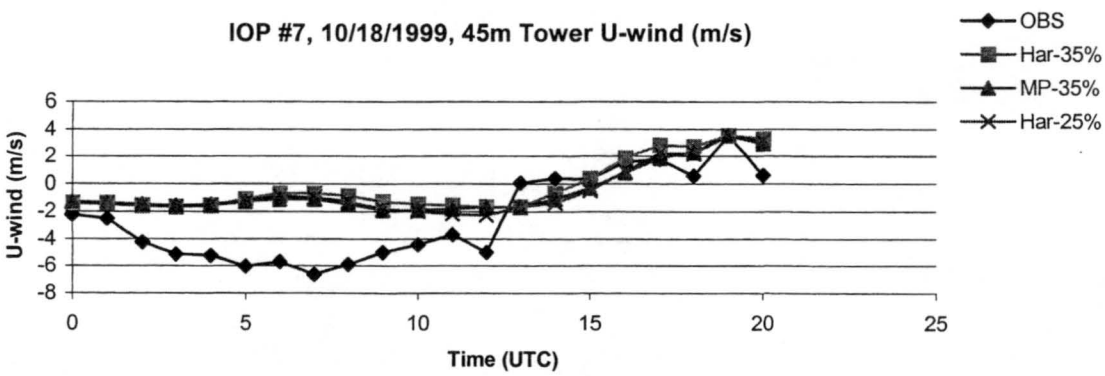
IOP #7, 10/18/1999, 45m Tower U-wind (m/s)
OBS
Har-35%
MP-35%
Har-25%
U-wind (m/s)
6
4
2
0
-2
-4
-6
-8
0
5
10
15
20
25
Time (UTC)

4.8.c.

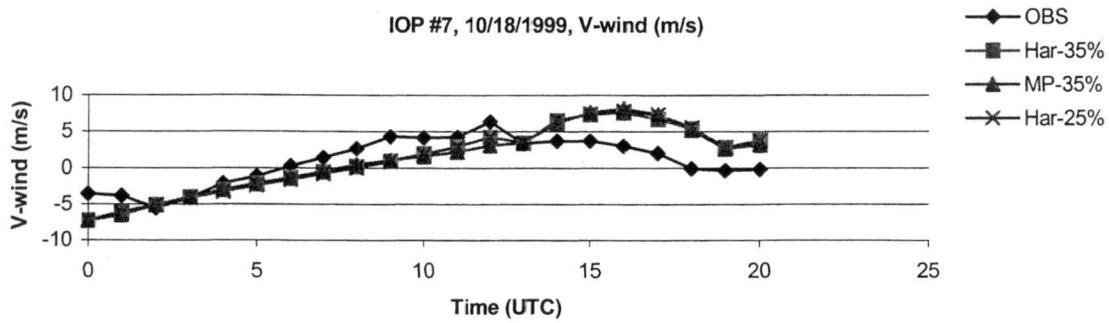

4.8.d

Figure 4.8 – IOP #7 Meteorological variables at 45m AGL, model data plotted with obs. taken at 45m AGL from central tower site: a) RH (%); b) Temperature (C); c) U-wind (m/s); and d) V-wind (m/s).

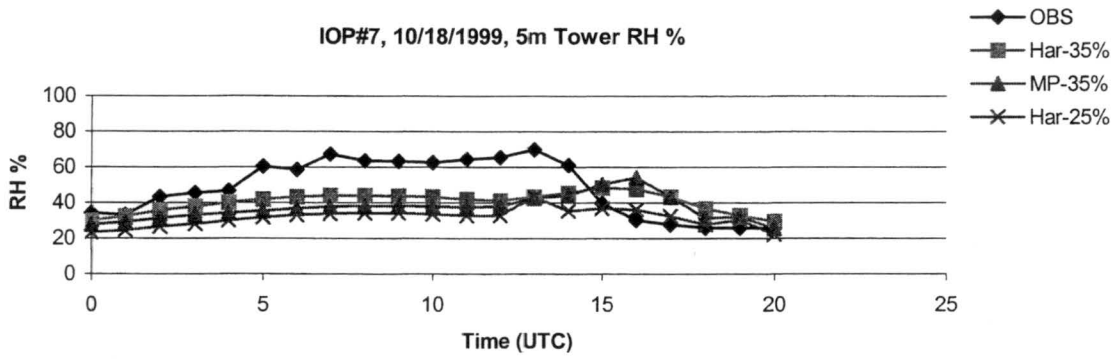

a.

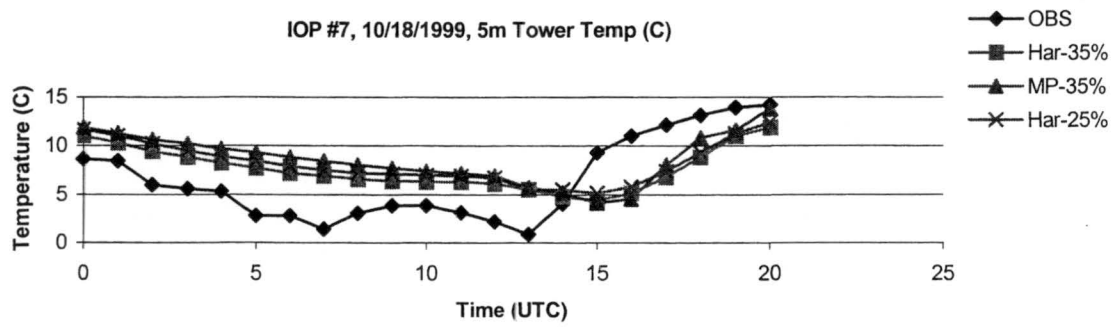

b.

Figure 4.9 - IOP #7 Meteorological variables at 5m AGL, model data plotted with obs. taken at 5m AGL from central tower site: a) RH (%); and b) Temperature (C).

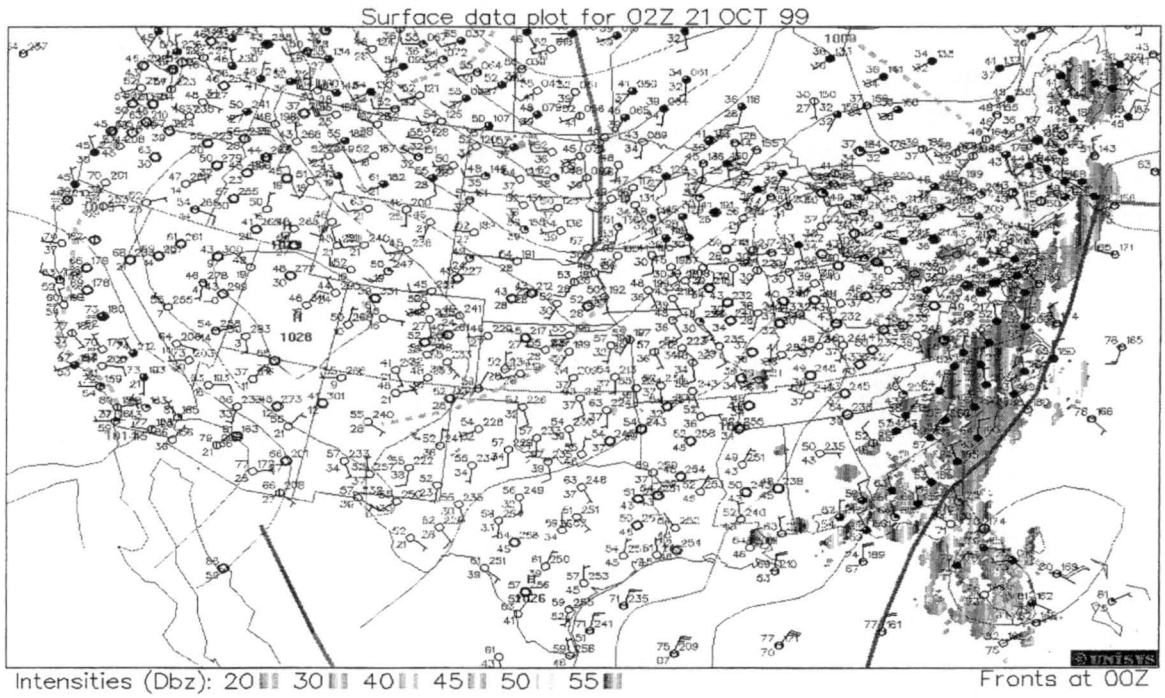

4.10.a

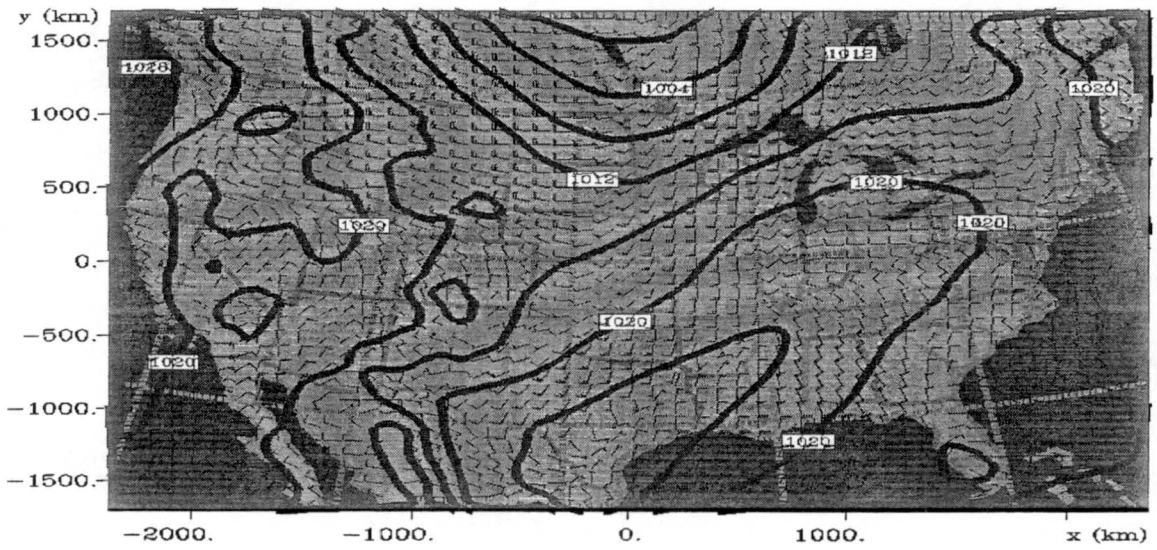

sea level pressure (mb)
min=996.6 max=1029 inc=4
Grid 1 z = 75.0 m
IOP9
Valid 10/21/99 0200 UTC

4.10.b

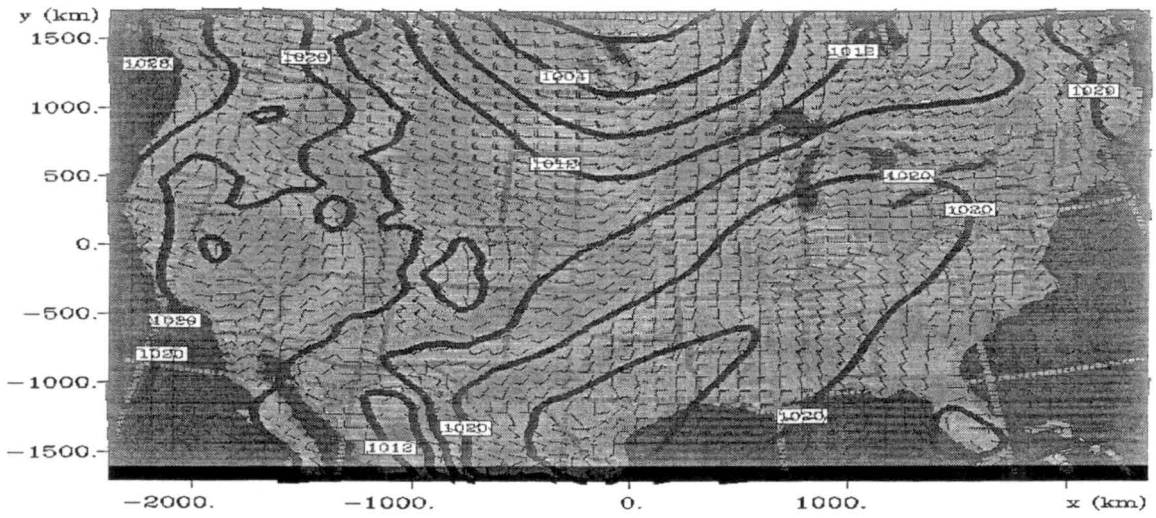

sea level pressure (mb)
min=996.6 max=1029 inc=4
Grid 1 z = 75.0 m
IOP9
Valid 10/21/99 0200 UTC

4.10.c

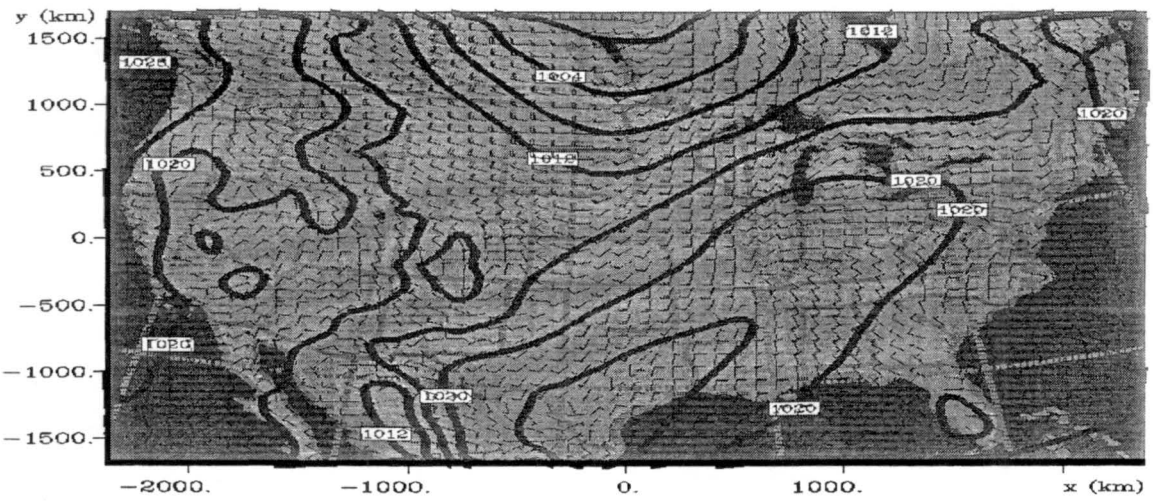

sea level pressure (mb)
min=996.5 max=1029 inc=4
Grid 1 z = 75.0 m
IOP9
Valid 10/21/99 0200 UTC

4.10.d

Figure 4.8 – IOP #9 (10/21/1999) sea level pressure at 02Z: a) observed; b) Harrington-35% model; c) Harrington-25% model; and d) Mahrer/Pielke-35% model.

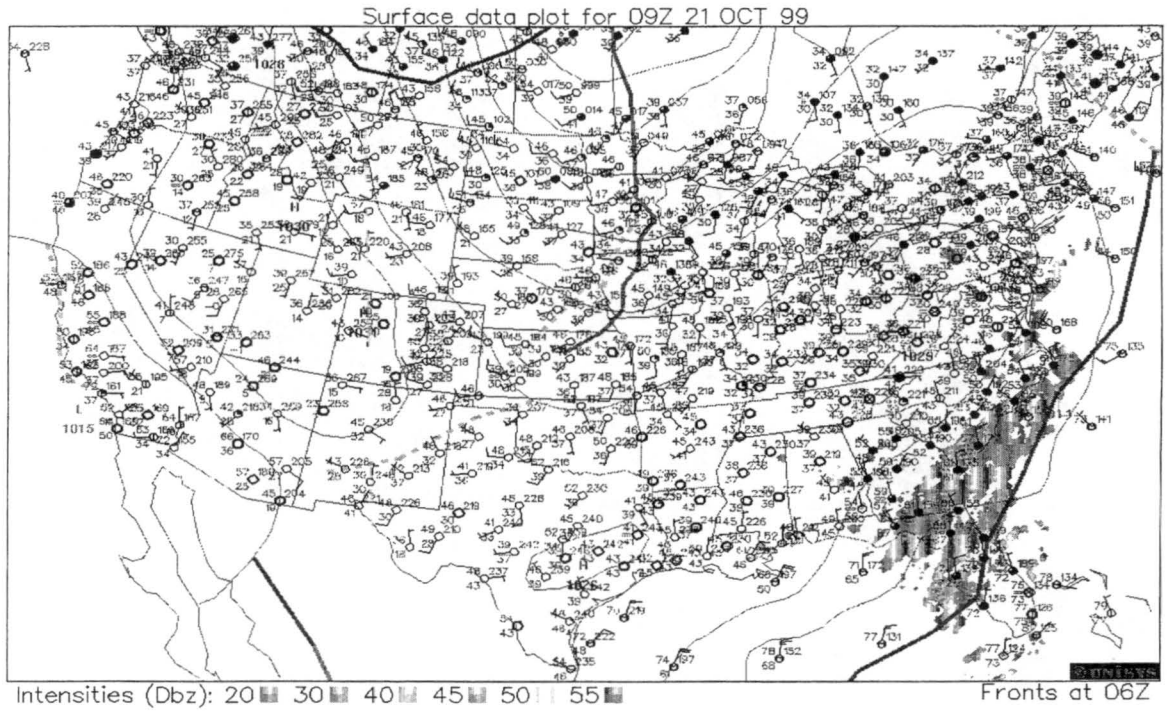
Surface data plot for 09Z 21 OCT 99
Intensities (Dbz): 20 30 40 45 50 55
Fronts at 06Z

4.11.a

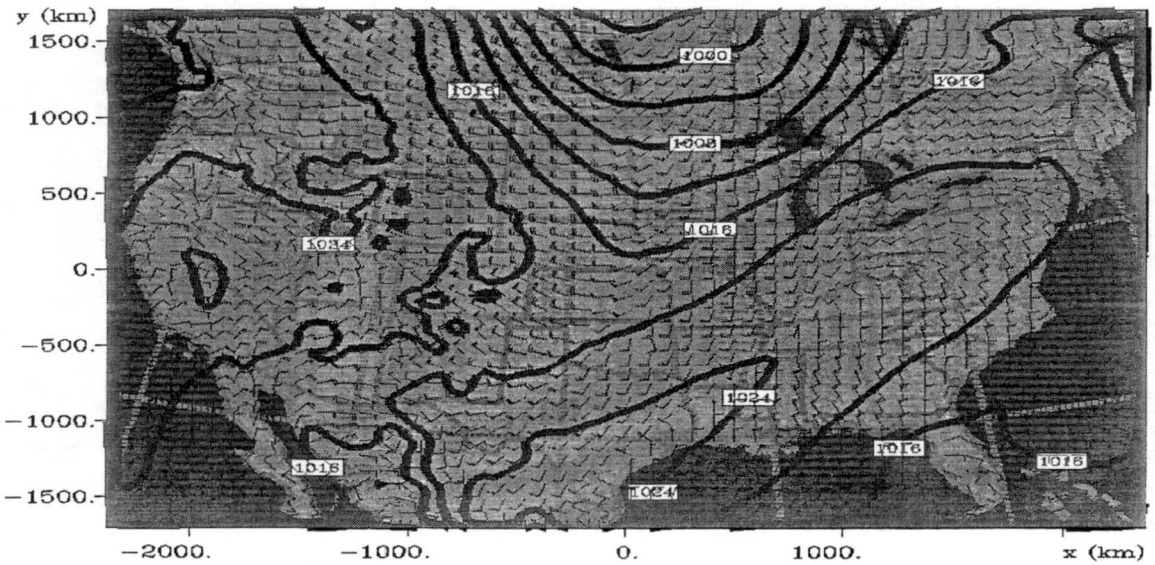
y (km)
1500.
1000.
500.
0.
−500.
−1000.
−1500.
−2000.
−1000.
0.
1000.
x (km)
1004
1008
1012
1016
1020
1024
1028
1015
1024
sea level pressure (mb)
min=993.6 max=1029 inc=4
Grid 1 z = 75.0 m
IOP9
Valid 10/21/99 0900 UTC

4.11.b

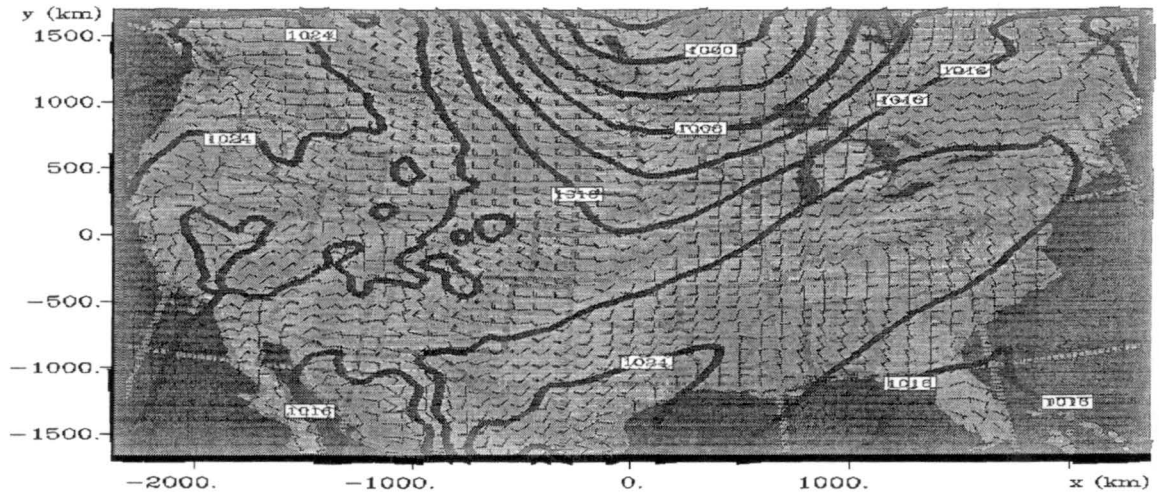

4.11.c

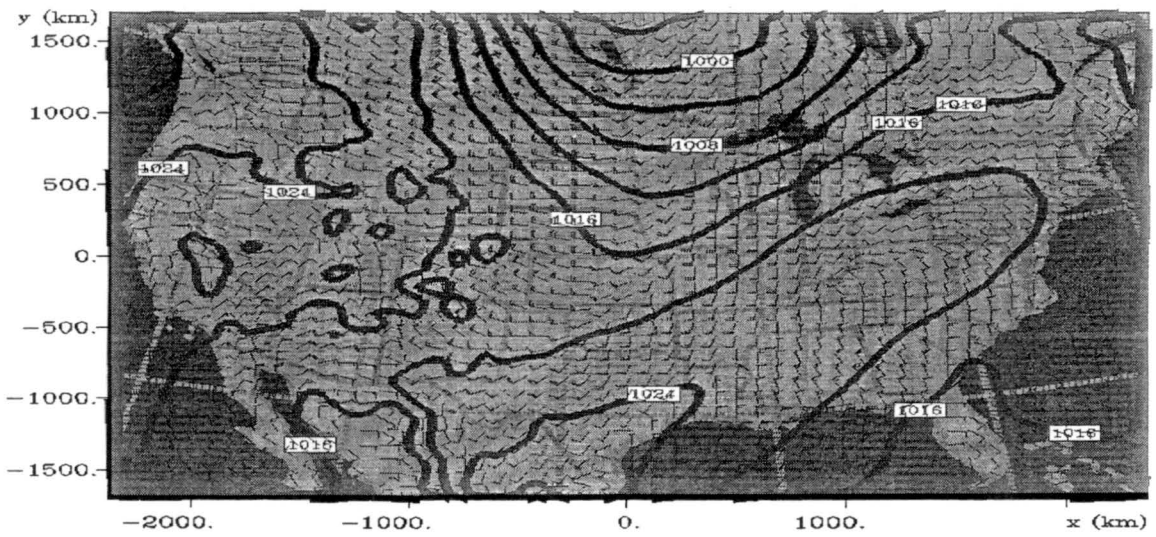

4.11.d

Figure 4.9 – IOP #9 (10/21/1999) sea level pressure at 09Z: a) observed; b) Harrington-35% model; c) Harrington-25% model; and d) Mahrer/Pielke-35% model.

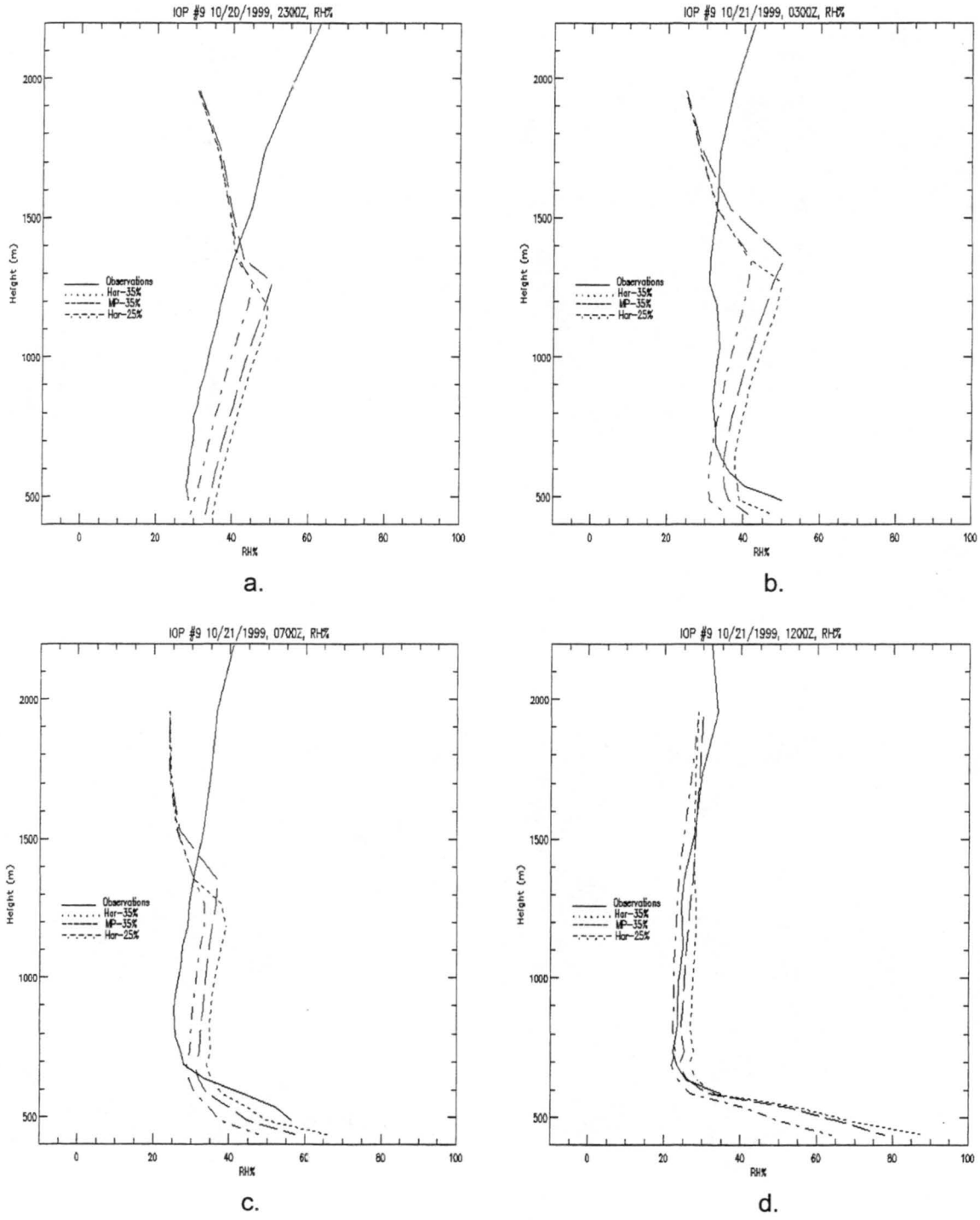

Figure 4.12 - IOP #9 (10/20-21/1999) relative humidity (%) profile at Leon, KA: a) 10/20 23Z; b) 10/21 03Z; c) 10/21 07Z; and d) 10/21 12Z. Legend: (.... Har-35, -.-.-.- Har-25, - - - - MP-35)

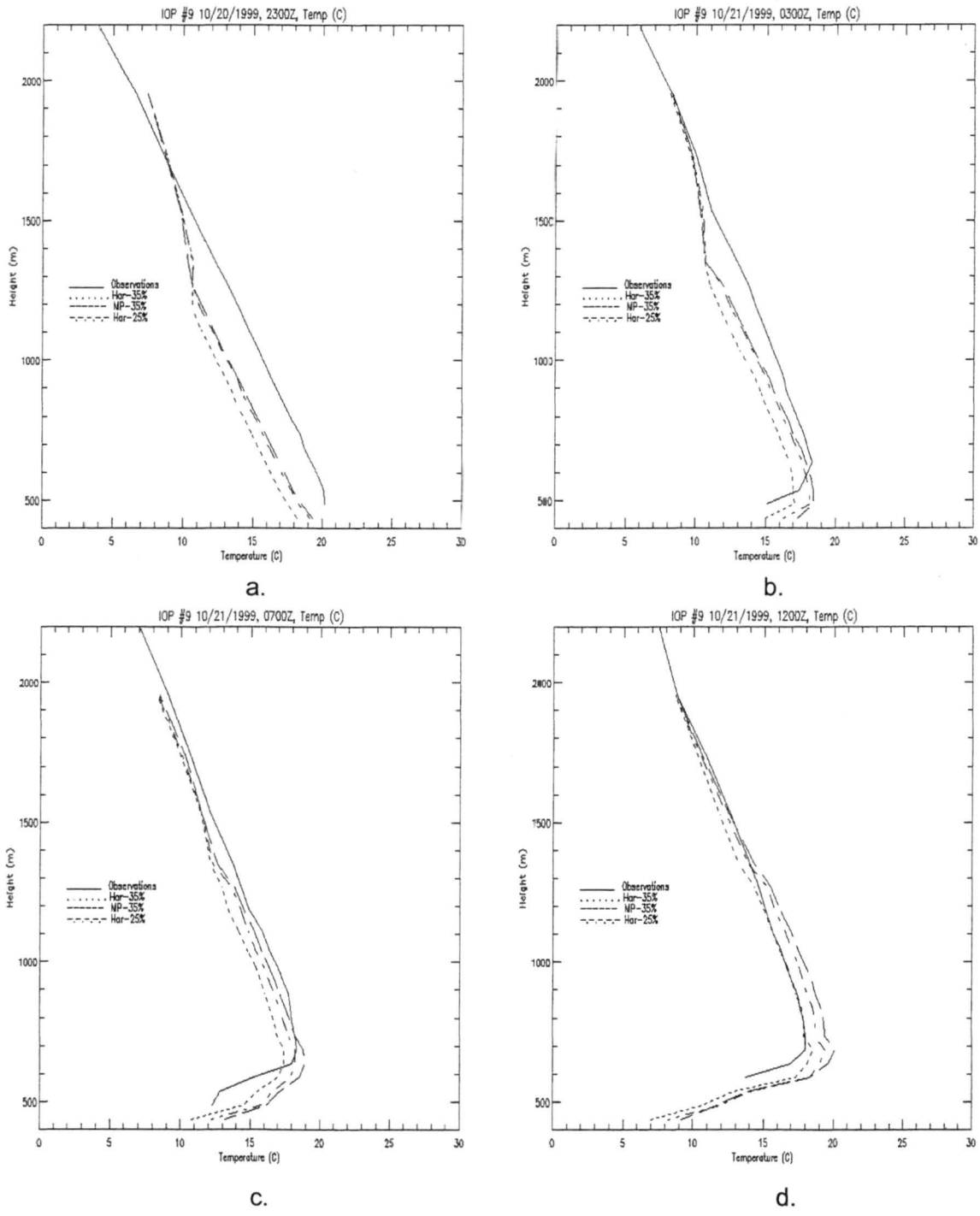

Figure 4.13 - IOP #9 (10/20-21/1999) temperature (C) profile at Leon, KA: a) 10/20 23Z; b) 10/21 03Z; c) 10/21 07Z; and d) 10/21 12Z. Legend: (.... Har-35, -.-.-.- Har-25, - - - - MP-35)

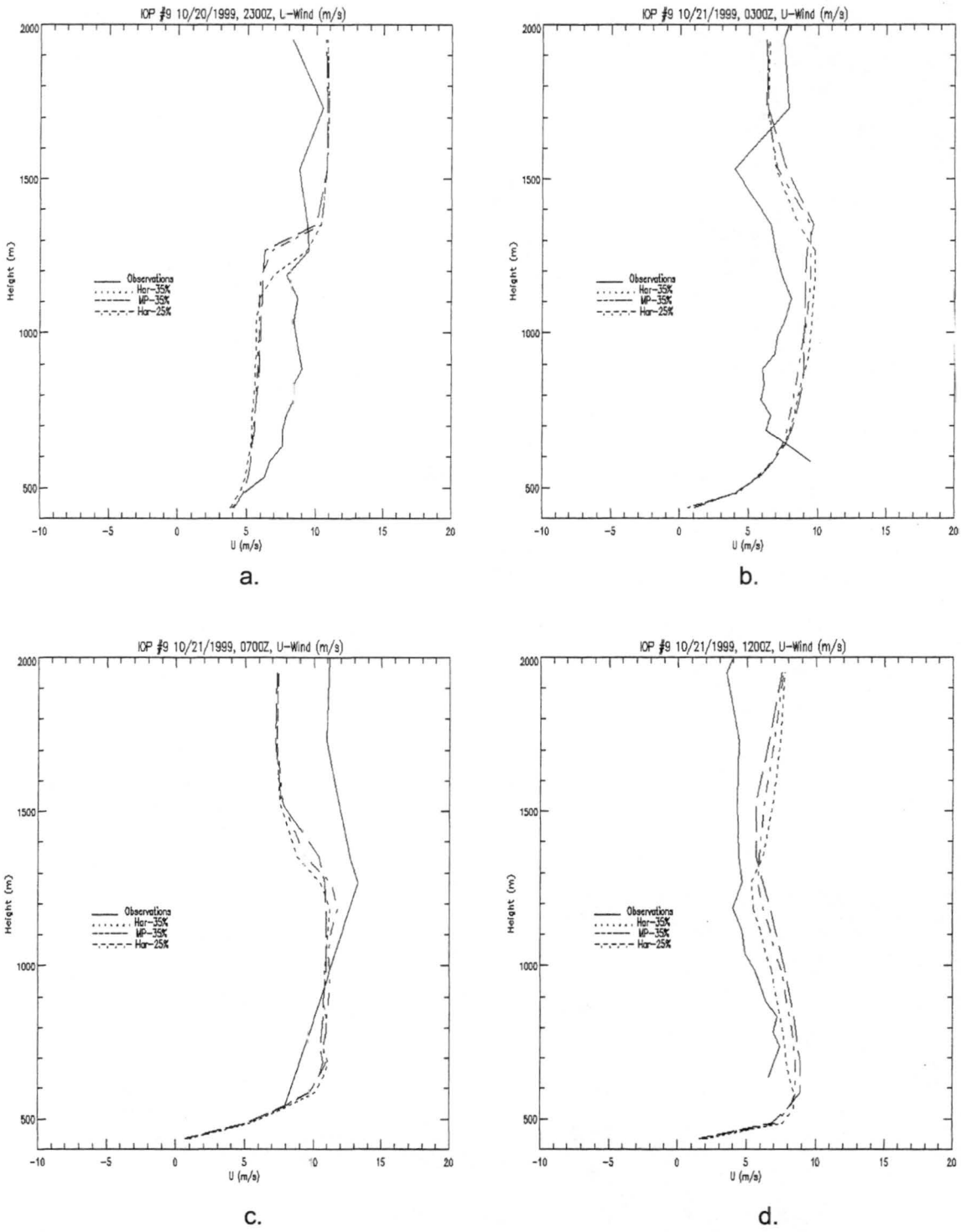

Figure 4.14 - IOP #9 (10/20-21/1999) U-wind speed (m/s) profile at Leon, KA: a) 10/20 23Z; b) 10/21 03Z; c) 10/21 07Z; and d) 10/21 12Z. Legend: (.... Har-35, -.-.-.- Har-25, - - - - MP-35)

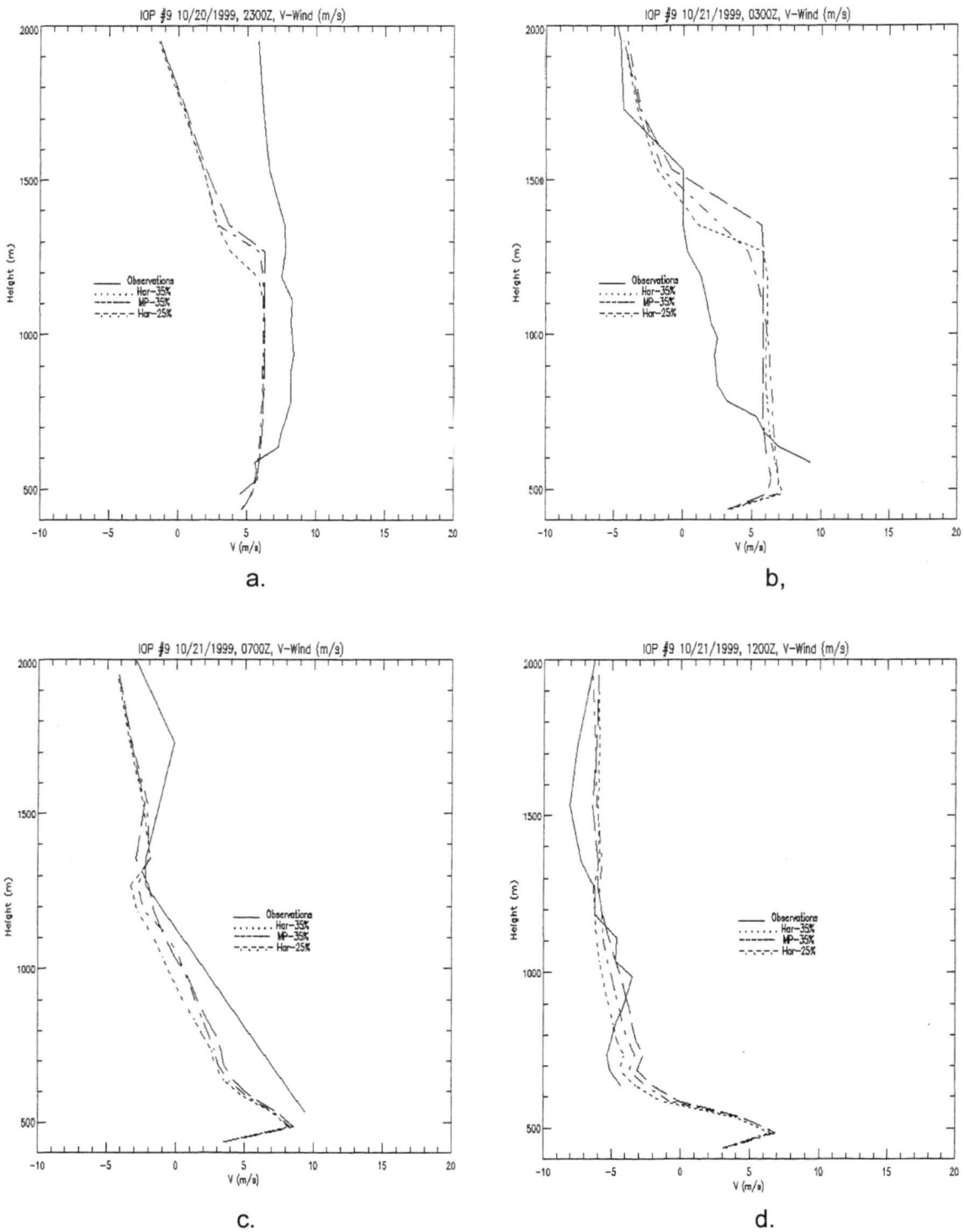

Figure 4.15 - IOP #9 (10/20-21/1999) V-wind speed (m/s) profile at Leon, KA: a) 10/20 23Z; b) 10/21 03Z; c) 10/21 07Z; and d) 10/21 12Z. Legend: (.... Har-35, -.-.-.- Har-25, - - - - MP-35)

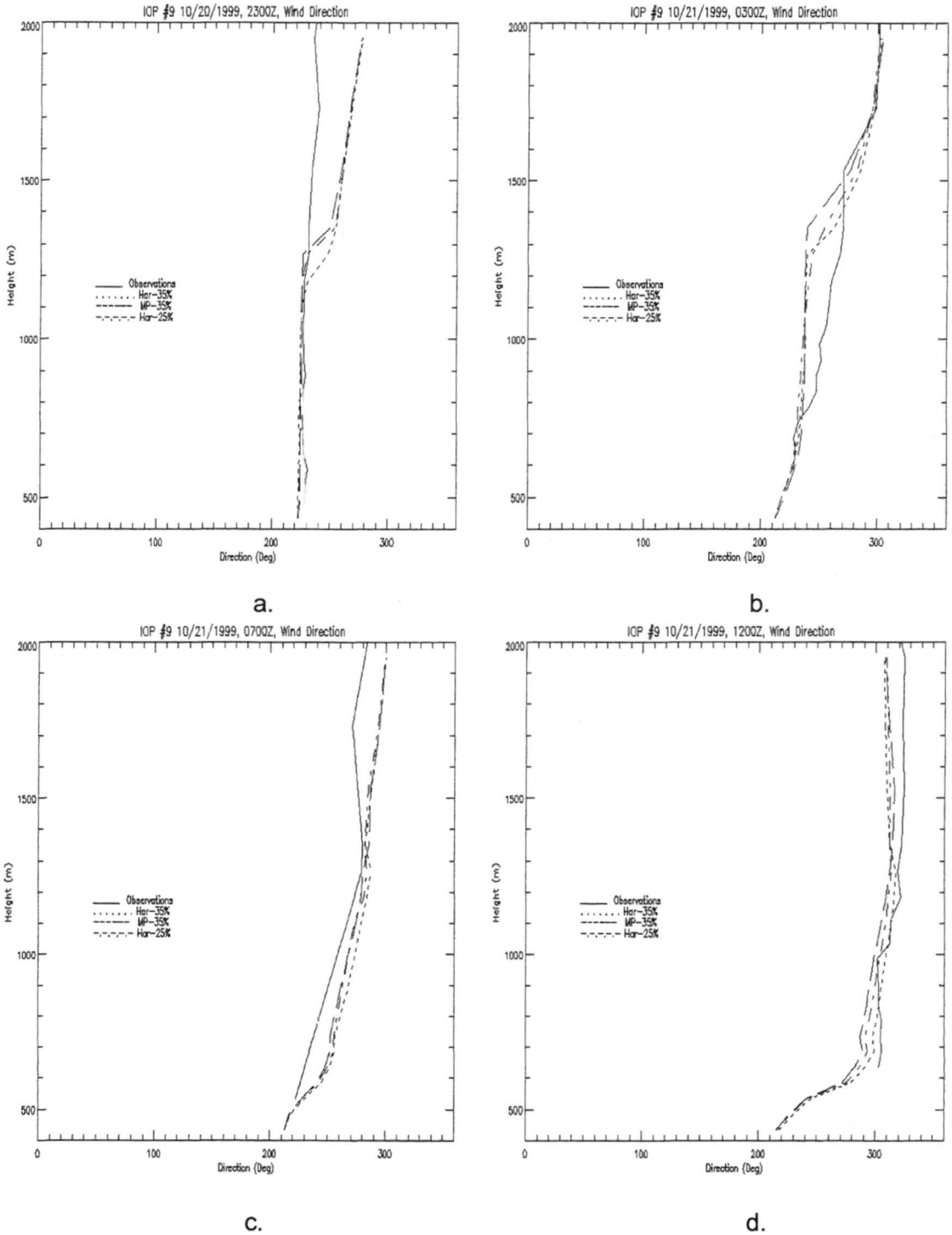

Figure 4.16 - IOP #9 (10/20-21/1999) wind direction (degrees) profile at Leon, KA: a) 10/20 23Z; b) 10/21 03Z; c) 10/21 07Z; and d) 10/21 12Z. Legend: (.... Har-35, -.-.-.- Har-25, - - - - MP-35)

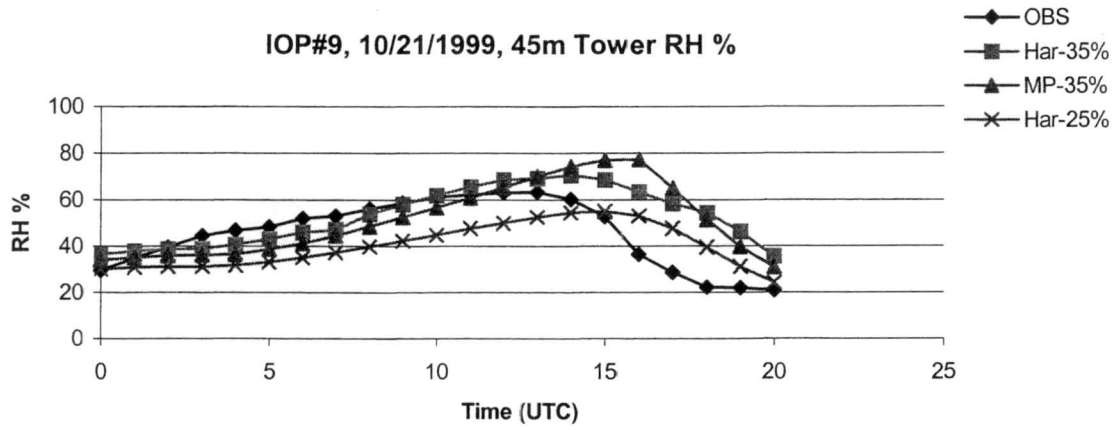

4.17.a

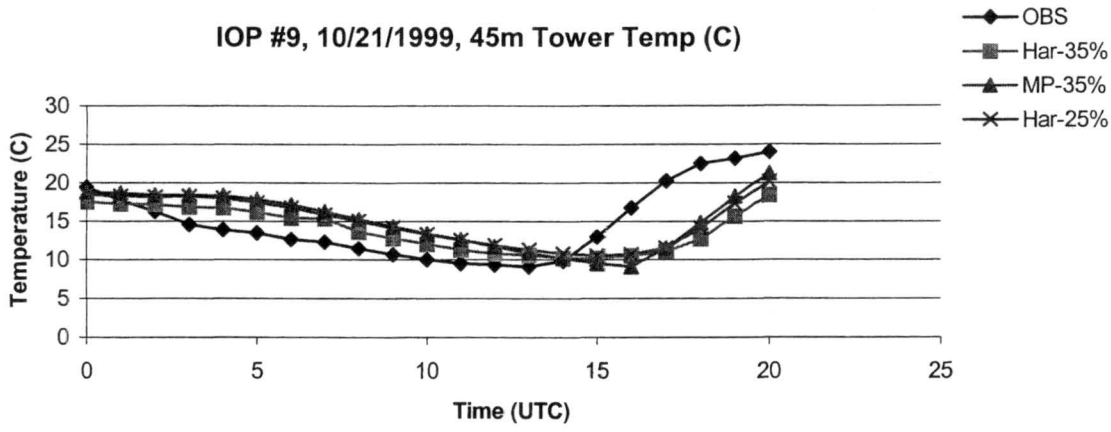

4.17.b

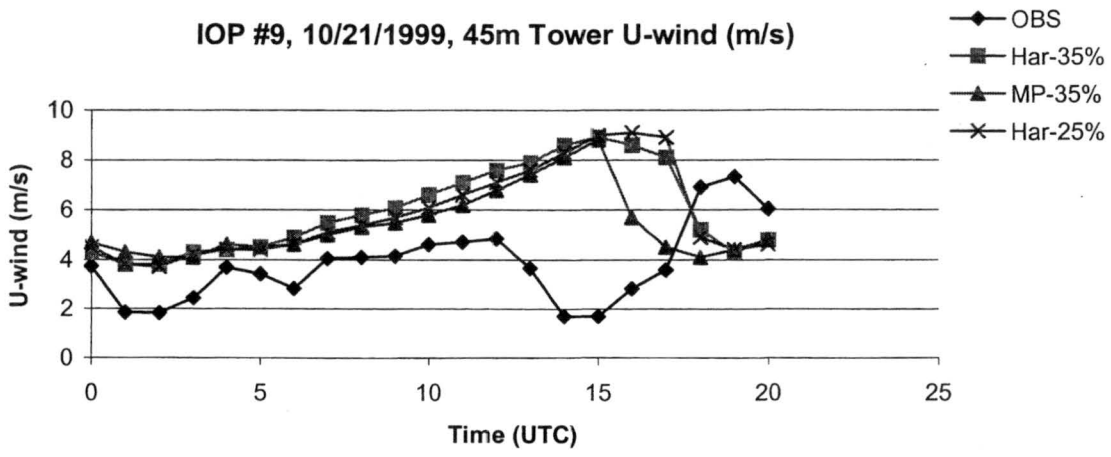

4.17.c

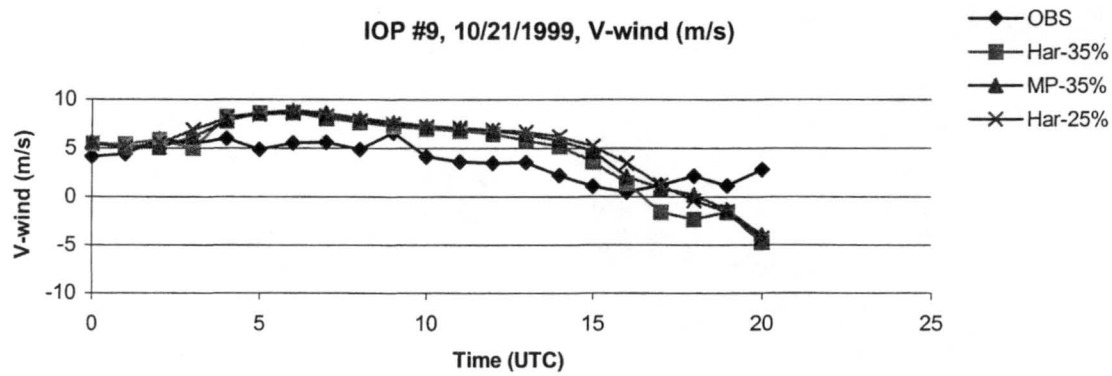

4.17.d

Figure 4.17 - IOP #9 Meteorological variables at 45m AGL, model data plotted with obs. taken at 45m AGL from central tower site: a) RH (%); b) Temperature (C); c) U-wind (m/s); and d) V-wind (m/s).

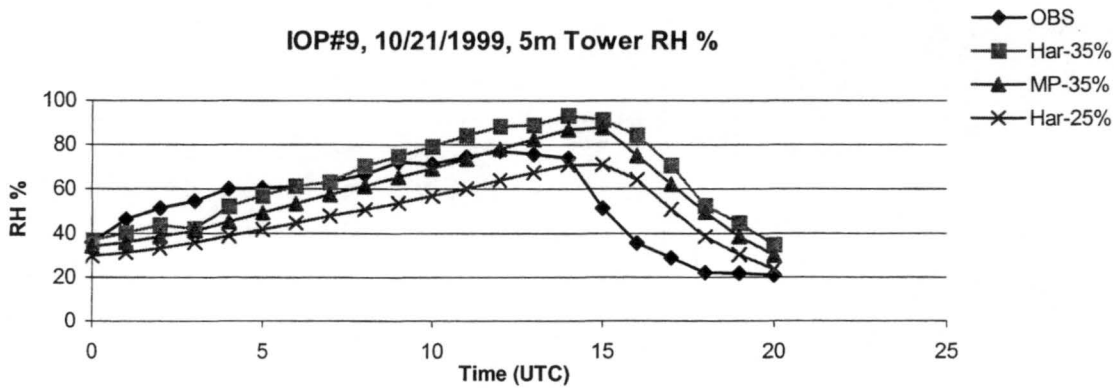

a.

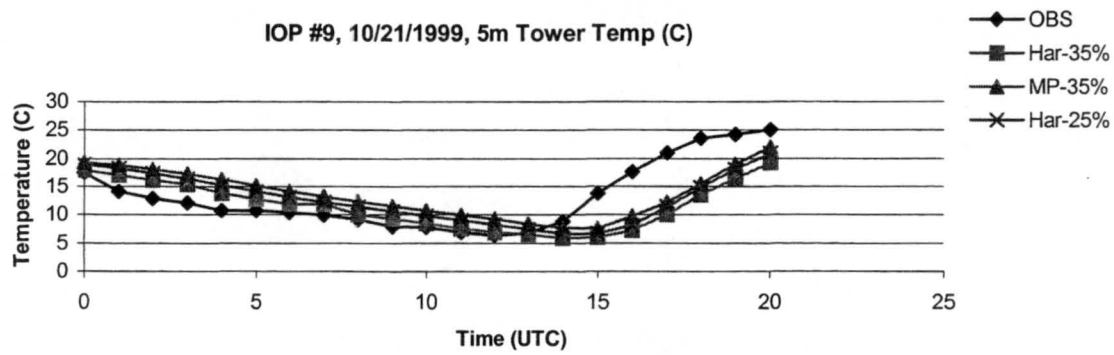

b.

Figure 4.18 - IOP #9 Meteorological variables at 5m AGL, model data plotted with obs. taken at 5m AGL from central tower site: a) RH (%); and b) Temperature (C).

5. Composite Forecast Analysis of CASES-99 Period

This section investigates composite model performance for each configuration through much of the CASES-99 operational period. Mean difference, mean absolute difference, and root mean square error were calculated for fixed forecast times at 100m, 200m, 500m, and 915m AGL incorporating data from all 4 sounding sites. Model bias and discrepancy from observed values for each configuration are discussed through examination of the statistics. Baseline plots of model and tower data at 5m and 45m AGL provide a general sketch of each model configuration's performance for forecast times less than 24 hours, and forecast times greater than 24 hours in terms of RH and temperature at 5m AGL, and RH, temperature, U-wind, and V-wind at 45m AGL. Data points for statistical comparison and baseline plots were chosen according to observational data availability.

5.1 Description and Procedure of Analysis

Methods used to analyze the effectiveness of each model configuration defined in chapter 5 were chosen to provide a rough sketch indicating if any consistent model biases existed through the CASES-99 period, and if a preferred configuration existed. Analysis involved comparison of model and observational data taken from the Leon

central site tower location and multiple sounding sites including Leon, Smileyberg, El Dorado, and Beaumont (Fig. 2.2 in chapter 2). Very limited data availability prevented a more robust approach.

Data from the central tower site was examined from October 5 to 21. Data points were chosen according to the availability of observational and model data, typically both available on dates when IOP's occurred. Time series plots were generated to compare the trends of model and observational data through the CASES-99 period at 5m and 45m AGL. Model data were taken from the closest point to the observational level for comparison. The tower data comparison involved analysis of forecast data produced within 24 hours of initialization, and forecast data produced for forecast times greater than 24 hours. Forecasts were compared over the same observational period, with one forecast period initialized 24 hours prior to the other. This provided a general look at the effectiveness of the model configurations as the forecast length increased. Variables analyzed at 45 m AGL included relative humidity, temperature, U-wind, and V-wind. At 5 m AGL, temperature and relative humidity were examined. The tower platform provided the utility of an observing system at a fixed point horizontally and vertically

Analysis of sounding data involved computation of mean difference (Eq. 5.1), mean absolute difference (Eq. 5.2), and root mean square error (Eq. 5.3) at forecast times when both observational and model data were available at all four sounding sites. Statistical variables were computed at 100 m, 200 m, 500 m, and 915m AGL to provide a general profile of model effectiveness through the lowest 1 km of the atmosphere. In this case, observational sounding data were linearly interpolated to the four fixed levels where model data were available. In the horizontal domain, model data were taken from the closest model point to a sounding launch location. Statistics were computed according equations 5.1-5.3.

$$MD = \frac{\sum_{j=1}^{m}\sum_{i=1}^{n}(x_{pij} - x_{oij})}{m\ n} \tag{5.1}$$

p = prediction
o = observation
i = station #
j = forecast day
n = number of soundings
m = number of days

$$MAD = \frac{\sum_{j=1}^{m}\sum_{i=1}^{n}|x_{pij} - x_{oij}|}{m\ n} \tag{5.2}$$

$$RMSE = \sqrt{\frac{\sum_{j=1}^{m}\sum_{i=1}^{n}(x_{pij} - x_{oij})^2}{m\ n}} \tag{5.3}$$

Mean difference was used to detect biases within model configurations, while mean absolute difference and root mean square error were used to examine model departure from observations and detect a possible preferential configuration. Atmospheric variables including relative humidity, temperature, U-wind, and V-wind were the focus of the examination. Due to very limited data availability, these parameters were calculated only to give a very rough indication of model performance. Missing sounding data at the required levels, along with a limited number of days where all four sites launched balloons synchronously at specified forecast hours seriously limited the amount of data for use in statistical analysis. Quality sounding data was available on four IOP days for calculation of the statistical parameters at forecast hours 11, 15, 19, 23, 35, 39, and 43. No sounding data was available during daytime hours at any of the four sites because daylight operations were not part of the CASES-99 project. Missing model data at forecast hour 47, due to problems with model operations mentioned in chapter 3, prevented that forecast hour from being included in the analysis.

5.2 Tower Data Analysis

Time series plots of atmospheric variables at 45 m and 5 m AGL provide insight on model performance through much of the period where CASES-99 operations took place. As with the individual IOP analysis in chapter 4, Har-35, Har-25, and MP-35 configurations are the focus of the analysis.

45m AGL Tower Analysis

Figure 5.1 displays plots of relative humidity (5.1.a), temperature (5.1.b), U-wind (5.1.c), and V-wind (5.1.d). The plots include observational data and model output from each of the three configurations at forecast times less than 24 hours (1 to 23 H). Comparison between model configurations shows no bias in the prediction of U and V-wind components. In terms of temperature and RH, Har-35 tended to produce the coolest temperatures, with the greatest RH of the three configurations through the period. Har-35 produced values 1 to 3 degrees C below temperatures produced by MP-35 through the majority of the forecast period. Har-25 produced temperatures within 1 degree C of MP-35 temperatures over the same period. Examination of RH shows that Har-25 produced the lowest values, 10% RH lower than Har-35 with the exception of the October 10th forecast period where MP-35 produced the lowest values. Other than the 10th, MP-35 split the difference between the other two configurations in RH values.

Comparison between model and observational data shows the model wind and temperature patterns to be consistent with observations, with a greater discrepancy displayed between model and observations in RH time evolution. From October 5th to 17th, model temperatures are 2 to 5 degrees C warmer than observed and correspondingly, RH values are up to 30% RH too low. After the 17th both RH and temperature values fit the observed pattern well in trends and magnitude. The

preferential configuration, with respect to predicting closest to observed values of temperature and RH, would be Har-35. Even though Har-35 followed observed trends no better than any other configuration, it was closest in magnitude to observed values. Examination of U and V-wind plots shows a good agreement between model and predicted wind patterns with the exception of U-winds on October 11 (IOP #4). During IOP #4, a slow moving cold front passed through the study area becoming stationary over northern Oklahoma causing the winds to shift east/northeasterly. All model configurations held the front in central Kansas, just north of the study area, and produced light southerly winds over the forecast area. This is the most evident synoptic scale problem displayed through the forecast period. Other than the 11th, all model configurations agree with observed trends and are within 5 m/s of observed U and V-wind speeds. No preferential configuration can be seen in predicting the observed wind fields.

Examination of tower plots at 45m AGL (Fig. 5.2) using model data produced at forecast times greater than 24 hours (25 to 48 H) shows an increase in discrepancy between model and observations with similar biases between model configurations in temperature and relative humidity as were displayed in the forecast times less than 24 hours model data. Comparison between model configurations shows Har-35 to again produce the coolest temperatures and highest RH values (Fig 5.2.a and b). In this case, Har-25 produced temperatures similar to Har-35 with RH values similar to MP-35. MP-35 produced temperatures 1 to 3 degrees greater than Har-35 and Har-25, and RH values 10% RH less than Har-35. Wind fields display consistent patterns and magnitudes between configurations with the exception of October 16th when Har-35 diverged from the other two configurations in the V-wind field, and Har-25 diverged from the other two configurations in the U-wind field (Fig. 5.2.c and d.). These divergences were most likely caused by discrepancies in the synoptic scale fields.

Comparison between model and observational data shows model fields produced larger discrepancies from the observations than seen in the 1 - 23 hour data. Temperature differences up to 10 degrees C greater than observed occurred from the 5th to 17th. Large discrepancies between model and observed RH of up to 30% RH below observations coincided with the temperature differences. Over the final two IOP's following the 17th, model and observations correspond well. As with the 1 – 23 hour data, Har-35 produced the closest results in terms of magnitude to observations, but did no better than the other configurations in reproducing the time evolution pattern of RH and temperature observations. Examination between model and observation wind fields shows that the model did a better job reproducing the observed time evolution of the V-wind structure than the U-wind structure. Additionally, it appears that the Har-35 configuration somewhat captured the wind shift on October 11 that was not captured in the < 24 H forecast, as the U-component turns easterly, but the V-wind component remains southerly. In terms of magnitude, both U and V-wind modeled components differed from observations by 5 to 10 m/s at times, a greater difference than seen in the < 24 H forecast. No preferential configuration can be seen in the wind field analysis.

5m AGL Tower Analysis

Figures 5.3 and 5.4 display time series plots of relative humidity and temperature at 5m AGL for forecast times less than 24 hours and forecast times greater than 24 hours respectively. As seen in the 45m AGL plots, Har-35 produced the coolest temperature values and corresponding greatest relative humidity values of the three model configurations at both ranges of forecast hours. MP-35 produced the warmest temperatures over both forecast time ranges, and RH values similar to those produced by Har-25, about 15 to 20 % RH lower than Har-35 values.

Comparison between model and observational data displays a similar trend in growing forecast error with time as displayed in the 45m AGL plots. Differences between observations and model produced RH values grow from a maximum of 30% RH seen in figure 5.3.a to 40% RH in figure 5.4.a. Additionally temperature differences grow from a maximum of 8 degrees C in figure 5.3.b to 12 degrees C in figure 5.4.b. Temperature and RH forecast data follow the time-evolving structure displayed in the observations fairly close in figures 5.3.a and b. As forecast times increase to greater than 24 hours, the model had more trouble resolving the time evolving pattern displayed in the observations. As discussed above some magnitude problems existed over both forecast time ranges. Plots of temperature and RH show a warm model bias, and dry RH bias through the majority of the period. In terms of magnitude, Har-35 produced values closest to observations over both forecast time ranges. With regards to following the time evolving structural pattern of the observations, no model configuration produced preferential results.

5.3 Sounding Data Analysis

Sounding data analysis involved computation of mean difference, mean absolute difference and root mean square error at 100 m, 200 m, 500 m, and 915 m AGL for relative humidity, temperature, U-wind, and V-wind as described in section 5.1. Analysis was completed for all model configurations to determine whether biases existed and which configuration produced results closest to observed values.

Examination of RH mean difference in figure 5.5 shows Har-35 consistently produced the highest RH values, as displayed in previous analysis. Har-25 produced the lowest RH values in forecast hours 11-23, while MP-35 produced the lowest RH values in forecast hours 35-43. Har-35 consistently produced the highest RH values of the three

configurations through all vertical levels at all forecast times. In terms of model bias compared to observations, a dry bias is displayed for all model configurations at 100 and 200 m AGL that grows as the forecast length increases to 35 – 43 hours. Further above ground level, at 500 m and 915 m AGL, the drying trend with increasing forecast length is consistent with the trend displayed at 100 m and 200m AGL. At 500 m and 915 m, no consistent dry or moist model bias is defined.

Figures 5.6 and 5.7 display mean absolute difference and root mean square error respectively calculated for relative humidity. At the two levels closest to the surface, 100 m and 200 m AGL, Har-35 displays the least amount of error with results within 15% RH of observed. At 500 m and 915 m AGL similar errors are produced by all model configurations of up to 20% RH. This might imply that the surface effects of the soil moisture adjustments have little impact except at vertical levels nearest the surface in the stable boundary layer forecast situation.

Examination of temperature mean difference (Fig. 5.8) shows consistent biases between model configurations at all levels of analysis. MP-35 produced the warmest temperatures, 1 to 2 degrees C warmer than the coolest readings produced by Har-35 at forecast hours 11 - 23. The difference increased to 2 to 3 degrees C at forecast hours 35 – 43, with Har-25 values approximately splitting the difference between the other configurations over both forecast time periods. At 100 m and 200 m AGL MP-35 and Har-25 have a warm bias compared to observed values, which increases with forecast length. Har-35 displays a warm bias at 100 m AGL, but little bias at 200 m AGL. A maximum warm bias of 6 degrees C was produced by MP-35 at 100 m AGL. At 500 m and 915 m AGL, a general 1 to 3 warm bias still exists for MP-35 and Har-25, with no consistent bias displayed in the Har-35 data. Har-35 stays within +/- 1 degree C of observations at these levels. When figures 5.8 and 5.5 are compared, it can be seen

that the warm biases displayed in the temperature data are consistent with the dry biases displayed in the RH data.

Plots of temperature mean absolute difference and root mean square error displayed in figures 5.9 and 5.10 respectively, show that Har-35 generally produced values closest to observations near the surface at 100 m and 200 m AGL, with no preferential configuration above 200m AGL. Errors also appear to grow less as forecast length increases to 35 – 43 hours in the Har-35 configuration compared to the other two configurations. Over those forecast hours, Har-35 produced the best results at all heights. In terms of magnitude, at all levels AGL Har-35 produced differences up to 3 degrees C from observations, while MP-35 produced the greatest errors, up to 6 degrees C from observed values.

Examination of U-wind component mean difference (Fig. 5.11) shows no bias between configurations. The only noticeable biases with respect to the observations would be an over-prediction of speeds by 2 to 4 m/s in the 11 – 23 forecast hour range, and an under-prediction of speeds by 2 to 4 m/s in the 35 – 43 forecast hour range. Wind direction is not taken into account in the analysis so directional problems may enhance or decrease the magnitude of biases.

Figures 5.12 and 5.13 display U-wind component mean absolute difference and root mean square error. Little difference in errors can be seen between model configurations. Generally, all three configurations predict wind magnitude within 4 m/s of observations at all forecast levels and times.

Differing from the U-wind component analysis, a bias between model configurations is displayed in the plots of V-wind component mean difference (Fig 5.14). Har-35 produced a mean difference generally 1 to 2 m/s lower than the other two configurations at all forecast times from 200 m to 915 m AGL. At 100 m AGL, all configurations produced similar results with the exception of forecast hour 19 where Har-35 diverged

from the other two configurations. No consistent biases with respect to observations are found in forecast hours 11 – 23. A consistent under-prediction of wind magnitude of up to 8 m/s occurs in forecast hours 35 – 43 by all model configurations.

Plots of V-wind component mean absolute difference and root mean square error (Figs. 5.15 and 5.16) show no preferential model configuration with respect to predicting closer to observed values. All configurations fall within 2 to 4 m/s of observed values in the 11 – 23 forecast hour range with the exception of the 19-hour Har-35 problem. Errors of up to 8 m/s at 100 m AGL appear in the 35 – 43 forecast hour range, and decrease with height. From the examination of both U and V-wind components, it appears the changes in soil moisture and radiation scheme have little impact on the wind fields, with similar synoptic scale conditions between configurations controlling wind speed and direction.

5.4 Summary of Tower and Sounding Data Analysis

From the examination of model vs. tower and sounding data in this chapter, it was shown how RAMS performed under various model configurations as a near surface high resolution forecasting tool through the time-evolution of the CASES-99 field project. Analysis of model and tower data at fixed levels of 5 m and 45 m AGL showed that Har-35 consistently produced the coolest temperatures and corresponding highest RH values of the three configurations, while MP-35 produced the warmest temperature values. Additionally, Har-35 produced results closest in magnitude to observed values of temperature and RH. In the wind field analysis, all configurations were similar in magnitude, with no preferred configuration displayed. Structural time evolution of all atmospheric fields were similar between model configurations, and followed the basic pattern displayed in the observations except for the RH fields. As forecast times

increased from less than 24 hours to greater than 24 hours, discrepancies between model and observations tended to increase as well.

Examination of rough statistics calculated at 100 m, 200 m, 500 m, and 915 m AGL utilizing sounding data from four spatially varying launch sites showed many similarities to the tower data analysis results at low levels. Mean difference analysis showed that Har-35 produced the coolest temperatures and highest RH values at all levels of examination, while MP-35 consistently produced the warmest temperatures, and shared the lowest RH values with Har-25. A warm temperature bias with respect to observations was displayed in mean difference plots of the Har-25 and MP-35 configurations at all vertical levels examined, with a corresponding dry RH bias at 100 m and 200 m AGL. Mean absolute difference and root mean square error plots for RH and temperature showed that Har-35 produced the smallest errors of the three configurations at 100 m and 200 m AGL, with no preferential configuration found above 200m AGL. U-wind mean difference plots showed no bias existed between model configurations. Between model and observation, U-wind magnitudes were generally over-predicted in the 11 – 23 hour range, and under-predicted in the 35 – 43 hour range. U-wind mean absolute difference and root mean square error plots displayed no preferential model configuration, with errors for all configurations ranging from 2 to 4 m/s at all vertical levels. Examination of V-wind statistics showed Har-35 produced results 1 to 2 m/s in magnitude less than the other two configurations above 100 m AGL. No consistent model bias existed with respect to observations in the 11 – 23 forecast hour range, while winds were under-predicted in magnitude in the 35 – 43 forecast hour range. V-wind mean absolute difference and root mean square error plots displayed no preferential model configuration with respect to predicting closer to observed values. Errors in magnitude ranged from 4 to 8 m/s.

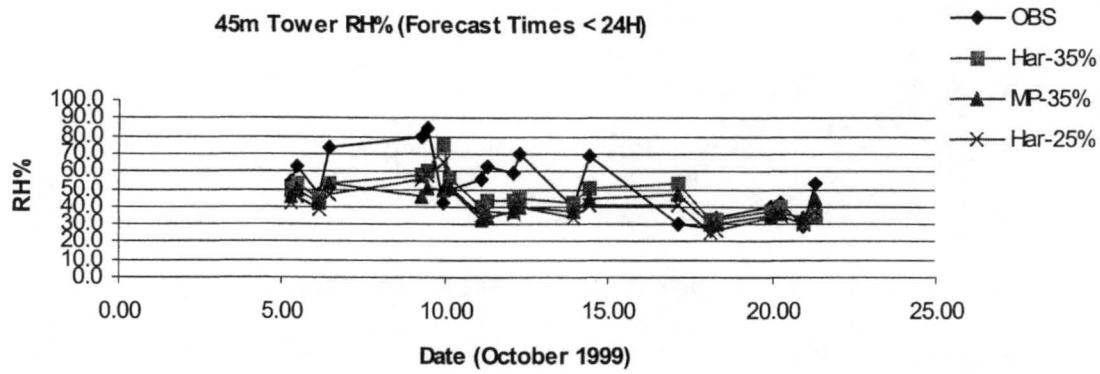

a.

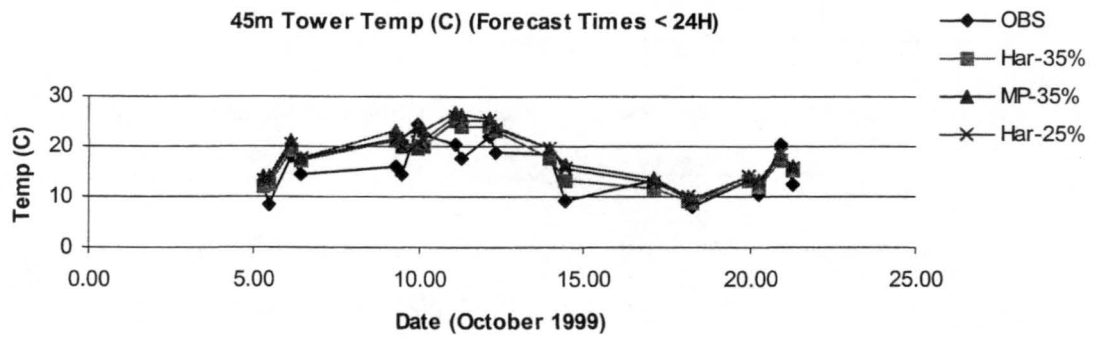

b.

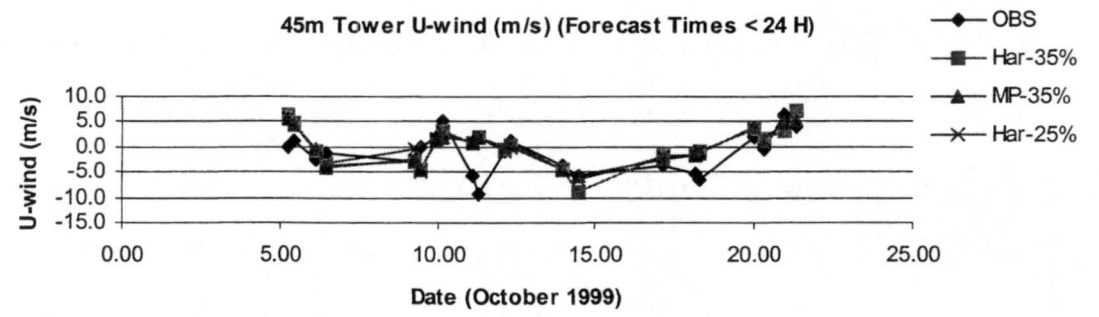

c.

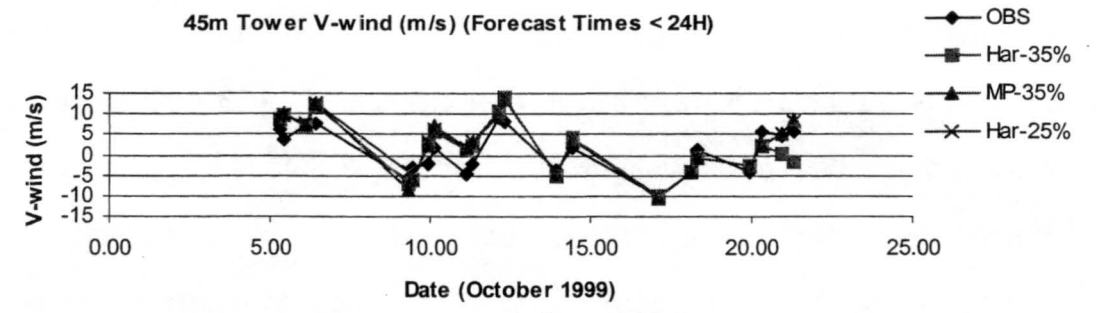

d.

Figure 5.1 – Model data at forecast times less than 24 hours plotted with observations taken at 45m AGL from central tower site: a) RH (%); b) Temperature (C); c) U-wind (m/s); and d) V-wind (m/s).

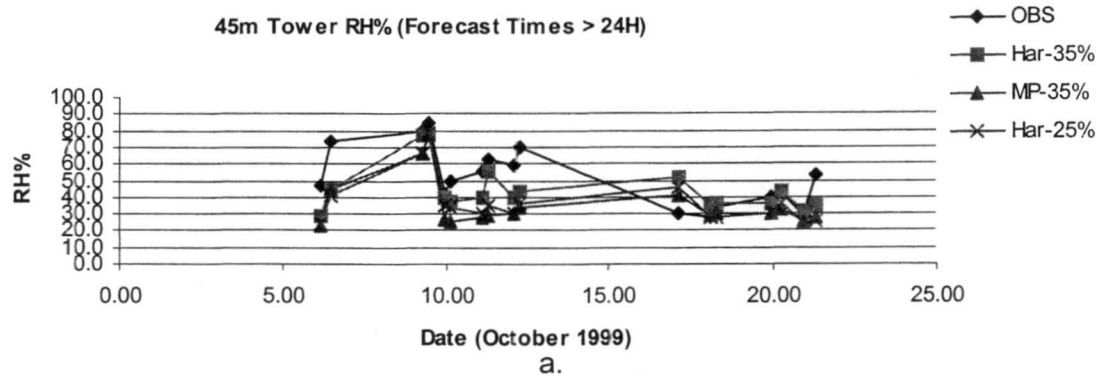

a.

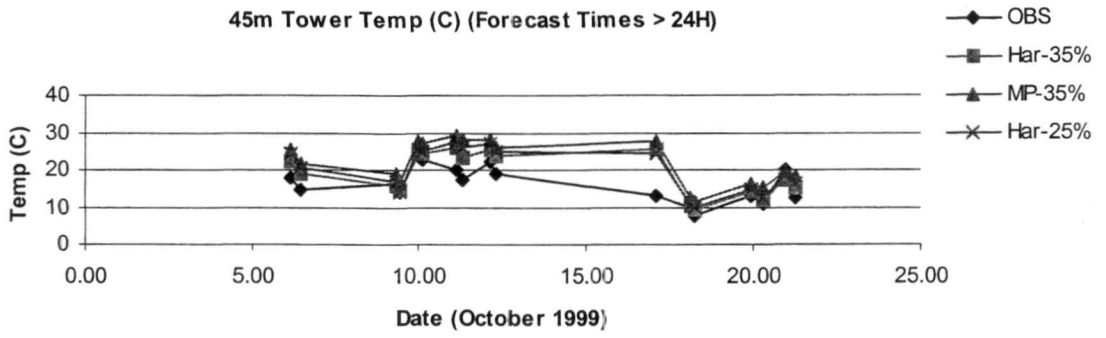

b.

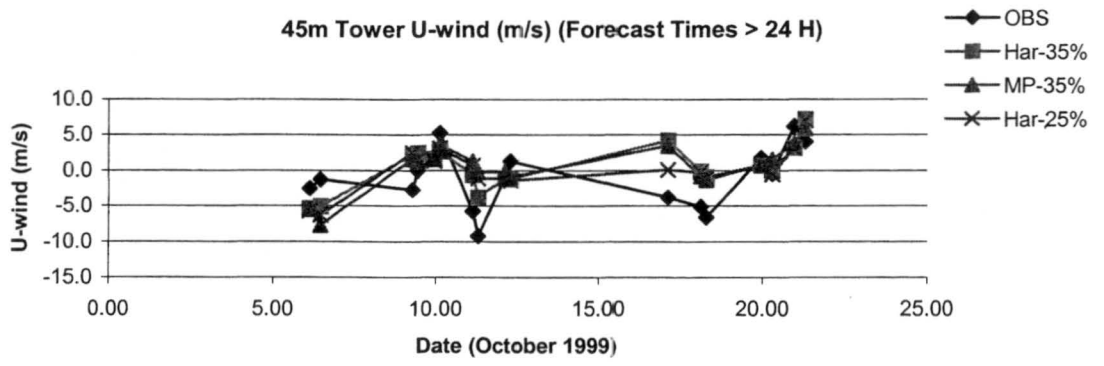

c.

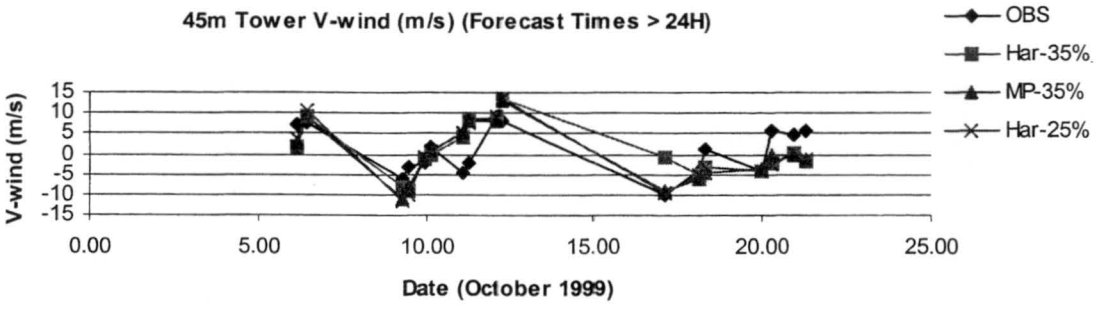

d.

Figure 5.2 – Model data at forecast times greater than 24 hours plotted with observations taken at 45m AGL from central tower site: a) RH (%); b) Temperature (C); c) U-wind (m/s); and d) V-wind (m/s).

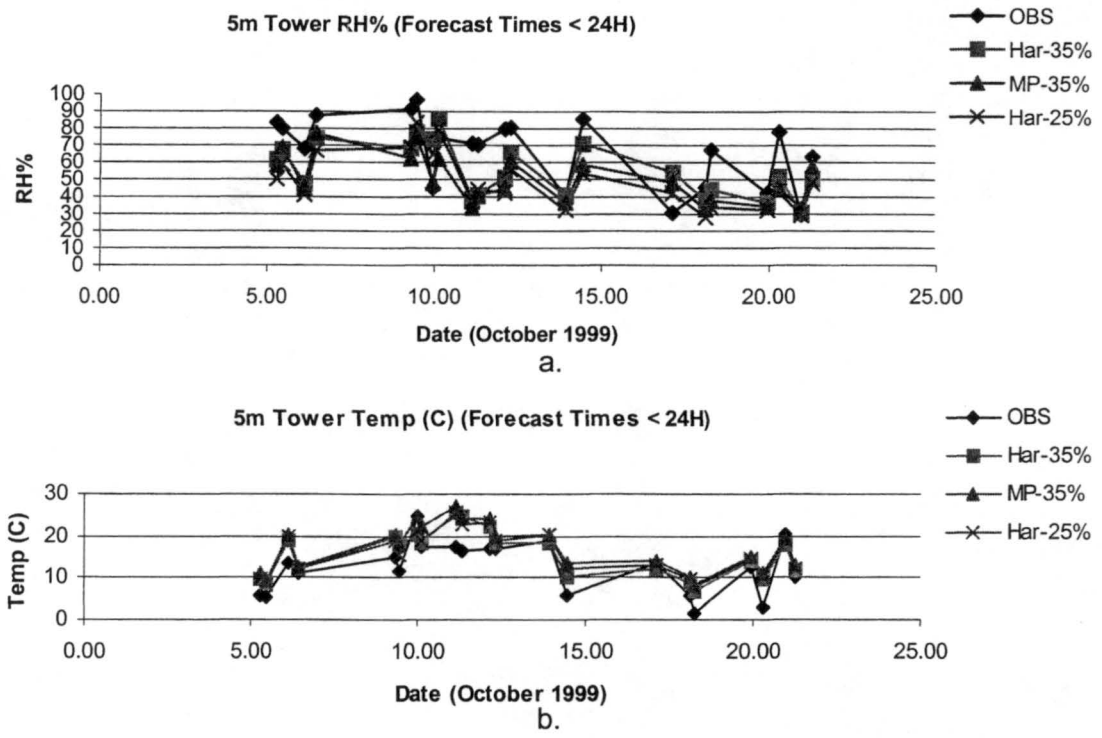

Figure 5.3 – Model data at forecast times less than 24 hours plotted with observations taken at 5m AGL from central tower site: a) RH (%); and b) Temperature (C).

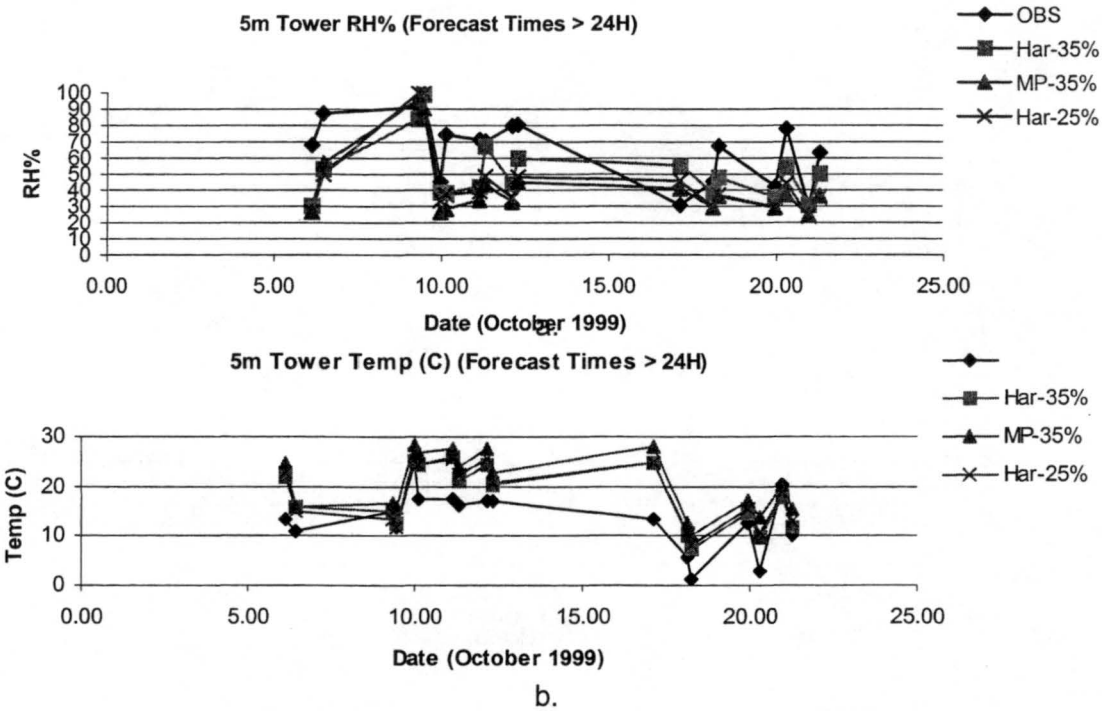

Figure 5.4 – Model data at forecast times greater than 24 hours plotted with observations taken at 5m AGL from central tower site: a) RH (%); and b) Temp. (C).

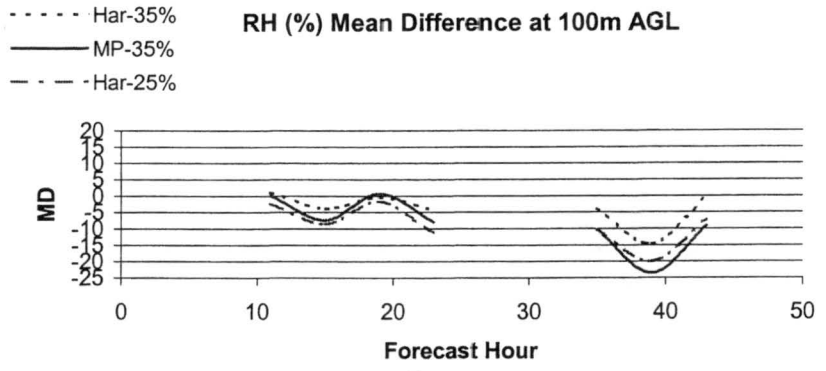

a.

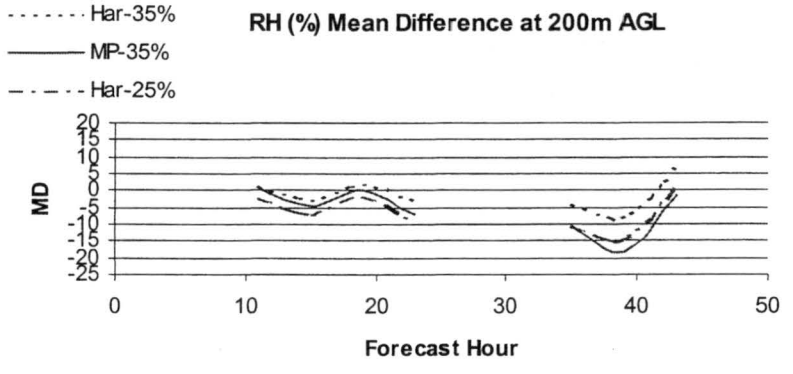

b.

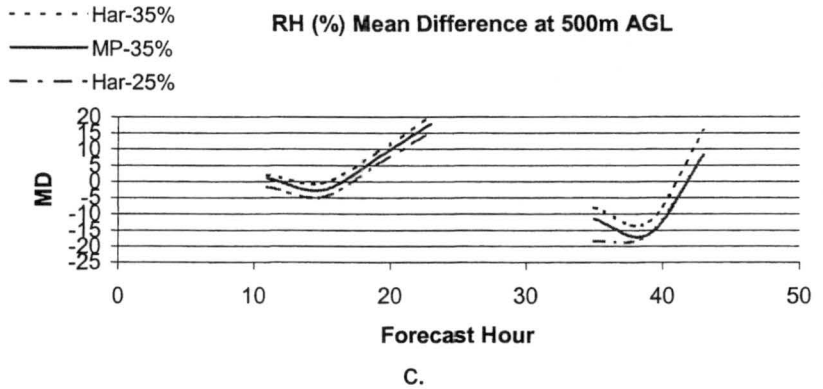

c.

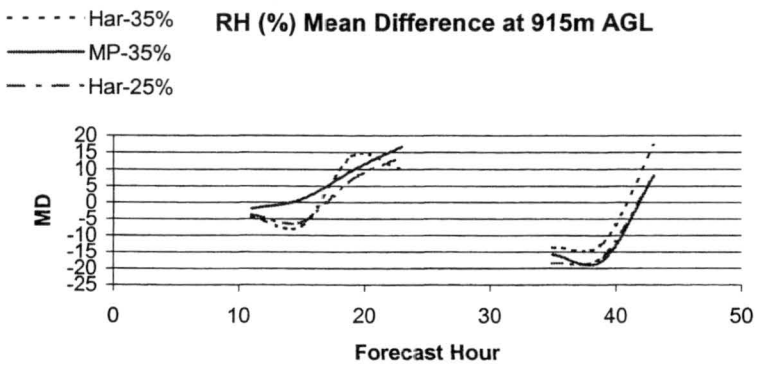

d.

Figure 5.5 – RH (%) Mean Difference at: a) 100m AGL; b) 200m AGL; c) 500m AGL; and d) 915m AGL.

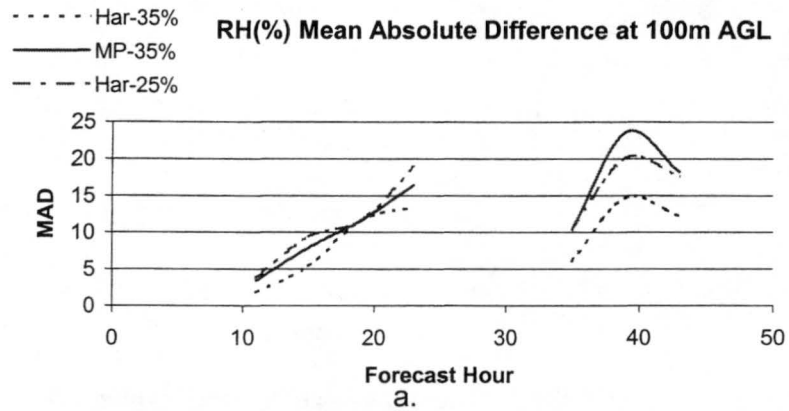

a.

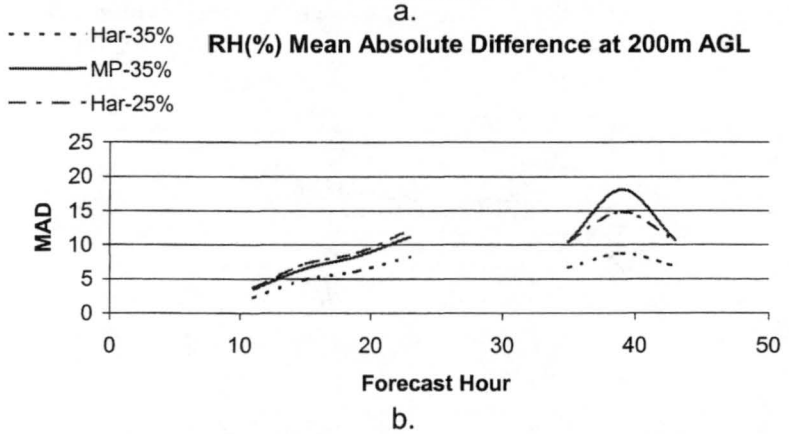

b.

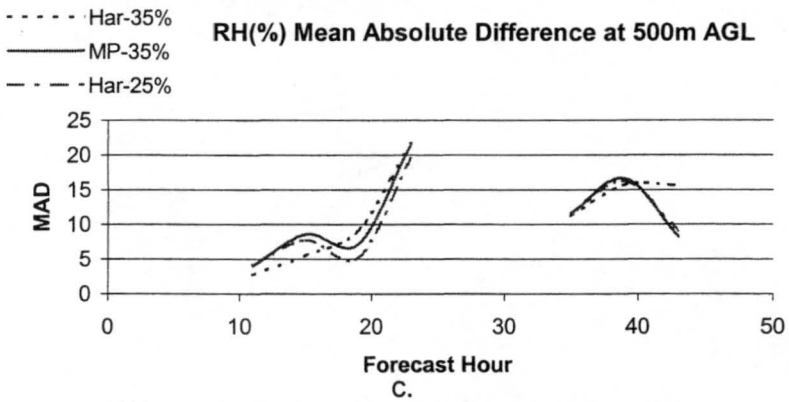

c.

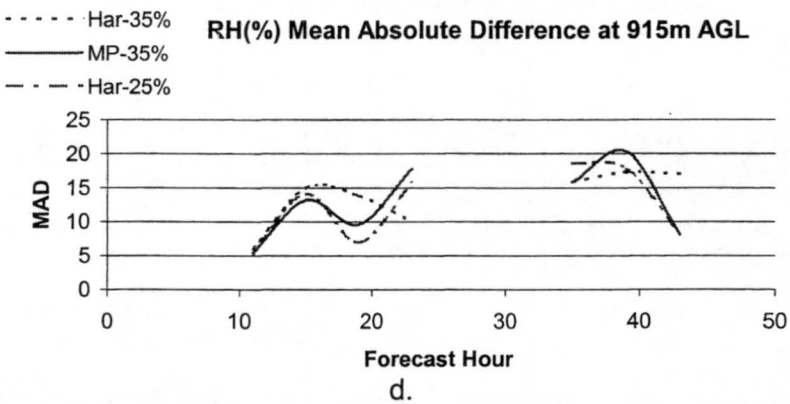

d.

Figure 5.6 – RH (%) Mean Absolute Difference at: a) 100m AGL; b) 200m AGL; c) 500m AGL; and d) 915m AGL.

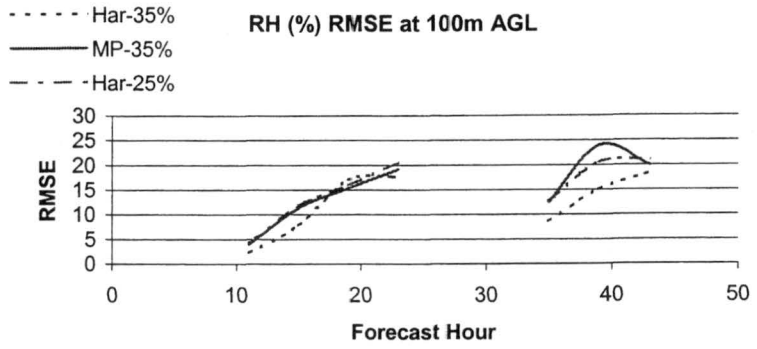

a.

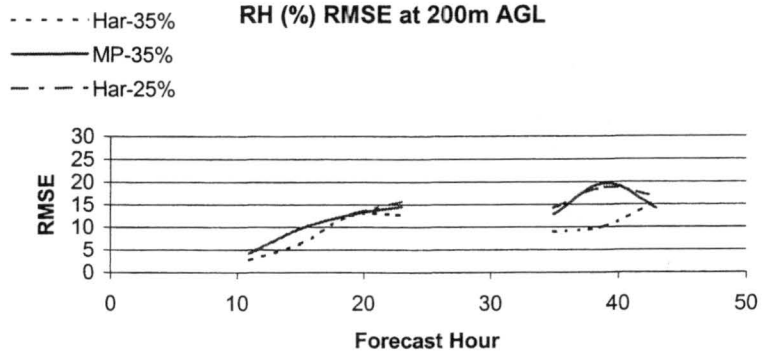

b.

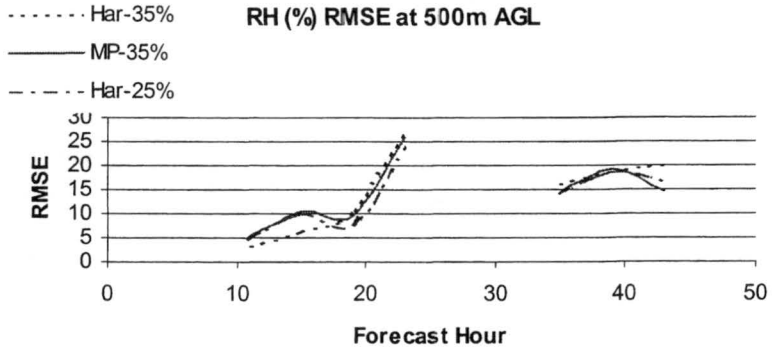

c.

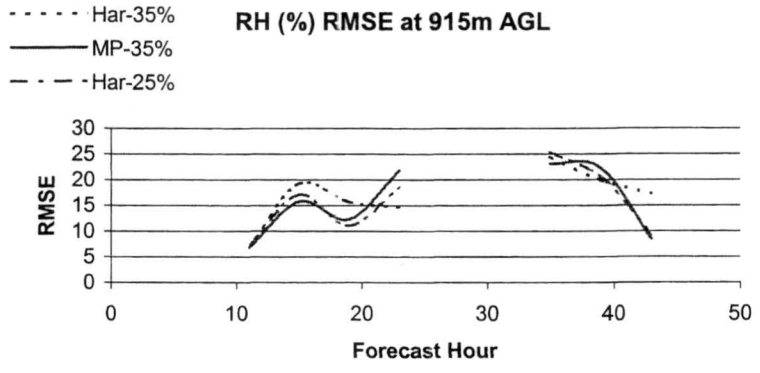

d.

Figure 5.7 - RH (%) Root Mean Square Error at: a) 100m AGL; b) 200m AGL; c) 500m AGL; and d) 915m AGL.

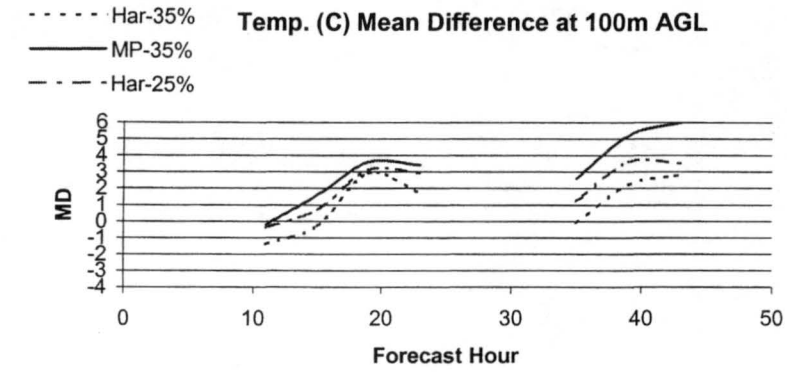

a.

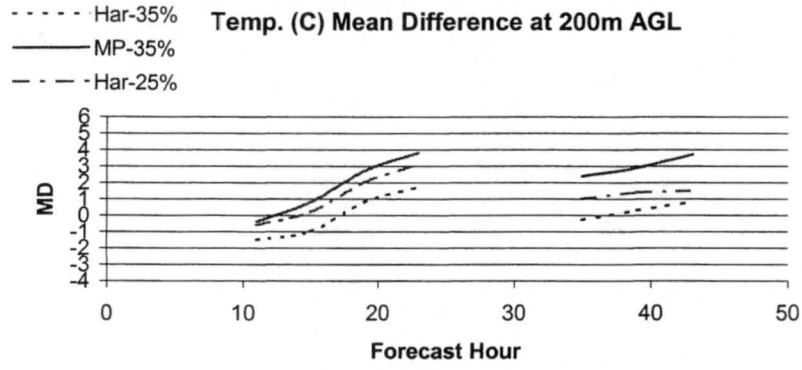

b.

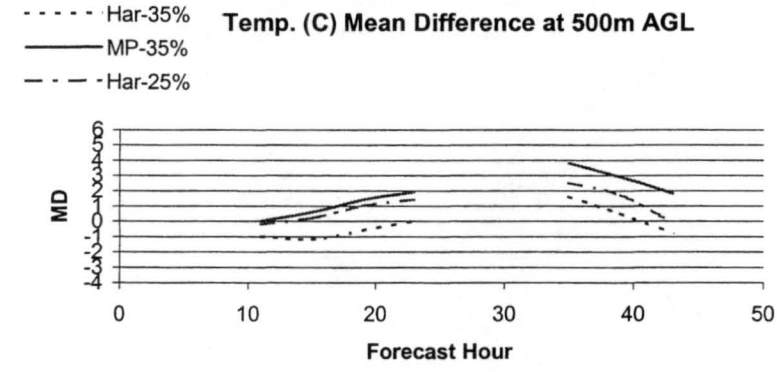

c.

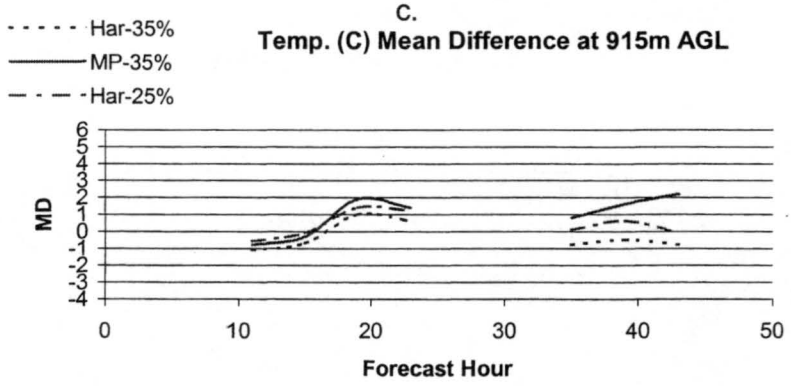

d.

Figure 5.8 – Temperature (C) Mean Difference at: a) 100m AGL; b) 200m AGL; c) 500m AGL; and d) 915m AGL.

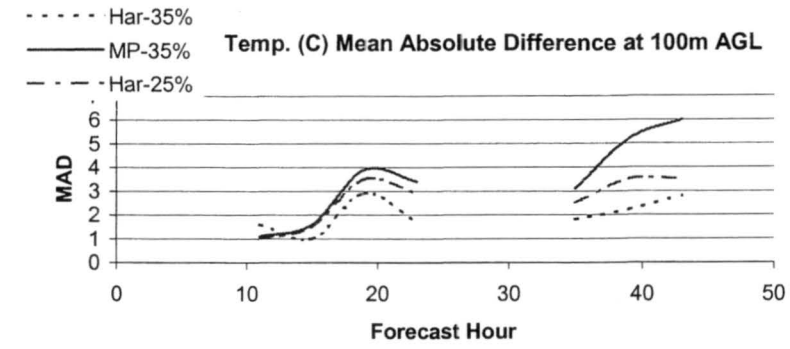

a.

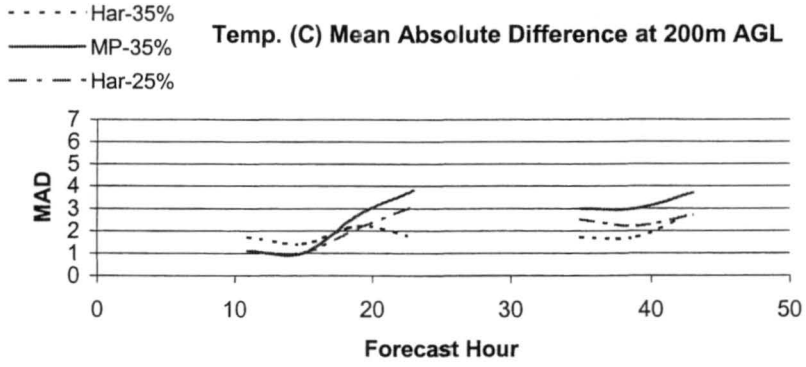

b.

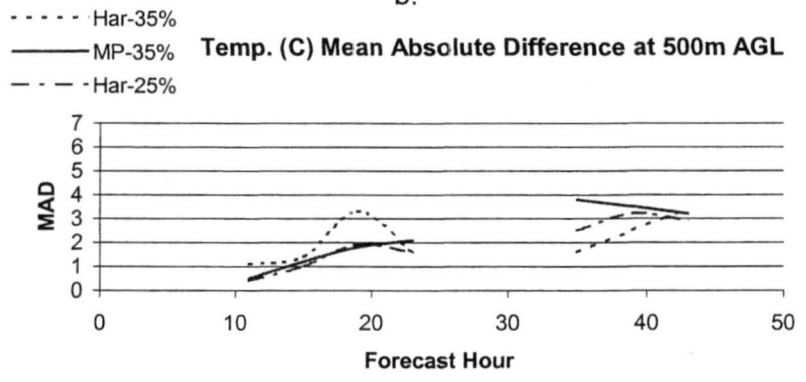

c.

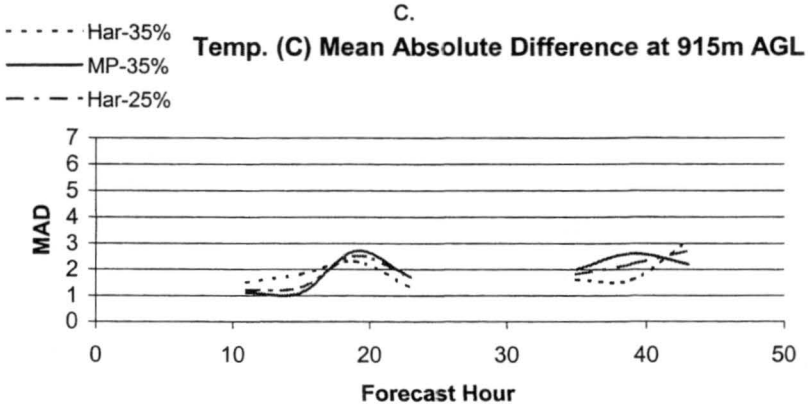

d.

Figure 5.9 – Temperature (C) Mean Absolute Difference at: a) 100m AGL; b) 200m AGL; c) 500m AGL; and d) 915m AGL.

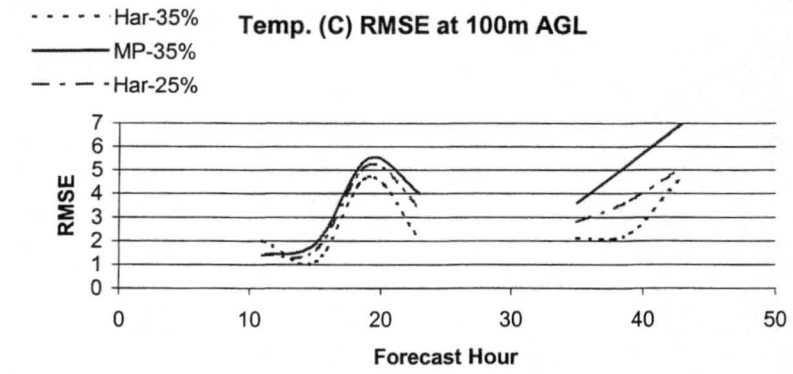

a.

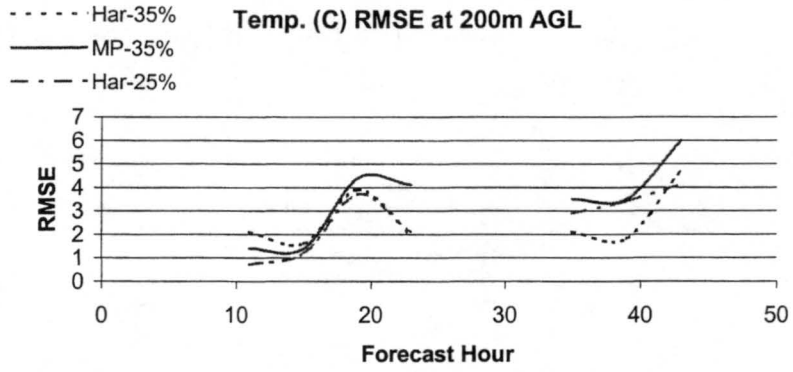

b.

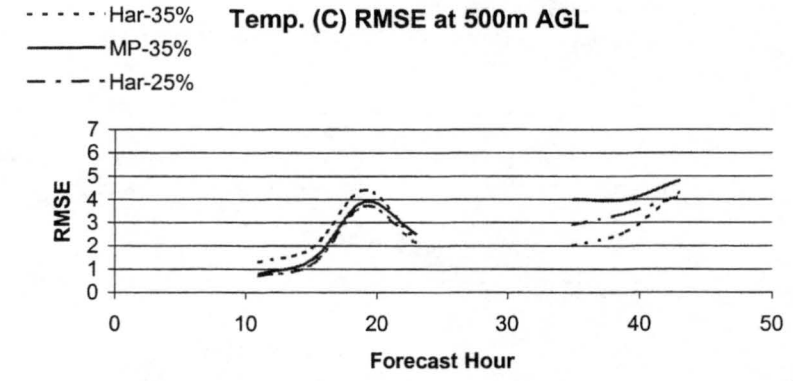

c.

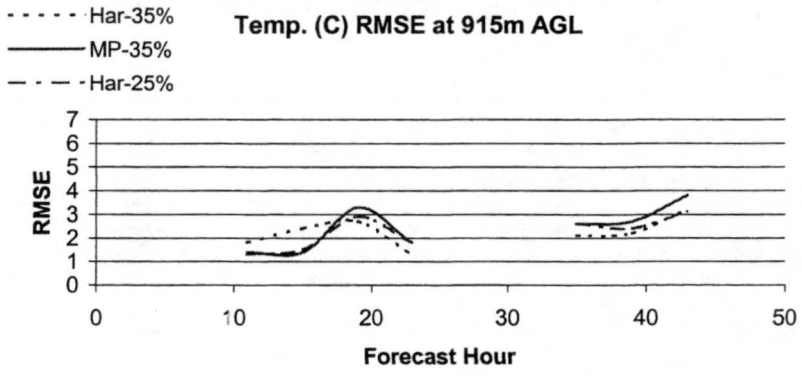

d.

Figure 5.10 – Temperature (C) Root Mean Square Error at: a) 100m AGL; b) 200m AGL; c) 500m AGL; and d) 915m AGL.

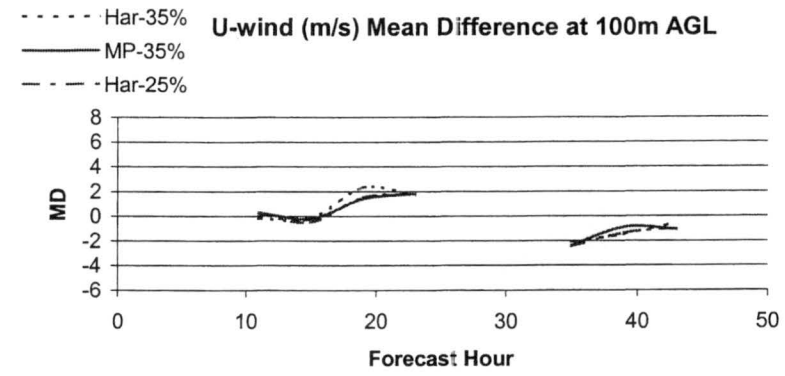

a.

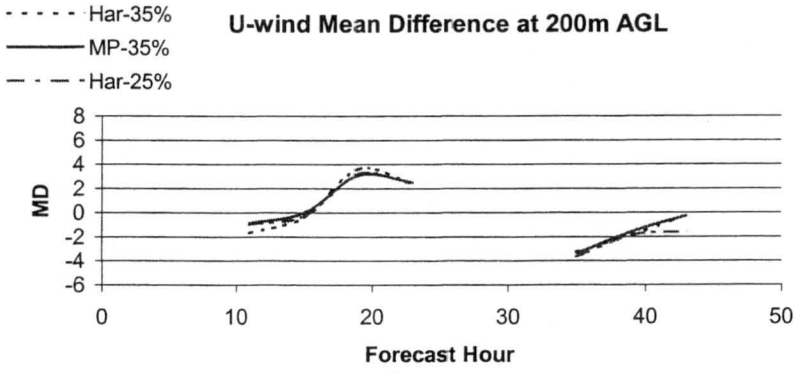

b.

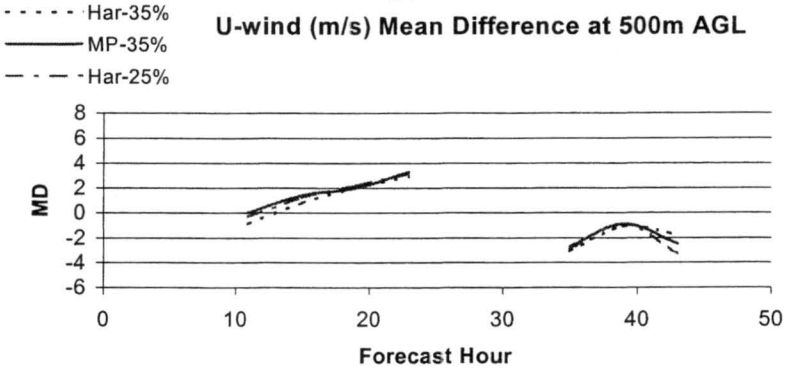

c.

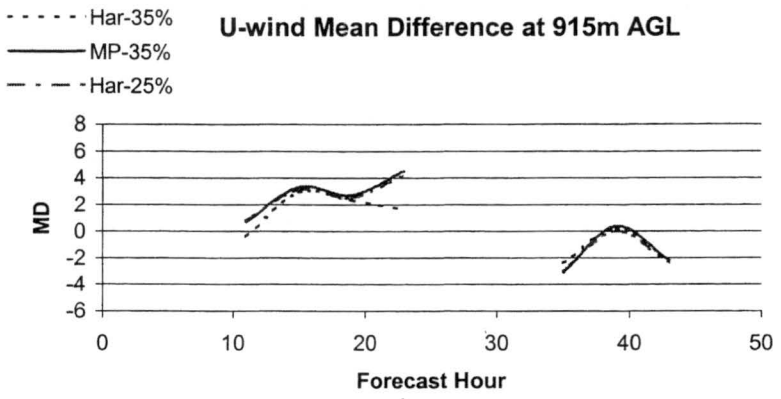

d.

Figure 5.11 – U-wind (m/s) Mean Difference at: a) 100m AGL; b) 200m AGL; c) 500m AGL; and d) 915m AGL.

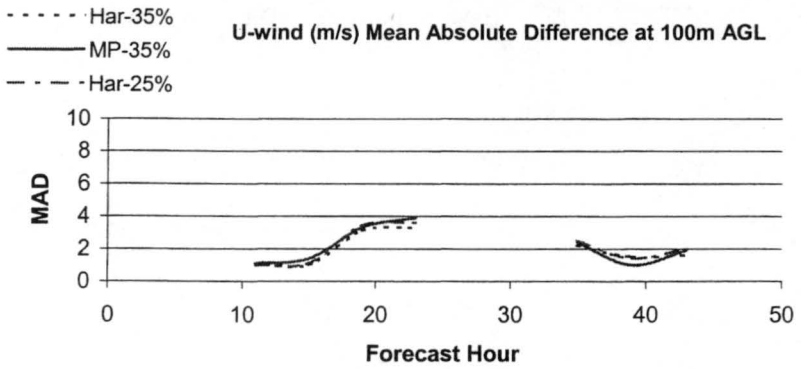

a.

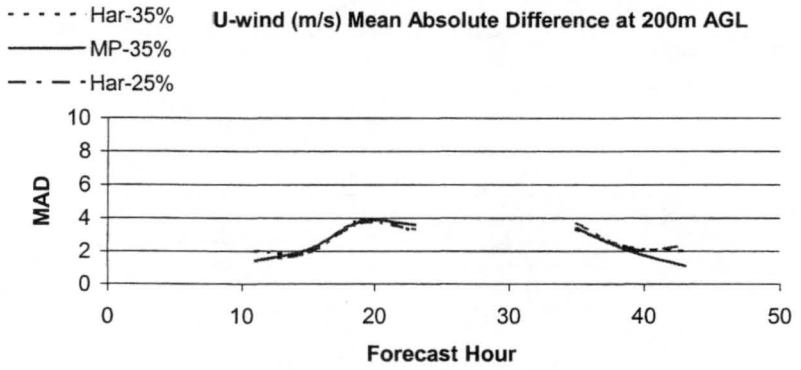

b.

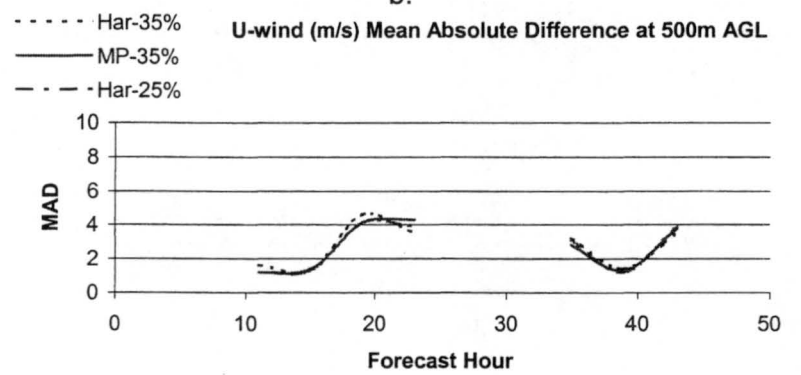

c.

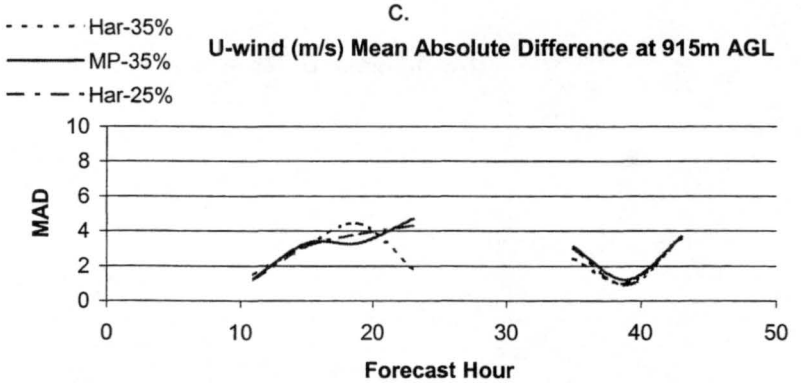

d.

Figure 5.12 – U-wind (m/s) Mean Absolute Difference at: a) 100m AGL; b) 200m AGL; c) 500m AGL; and d) 915m AGL.

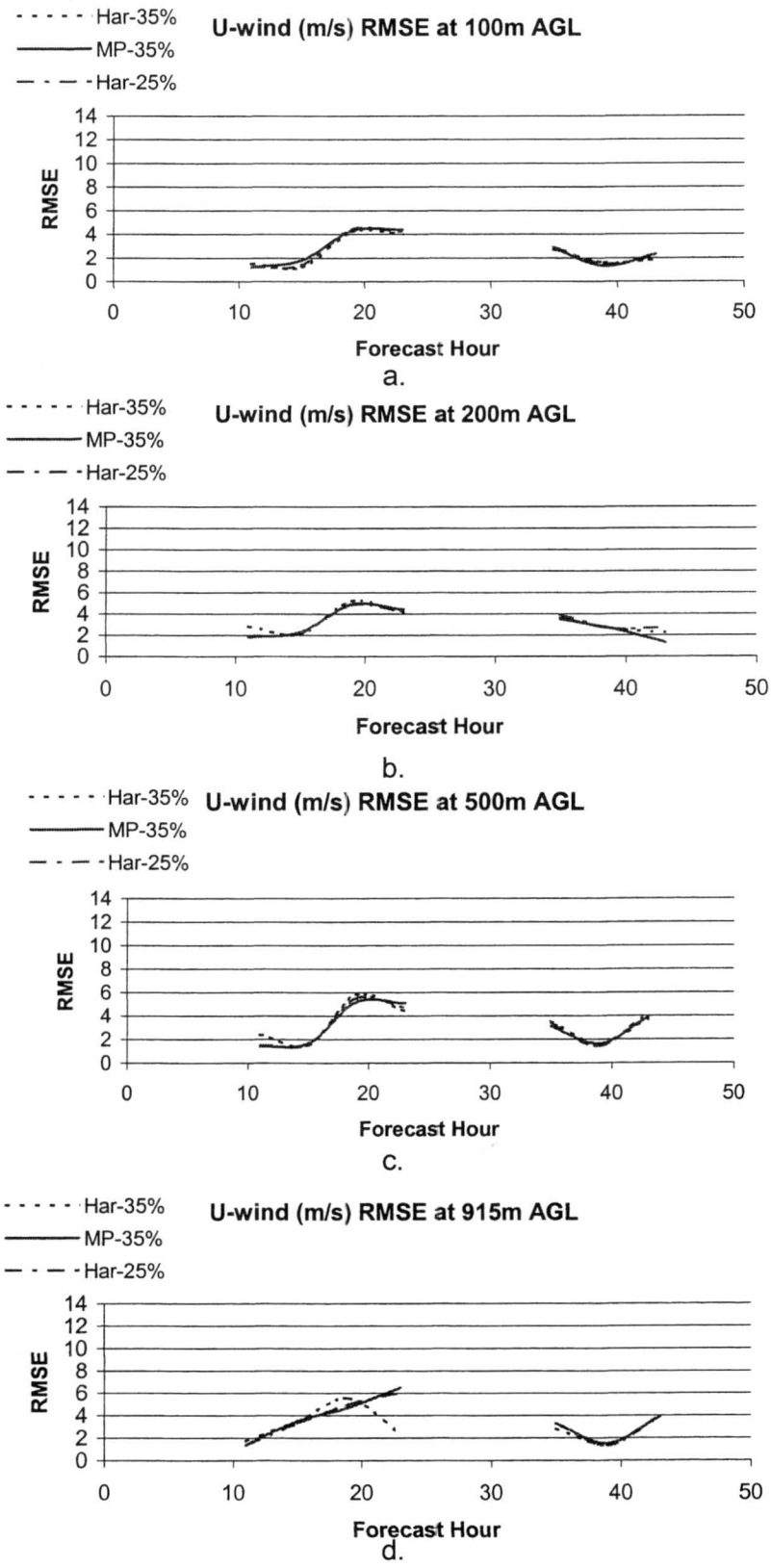

Figure 5.13 – U-wind (m/s) Root Mean Square Error at: a) 100m AGL; b) 200m AGL; c) 500m AGL; and d) 915m AGL.

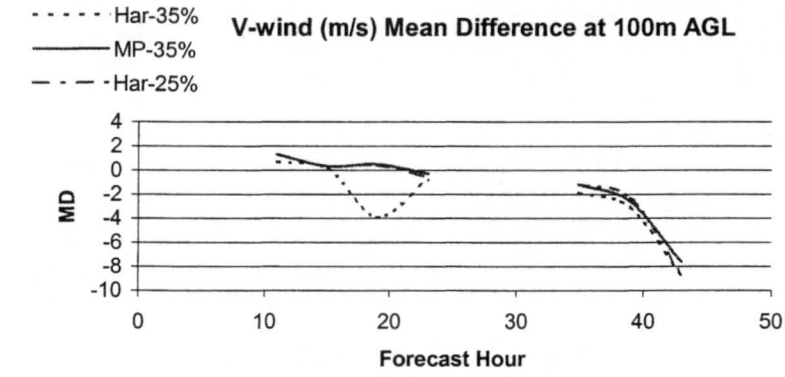

a.

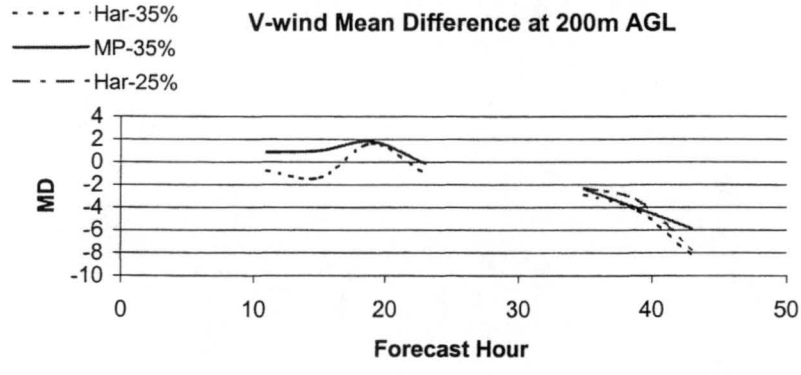

b.

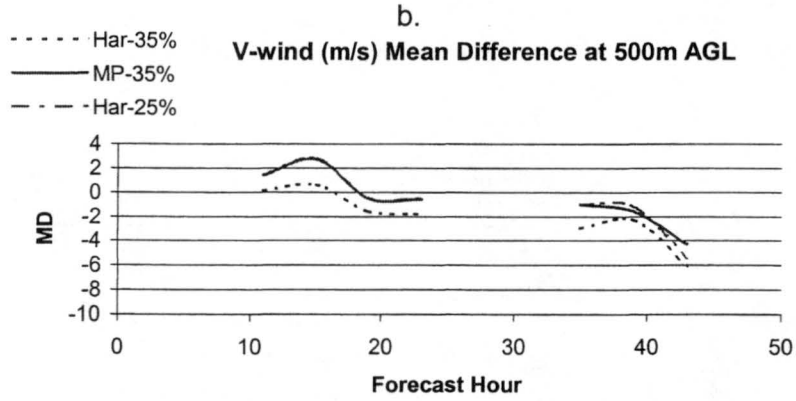

c.

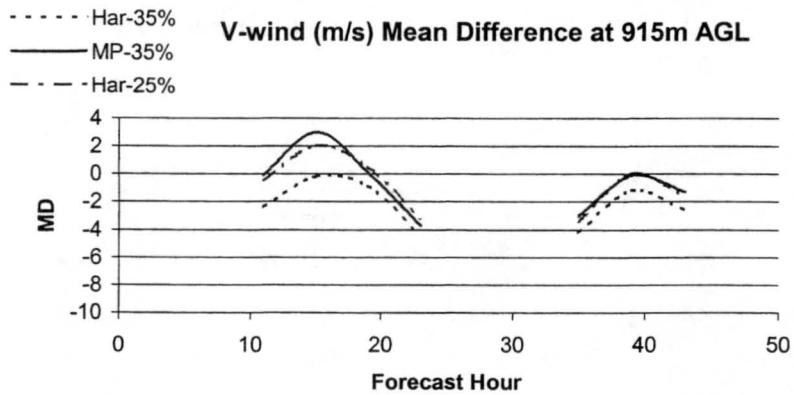

d.

Figure 5.14 – V-wind (m/s) Mean Difference at: a) 100m AGL; b) 200m AGL; c) 500m AGL; and d) 915m AGL.

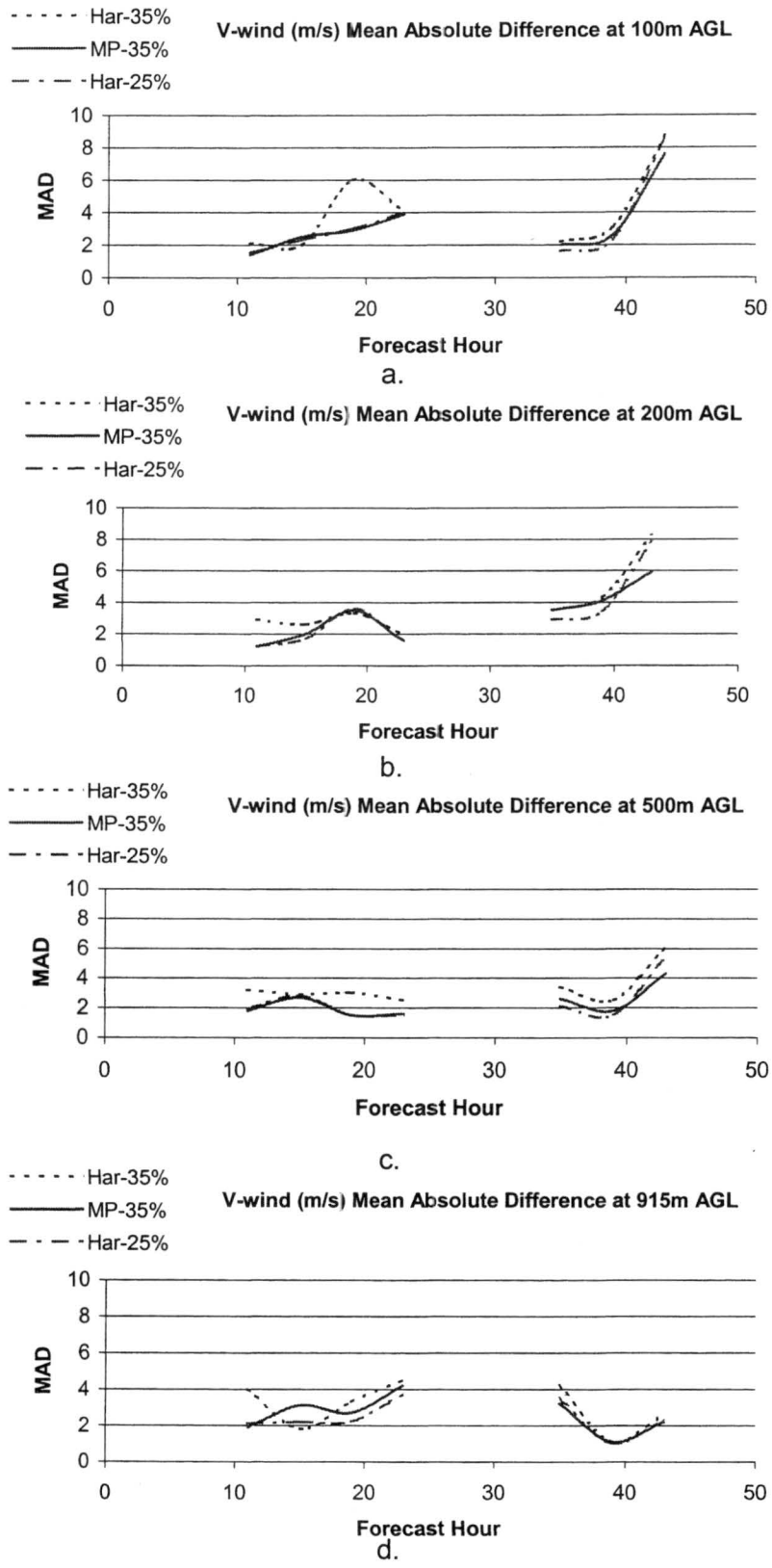

Figure 5.15 – V-wind (m/s) Mean Absolute Difference at: a) 100m AGL; b) 200m AGL; c) 500m AGL; and d) 915m AGL.

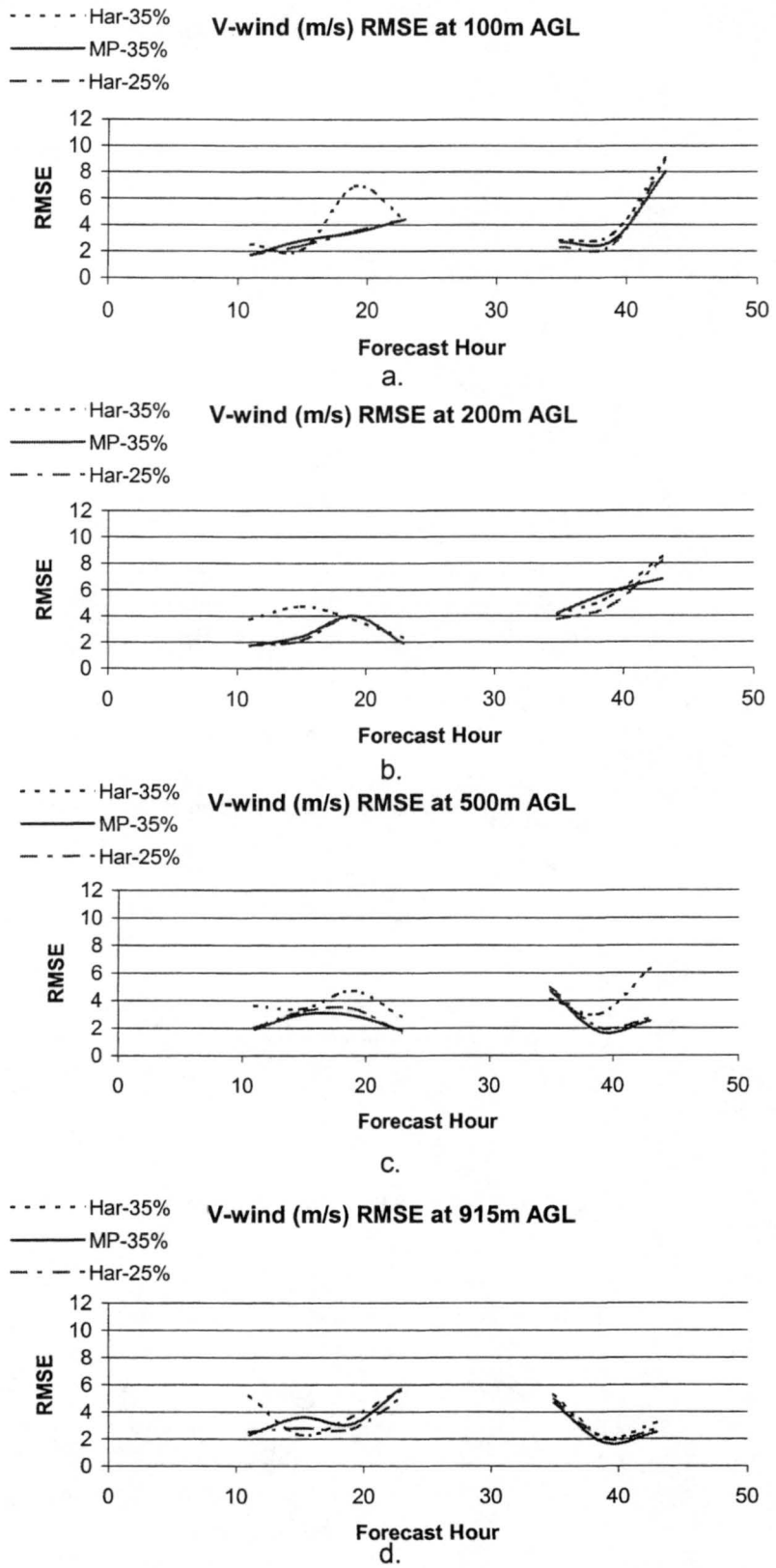

Figure 5.16 – V-wind (m/s) Root Mean Square Error at: a) 100m AGL; b) 200m AGL; c) 500m AGL; and d) 915m AGL.

6. Conclusions

6.1 Summary and Interpretation of Results

In September 1999, RAMS version 4.29 was implemented on a cluster of 16 Pentium class PC's for use as a real-time forecast system. Its initial project was to provide high-resolution boundary layer forecast data for the CASES-99 nocturnal boundary layer field project over October 1999. By late September 1999, an initial configuration of the model had been implemented with development of automation scripts, and graphical model web output ongoing. The initial operational model configuration provided CASES-99 forecasters real-time numerical guidance in support of field operations. Real-time model output was utilized to complement both the planning of observational periods, and provide information to assist in the near real-time interpretation of observed events. Over the initial forecast days of the CASES-99 field project, issues involving development of automation scripts and graphical output products were resolved with the help of input from the CASES-99 principal investigators. After some initial experimentation, an appropriate model time-step was implemented to provide reliable and timely forecasts for field investigators. Forecasts were initialized and nudged with 12 Z NCEP ETA model initialization and forecast data, daily by 10:30 AM MDT. Typically 24 hours of forecast data were available to CASES-99 forecasters by the required 2:00 MDT deadline to assist in making a decision on the initiation of operations

that evening. 48 hours worth of data were available to forecasters by 5:00 PM MDT to assist forecasters in planning for operations on the following evening. Through the period of the field project, the model proved to be reliable, producing timely forecasts, with the exception of a few dates where problems receiving initialization data occurred. Upon conclusion of the CASES-99 project, the high-resolution grids were relocated to varying geographical sites within the CONUS including White Sands, NM, Littlefield, TX, Tucson, AZ, WLEF Tower, WI, southern MN, Leon, KA, north central and northeast Colorado (Fig 3.2) to provide forecast support for a variety of interests and demonstrate grid mobility. This study focused on analysis of model performance through the period of the CASES-99 field project utilizing observational tower and sounding data gathered throughout the project for comparison with model data.

The overall performance of the model, determination of potential model biases and a preferential configuration for the forecasting situation were analyzed through examination of individual forecast performance on two representative IOP's, and forecast performance through the duration of the CASES-99 project. Three model configurations were examined to determine potential model biases and a preferential configuration for the forecasting situation. The three configurations varied only in the soil moisture and radiation scheme, with all other parameters uniform between configurations. Model configurations included: 1) Harrington radiation at 35% homogeneous volumetric soil moisture (Har-35); 2) Harrington radiation at 25% homogeneous volumetric soil moisture (Har-25); and 3) Mahrer/Pielke radiation at 35% homogeneous volumetric soil moisture (MP-35). Mahrer/Pielke was included in the analysis because it was operational at the time of the CASES-99 field project, while the Harrington scheme did not come online until a later date. When Harrington came online, it was implemented in the real-time model because of its inclusion of clouds in radiation calculations, which could pertain to future forecasting situations. Soil moisture was

decreased to 25% in accordance with point observations from the Kansas field site. Uniform characteristics between model configurations included a three-grid setup, with grid 1 covering the CONUS at 48 km resolution, grid 2 covering 552 x 552 km at 12 km resolution, and grid 3 covering 114 x 114 km at 3 km resolution. Vertically, grid 3 provided 50 m resolution up to 600 m AGL, increasing to 75 m resolution up to 1000 m AGL. For the duration of the CASES-99 field project, grids 2 and 3 were centered near Leon, KA, which was the central location for the field project.

Methods used to analyze model performance, potential biases between configurations, and determination of a preferential configuration involved analysis of two specific individual forecasts representative of the general atmospheric conditions observed on all IOP's, and comprehensive analysis of forecasts through the duration of the CASES-99 project. Both analyses focused on meteorological variables important to field forecasters including relative humidity, temperature, U-wind speed, V-wind speed and wind direction. The individual forecast analysis involved comparison of model and observed synoptic scale conditions, model and sounding data from the Leon launch site through the lowest 1500 m AGL of the atmosphere, and comparison of model and tower data from the Leon central 55 m tower site at 45 m and 5 m AGL, through the time evolution of two individual forecast periods. This analysis method provided insight on model performance regarding the time evolution of boundary layer structure through specific forecast periods. High-resolution features were captured in the sounding analysis that could not be captured in the comprehensive forecast analysis. The comprehensive forecast analysis involved comparison of model and tower data at 45 m and 5 m AGL through the duration of the CASES-99 period. Additionally, statistical parameters were computed at 100 m, 200 m, 500 m, and 915 m AGL utilizing limited sounding data from four sites to roughly analyze tendencies in model performance and discover possible model biases.

Examination of the results of both analyses showed similar tendencies. Har-35 produced the coolest temperatures and corresponding highest RH values of all model configurations, especially at vertical levels closest to the surface. MP-35 generally produced the warmest temperatures, while Har-25 produced the lowest RH values at similar vertical levels. Additionally, both analyses showed Har-35 to be in closest agreement with observations nearest the surface in terms of relative humidity and temperature magnitude, with no preferential configuration with regard to winds at low levels. Above the 200 m AGL statistical analysis, no preferential configuration was displayed with regards to relative humidity, temperature, U-wind, and V-wind. All configurations followed the pattern of observed time evolution of atmospheric variables fairly well but had problems with magnitude, with the largest error displayed in relative humidity fields.

Specific highlights from the analysis of IOP #7 and IOP #9 displayed how RAMS performed under various model configurations as a near surface high resolution forecasting tool on specific dates of a field project. Synoptic scale guidance displayed consistency between all model configurations in predicting the observed sea-level pressure structure at various times, with some problems in prediction of SE wind direction ahead of troughs approaching the Midwest. Comparison between model and observed sounding data showed a tendency of all model configurations to produce temperature inversions at heights lower than observed, or fictitious inversions that never existed within the observations, potentially associated with fictitious directional wind shear at similar heights as displayed in IOP# 9. Below predicted inversion levels model and observed values agreed fairly well in structural appearance. All configurations performed adequately in predicting the observed direction of wind components, but had some problems with magnitude. Additionally, all configurations resolved the formation and development of low level jets near the surface and indicated the presence of high

resolution wind features, such as the vertical shear in IOP #9, which indicated to forecasters that turbulence might develop. Comparison of model and tower data displayed a 2 to 3 hour lag in transition from stable to convective boundary layer that was linked to conservative numerical parameters in the LEAF-2 surface model, which have been adjusted in version 4.3.

Tower and sounding analysis in chapter 5 backed up some on the general trends displayed in the individual forecast analyses and added information through a rough statistical analysis. Tower analysis at 45 and 5 m AGL showed that the structural time evolution of all atmospheric fields were similar between model configurations, and followed the basic pattern displayed in the observations except for the RH fields. As forecast times increased from less than 24 hours to greater than 24 hours, discrepancies between model and observations tended to increase as well. Examination of sounding statistics displayed temperature and RH biases discussed above. Wind statistics showed that U-wind magnitudes were generally over-predicted in the 11 – 23 forecast hour range, and under-predicted in the 35 – 43 forecast hour range. V-wind statistics showed no consistent model bias in the 11 – 23 forecast hour range, while winds were under-predicted in the 35 – 43 forecast hour range. Little difference existed between model configurations in the prediction of wind fields.

From the results of this study, it appears that all three model configurations could have been used as effective forecast tools in support of the CASES-99 field project. Analysis of individual forecast periods showed that the model provided insight to forecasters on the development of high-resolution features such as low level jets within 100 m of the surface, and strong directional wind shear with height. At levels near the surface, the Har-35 proved to produce temperature and RH results closest in magnitude to observations. At similar levels no model bias was seen in the prediction of wind fields. At levels greater than 200 m AGL, no model bias with respect to observations was

displayed in terms of RH, temperature, or winds. In terms of predicting the time evolution of atmospheric fields, all configurations displayed their effectiveness in predicting the trends displayed in the observations, with some discrepancies appearing in magnitudes. Overall, the results of the study displayed the utility of RAMS in providing near-surface high vertical resolution forecast data, that is currently unavailable from other operational forecast models, running on a relatively inexpensive cluster of Pentium class PC's. As upgrades in processor speed continue, RAMS' ability to provide high resolution forecast data should only grow.

6.2 Future Work

Suggestions for future research involve additional work on the CASES-99 study, and a broader examination of model performance over seasonal periods and varied locations. Additional work on the CASES-99 project could involve the inclusion of higher resolution data sets, such as lidar data, for further verification analysis of wind fields. A more thorough investigation into what physical mechanisms caused model errors could also be included in future work. The effectiveness of vertical nesting could be examined by comparing model configurations with high-resolution vertical nesting, and lower resolution vertical spacing, where no vertical nesting is implemented. Additionally, initialization and nudging datasets could be varied, for example utilizing FSL high-resolution maps analysis data for initialization, to study the model's sensitivity to such datasets. Also, when real-time heterogeneous soil moisture initialization becomes an option with the real-time model, it would be good to study the impacts of heterogeneous soil moisture initialization on the CASES-99 study to see which initialization methods work best in a real-time environment. Finally, reproduction of runs without the LEAF-2

transitional lag bug would provide insight on what effects the transitional lag from stable to convective boundary layer had on forecast results.

The other focus of future work could involve a much more comprehensive study that examines model performance at varied locations over seasonal time scales. One problem with the CASES-99 study was that it covered dates only within the month of October 1999, and primarily covered nocturnal hours in clear sky conditions at a single location. The primary attractions to the CASES-99 study were the real-time RAMS support, and the availability of near-surface high-resolution datasets. A much more rigorous examination of model performance over varied terrain could be completed if multiple field projects over varying locations could be supported in real-time and re-examined at a later date. With the emphasis on grid mobility it would be helpful to accumulate a database of model performance at varied locations. Another possibility would be for the forecast model to provide real-time forecast data at a fixed site through seasonal time scales to thoroughly analyze how the model performed on a specific type of terrain over the coarse of a year. In either case, availability of high-resolution observational data would most likely be the limiting factor in determining model performance.

7. References

Businger, J.A., W.F. Dabberdt, A.C. Delany, T.W. Horst, C.L. Martin, S.P. Oncley, and S.R. Semmer, 1990: ASTER: the Atmospheric-Surface Turbulent Exchange Research Facility at NCAR. *Eos.* 693-702.

Cotton, W.R., M.A. Stephens, T. Nehrkorn, and G. J. Tripoli, 1982: The Colorado State University three-dimensional cloud/mesoscale model—1982. Part II: An ice parameterization. *J. Rech. Atmos.*, **16**, 295-320.

Cotton, W.R., G. Thompson, and P.W. Mielke, 1994: Real-time mesoscale prediction on workstations. *Bull. Amer. Meteor. Soc.,* **75**, 349-362.

Clark, T.L., 1977: A small-scale dynamic model using a terrain-following coordinate transformation. *J. Comput. Phys.,* **24**, 186-215.

Cram, J.M., 1990: Numerical simulation and analysis of the propagation of a prefrontal squall line. PhD dissertation, Atmos. Sci. Paper No. 471, Colorado State University, Dept of Atmos. Sci., Fort Collins, CO, 332pp.

Day, C.H., 1998: The WMO format for the storage of weather product information and the exchange of weather product messages in gridded binary form as used by NCEP central operations. U.S. Dept. of Commerce, NOAA, NWS, NCEP. Office Note 388, p29.

Gal-Chen, T., and R.C.J. Somerville, 1975: On the use of a coordinate transformation for the solution of the Navier Stokes equations. *J. Comput. Phys.,* **17**, 209-228.

Harrington, J.Y., 1997: The effects of radiative and microphysical processes on simulated warm and transition season arctic stratus. PhD dissertation, Atmos. Sci. Paper No. 637, Colorado State University, Dept. of Atmos. Sci., Fort Collins, CO, 278pp.

Henmi, T. and R. Dumais, Jr., 1998: Description of the Battlescale Forecast Model, TR-1032, U.S. Army Research Laboratory.

Lemone, M.A., R.L. Grossman, R.L. Coulter, M.L. Wesley, G.E. Klazura, G.S. Poulos, W. Blumen, J.K. Lundquist, R.H. Cuenca, S.F. Kelly, E.A. Brandes, S.P. Oncley, R.T. McMillen, and B.B. Hicks, 2000: Land-atmosphere interaction research, early results, and opportunities in the Walnut River Watershed in southeast Kansas: CASES and ABLE. *Bull. Amer. Meteor. Soc.,* **81**, 757-779.

Mahrer, Y. and R.A. Pielke, 1977: A numerical study of airflow over irregular terrain. *Beitrage zur Physik der Atmosphare*, **50**, 98-113.

Mellor, G.L., and T. Yamada, 1974: A hierarchy of turbulence closure models for planetary boundary layers. *J. Atmos. Sci.,* **31**, 1791-1806.

Mesinger, F. and A. Arakawa, 1976: Numerical Methods used in atmospheric models. GARP Publication Series, No. 14, WMO/ICSU Joint Organizing Committee, 64pp.

Mesinger, F., T.L. Black, and M.E. Baldwin, 1999: Impact of resolution and of the Eta coordinate on skill of the Eta Model precipitation forecasts. *Numerical Methods in Atmospheric and Oceanic Modeling: the Andre J. Robert Memorial Volume,* 399 – 423.

Pielke, R.A., W.R. Cotton, R.L. Walko, C.J. Tremback, W.A. Lyons, L.D. Grasso, M.E. Nicholls, M.D. Moran, D.A. Wesley, T.J. Lee and J.H. Copeland, 1992: A comprehensive meteorological modeling system – RAMS. *Meteorol. Atmos. Phys.*, **49**, 69-91.

Poulos, G.S., W. Blumen, D.C. Fritts, J.K. Lundquist, J. Sun, S.P. Burns, C. Nappo, R. Banta, R. Newsom, J. Cuxart, E. Terradellas, B. Balsley, and M. Jensen, 2001: CASES-99: A comprehensive investigation of the stable nocturnal boundary layer. Submitted *Bull. Amer Meteor. Soc.*

Rogers, E., M.E. Baldwin, T.L. Black, K. Brill, F. Chen, G.J. Dimego, J. Manikin, F. Messinger, K.E. Mitchell, D.F. Parrish, and Q. Zhao, 1998: Changes to the NCEP operational "early" eta analysis / forecast system. http://www.nws.noaa.gov/er/buf/etamodel.htm.

Thompson, G., 1993: Prototype real-time mesoscale prediction during the 1991-92 winter season and statistical verification of model data. Masters thesis, Atmos. Sci. Paper No. 521, Colorado State University, Dept. of Atmos Sci., Fort Collins, CO, 105pp.

Tremback, C.J., 1990: Numerical simulation of a mesoscale convective complex: model development and numerical results. PhD dissertation, Atmos. Sci. Paper No. 465, Colorado State University, Dept. of Atmos. Sci., Fort Collins, CO, 274pp.

Tremback, C.J., G.J. Tripoli, and W. R. Cotton, 1985: A regional scale atmospheric numerical model including explicit moist physics and a hydrostatic time-split scheme. *Preprints, 7th Conf. On Numerical Weather Prediction*, AMS, Montreal, Canada, 355-358.

Tripoli, G.J., 1986: A numerical investigation of an orogenic mesoscale convective system. PhD dissertation, Atmos. Sci. Paper No. 401, Colorado State University, Dept. of Atmos. Sci., Fort Collins, CO, 290pp.

Tripoli, G.J. and W.R. Cotton, 1982: The Colorado State University three-dimensional cloud/mesoscale model–1982. Part I: General theoretical framework and sensitivity experiments. *J. Rech. Atmos.*, **16**, 185-220.

Walko, R.L., L.E. Band, J. Baron, T.G.F. Kittel, R. Lammers, T.J. Lee, D. Ojima, R.A. Pielke, C. Taylor, C. Tague, C.J. Tremback, and P.R. Vidale, 2000: Coupled atmosphere-biophysics-hydrology models for environmental modeling. *J. Appl. Meteor.,* **39**, 931-944.

Walko, R.L., W.R. Cotton, M.P. Meyers, and J.Y. Harrington, 1995: New RAMS cloud microphysics parameterization. Part I: The single moment scheme. *Atmos. Res.,* **38**, 29-62.

Warner, T.T. and N.L. Seaman, 1990: A real-time mesoscale numerical weather-prediction system for research, teaching, and public service at Pennsylvania State University. *Bull. Amer. Meteor. Soc.,* **71**, 792-805.